Inaugural dissertation

for

obtaining the doctoral degree

of the

Combined Faculty of Mathematics, Engineering and Natural Sciences

of the

Ruprecht - Karls - University

Heidelberg

Presented by

M.Sc. Minh Tu Pham

born in: Cantho, Vietnam

Oral examination: October 19, 2022

Intercellular transmission of viral RNA by Apolipoprotein E-associated extracellular vesicles

Referees:

Prof. Dr. Ralf Bartenschlager

Prof. Dr. Britta Brügger

Declaration

The applicant, Minh Tu Pham declares that he is the sole author of the submitted dissertation and no other sources or help from those specifically referred to have been used. Additionally, the applicant declares that he has not applied for permission to enter the examination procedure at another institution and this dissertation has not been presented to other faculty and not used in its current or in any other form in another examination.

Heidelberg, *01 August 2022*

Minh Tu Pham

TABLE of CONTENTS

LỜI CẢM TẠ

Con xin đội ơn Thượng Đế, Thánh Thần, Tổ Thầy, Chư Vị và sư huynh dạy dỗ và ban cho con ơn phước. Con xin được mượn lời của cô Triệu Ân để bày tỏ lòng mình: *"Một trận mưa xối xuống, vạn vật tùy theo chủng loại được thấm nhuần khác nhau. Con, phận cỏ thấp bé cũng hưởng được cơn mưa phước của Thánh Thần, mười phương Phật"*.

Con xin được cảm ơn nguồn cội, và con cảm ơn mẹ vì tất cả. Tình yêu của mẹ chắp cho con đôi cánh tự do.

"Science without religion is lame, religion without science is blind"

Albert Einstein, 1954

v

ACKNOWLEDGEMENTS

LIST of FIGURES

LIST of TABLES

LIST of MOVIES

Movie 1. Long-term time-lapse confocal imaging of ApoE, NS5A, and E2 trafficking in a HCV-replicating hepatocyte

Movie 2: Spatio-temporal convergence and divergence events of ApoE and NS5A-E2 double-positive signals

Movie 3. Abundance of ApoE-NS5A foci in a HCV-replicating hepatocyte

Movie 4. Intracellular co-trafficking of ApoE-CD63 complexes in an uninfected hepatocyte

Movie 5. Secretion of an ApoE-associated CD63 intraluminal vesicle in an uninfected hepatocyte

Movie 6. The uptake of donor-derived ApoE-CD63 complexes in a recipient cell

APPENDIX

LIST OF ABBREVIATIONS

AF	Alexa flour		IRES	internal ribosome entry site
ApoE	Apolipoprotein E		IV	intraluminal vesicle
ApoE-KD	ApoE-knockdown		IVT	in vitro transcript
BSA	bovine serum albumin		JFH1	Japanese fulminant hepatitis 1
Caco	sodium cacodylate		KDEL	ER retention signal
CD63	cluster of differentiation 63		LCS	low complexity sequence
CD81	cluster of differentiation 81		LDL	low density lipoprotein
CLEM	correlative light electron microscopy		LDLR	very low density receptor
CMIA	chemiluminescent microparticle immunoassay		LRP1	lipoprotein receptor-related protein 1
COVID-19	Coronavrus Disease 2019		miR-122	microRNA-122
CRAC	cholesterol recognition/interaction amino acid consensus sequence		mRNA	messenger ribonucleic acid
Cryo-FIB-SEM	cryogenic focused ion beam scanning electron microscopy		MSD	mean squared displacement
CsA	cyclosporin A		mT2	mTurquoise 2
CypA	cyclophilin A		mTOR	mechanistic target of rapamycin
DGAT1	diacylglycerol-O-acyltransferase 1		MTTP	microsomal triglyceride transfer protein
DMEMcplt	Dulbecco's modified Eagle medium complete		NEB	New England Biolabs
DMV	double membrane vesicle		Neo	Neomycin
DNA	deoxyribonucleic acid		Nluc	nanoluciferase
dsDNA	double-stranded ribonucleic acid		NS2	nonstructural protein 2
DTT	dithiothreitol		NS5A	nonstructural protein 5A
E. coli	Escherichia coli		NTR	nontranslated region
EBV	Epstein-Barr virus		PBS	phosphate-buffered saline
eIFs	eukaryotic *initiation* factors		PCR	polymerase chain reaction
EM	electron microscopy		PFA	paraformaldehyde
ER	endoplasmic reticulum		PI4KIIIα	phosphatidylinositol-4 kinase III alpha
ESCRT	endosomal sorting complex required for transport		PM	plasma membrane
EV	extracellular vesicle		RNA	ribonucleic acid
eYFP	enhanced yellow fluorescent protein		RT	room temperature
FCS	fetal calf serum		RT-qPCR	real time quantitative PCR
FP	fluorescent protein		SARS-CoV2	severe acute respiratory syndrome coronavirus 2
GA	glutaraldehyde		SDS-PAGE	sodium dodecyl sulfate–polyacrylamide gel electrophoresis
GFP	green fluorescent protein		SEF	spot-enhancing filter
h.p.e	hour post-electroporation		SEM	standard error of the mean
h.p.t	hour post-transfection		shRNA	short hairpin
HBV	hepatitis B virus		smFISH	single molecule fluorescence in situ hybridization
HCV	Hepatitis C virus		SR-BI	scavenger receptor class B type I
HCV LVP	HCV lipoviroparticle		ssRNA	single-stranded ribonucleic acid
HCVcc	HCV cell culture		STED	stimulated emission depletion microscopy
HEK293T	human embryonic kidney 293 with T-antigen		SVP	subviral particle
HIV	human immunodeficiency virus		TAE	Tris-acetate-EDTA
HPV	human papillomavirus		TAR	trans-activation response element
HSP70	heat shock protein 70		TCP	transcomplemented particle
HSP90	heat shock protein 90		TEM	transmission electron microscopy
HSPG	heparin sulfate proteoglycans		TLR3	toll-like receptor 3
HSV	Herpes simplex virus		tub	tubulin
Hyg	Hygromycin		VLDL	very low density lipoprotein
IF	immunofluorescence		WHO	World Health Organization

SUMMARY

Hepatitis C virus is a major causative agent of liver-associated diseases including liver cirrhosis and liver cancer. A prophylactic vaccine is not available and highly efficient antiviral therapy that can eliminate the virus in infected individuals is not affordable in many high-prevalence countries. Therefore, more efforts are required regarding the global eradication of HCV infection.

The HCV life cycle has been extensively studied since the discovery of HCV in 1989 and it has become an excellent research model for the studying of other pathogenic positive-strand RNA viruses. However, important gaps in the understanding of the HCV life cycle remain, especially the mechanism of HCV assembly, the site within the cells where virions are forming, and involved viral and host cell factors. Recently, it has been suggested that HCV possibly coordinates viral RNA replication and particle assembly by generating and using double-membrane vesicles (DMVs) that are tightly connected to the endoplasmic reticulum (ER), which wraps around lipid droplets. However, thus far it has not been possible to visualize assembling HCV particles.

In the first part of my thesis, I describe my efforts to faithfully identify HCV assembly sites. To this end, I established a triple-label live-cell imaging approach by fluorescently tagging Apolipoprotein E (ApoE), a host cell component of infectious HCV particles, the viral envelope glycoprotein E2, and the HCV replicase factor NS5A. Based on the available literature, I originally hypothesized that nascent HCV particles bud into the ER lumen at the sites where NS5A, E2, and ApoE are enriched and colocalize. Therefore, I investigated HCV assembly events by time-lapse live-cell confocal imaging coupled with light and electron microscopy (CLEM). I found that the triple-positive signals of ApoE, NS5A, and E2 exist, but only at a very low frequency. Unfortunately, ultrastructural analysis by CLEM did not allow the unambiguous detection of nascent or mature intracellular HCV particles.

In the course of these studies, I observed that ApoE associates with NS5A to a large extent and this occurs independent of HCV assembly. Therefore, I focused my project to study the **role of the association between ApoE and NS5A in processes other than HCV assembly, which is described in the second part of my thesis.** Since NS5A also is involved in the formation of HCV-produced extracellular vesicles (EVs), reported to contribute to *de novo* infection and virus-induced pathogenesis, I employed HCV as a model system to investigate the intracellular

association, co-secretion and co-transmission of ApoE-containing lipoproteins with EVs generated in and released from infected cells.

EVs and lipoproteins are two essential ways exploited by cells and viruses for intercellular communication. The former is responsible for cell-to-cell transmission of encapsulated nucleic acids, proteins, lipids, and metabolites while the latter is crucial for the transport of cholesteryl esters and triglycerides. Several lines of evidence suggest an association of lipoproteins with EVs but the role of this interplay is not well known. Moreover, the intercellular co-transmission of these two vesicle species has not been documented. Distinct from a variety of viruses that modify the host endosomal pathway and release virus-produced EVs, HCV generates, in addition to classical virus particles, EVs containing the complete viral genome and supporting the dissemination of infection in addition to the virus particle route. Moreover, HCV also induces drastic changes in the lipid homeostasis of infected host cells, including the lipoprotein pathway. In this study, I found that in HCV-replicating cells, NS5A is enriched in ApoE and CD63 double-positive late endosomes. There, ApoE interacts with NS5A-positive intraluminal vesicles (IVs) which are the precursors of EVs. In addition, I found that infected cells release EVs containing NS5A and viral RNA. These EVs interact with ApoE either in infected cells or after release from cells into the extracellular medium. ApoE-associated EVs are taken up by non-infected bystander cells, thus transmitting viral RNA. Importantly, ApoE-NS5A interaction appeared to be important for efficient EV-mediated secretion of HCV RNA.

In the third part of my thesis, I describe the characterization of the association of ApoE-containing lipoproteins with EVs in the context of non-infected cells. I found that ApoE and CD63 double-positive IVs traffic along the pathway of late endosomes. Importantly, secreted ApoE associates with a fraction of EVs and co-enters neighboring bystander cells. These results suggest a more general role of ApoE in EV-mediated cell-to-cell communication and reveal genuine intercellular co-transmission of EVs in association with ApoE.

ZUSAMMENFASSUNG

Das Hepatitis-C-Virus ist einer der Hauptverursacher von leberbedingten Krankheiten wie Leberzirrhose und Leberkrebs. Ein prophylaktischer Impfstoff steht nicht zur Verfügung, und eine hochwirksame antivirale Therapie, die das Virus bei infizierten Personen eliminieren kann, ist in vielen Ländern mit hoher Prävalenz nicht erschwinglich. Daher sind weitere Anstrengungen erforderlich, um die HCV-Infektion weltweit auszurotten.

Der HCV-Lebenszyklus wurde seit der Entdeckung von HCV im Jahr 1989 eingehend untersucht und hat sich zu einem hervorragenden Forschungsmodell für die Untersuchung anderer pathogener Positivstrang-RNA-Viren entwickelt. Allerdings gibt es noch immer große Lücken im Verständnis des HCV-Lebenszyklus, insbesondere im Hinblick auf den Mechanismus der HCV-Assemblierung, den Ort innerhalb der Zellen, an dem die Virionen gebildet werden, und die beteiligten Virus- und Wirtszellfaktoren. Kürzlich wurde vorgeschlagen, dass HCV möglicherweise die virale RNA-Replikation und den Zusammenbau von Partikeln koordiniert, indem es Doppelmembranvesikel (DMVs) erzeugt und nutzt, die eng mit dem endoplasmatischen Retikulum (ER) verbunden sind, das Lipidtröpfchen umhüllt. Bislang war es jedoch nicht möglich, den Zusammenbau von HCV-Partikeln sichtbar zu machen.

Im ersten Teil meiner Dissertation beschreibe ich meine Bemühungen, die HCV-Assemblierungsstellen genau zu identifizieren. Zu diesem Zweck habe ich einen dreifachen Markierungsansatz für die Bildgebung in lebenden Zellen entwickelt, indem ich Apolipoprotein E (ApoE), eine Wirtszellkomponente infektiöser HCV-Partikel, das virale Hüllglykoprotein E2 und den HCV-Replikasefaktor NS5A fluoreszierend markierte. Auf der Grundlage der verfügbaren Literatur stellte ich ursprünglich die Hypothese auf, dass naszierende HCV-Partikel an Stellen in das ER-Lumen eindringen, an denen NS5A, E2 und ApoE angereichert und kolokalisiert sind. Daher untersuchte ich die HCV-Assemblierung mit konfokaler Bildgebung im Zeitraffer, gekoppelt mit Licht- und Elektronenmikroskopie (CLEM). Dabei stellte ich fest, dass die dreifach positiven Signale von ApoE, NS5A und E2 zwar vorhanden sind, aber nur in sehr geringer Häufigkeit. Leider erlaubte die ultrastrukturelle Analyse mittels CLEM nicht den eindeutigen Nachweis von naszierenden oder reifen intrazellulären HCV-Partikeln.

Im Laufe dieser Studien stellte ich fest, dass ApoE in hohem Maße mit NS5A assoziiert und dies unabhängig von der HCV-Assemblierung geschieht. Daher konzentrierte ich mein Projekt darauf, die Rolle der Assoziation zwischen ApoE und NS5A bei anderen Prozessen als der HCV-Assemblierung zu untersuchen, was im zweiten Teil meiner Arbeit beschrieben wird. Da NS5A auch an der Bildung von HCV-produzierten extrazellulären Vesikeln (EVs) beteiligt ist, von denen berichtet wird, dass sie zur De-novo-Infektion und virusinduzierten Pathogenese beitragen, habe ich HCV als Modellsystem verwendet, um die intrazelluläre Assoziation, Ko-Sekretion und Ko-Übertragung von ApoE-haltigen Lipoproteinen mit EVs zu untersuchen, die in infizierten Zellen erzeugt und aus diesen freigesetzt werden.

EVs und Lipoproteine sind zwei wesentliche Wege, die von Zellen und Viren für die interzelluläre Kommunikation genutzt werden. Erstere sind für die Übertragung von eingekapselten Nukleinsäuren, Proteinen, Lipiden und Metaboliten von Zelle zu Zelle verantwortlich, während letztere für den Transport von Cholesterinestern und Triglyceriden entscheidend sind. Es gibt mehrere Hinweise darauf, dass Lipoproteine mit EVs assoziiert sind, aber die Rolle dieses Zusammenspiels ist nicht genau bekannt. Darüber hinaus wurde die interzelluläre gemeinsame

Übertragung dieser beiden Vesikelarten bisher nicht dokumentiert. Im Unterschied zu einer Reihe von Viren, die den endosomalen Weg des Wirts modifizieren und virusproduzierte EVs freisetzen, erzeugt HCV zusätzlich zu den klassischen Viruspartikeln EVs, die das gesamte virale Genom enthalten und die Verbreitung der Infektion zusätzlich zum Viruspartikelweg unterstützen. Darüber hinaus führt HCV auch zu drastischen Veränderungen in der Lipid-Homöostase infizierter Wirtszellen, einschließlich des Lipoprotein-Wegs. In dieser Studie habe ich festgestellt, dass NS5A in HCV-replizierenden Zellen in ApoE- und CD63-positiven späten Endosomen angereichert ist. Dort interagiert ApoE mit NS5A-positiven intraluminalen Vesikeln (IVs), die die Vorläufer von EVs sind. Darüber hinaus habe ich festgestellt, dass infizierte Zellen EVs freisetzen, die NS5A und virale RNA enthalten. Diese EVs interagieren mit ApoE entweder in infizierten Zellen oder nach der Freisetzung aus den Zellen in das extrazelluläre Medium. ApoE-assoziierte EVs werden von nicht-infizierten Bystander-Zellen aufgenommen und übertragen so die virale RNA. Wichtig ist, dass die ApoE-NS5A-Wechselwirkung für eine effiziente EV-vermittelte Sekretion von HCV-RNA wichtig zu sein scheint.

Im dritten Teil meiner Dissertation beschreibe ich die Charakterisierung der Assoziation von ApoE-haltigen Lipoproteinen mit EVs im Zusammenhang mit nicht-infizierten Zellen. Ich fand heraus, dass ApoE und CD63 doppelt-positive IVs entlang des Weges der späten Endosomen transportiert werden. Wichtig ist, dass sezerniertes ApoE mit einem Teil der EVs assoziiert und in benachbarte Bystander-Zellen eindringt. Diese Ergebnisse deuten auf eine allgemeinere Rolle von ApoE in der EV-vermittelten Zell-zu-Zell-Kommunikation hin und offenbaren eine echte interzelluläre Co-Übertragung von EVs in Verbindung mit ApoE.

I. INTRODUCTION

1. Hepatitis C Virus

1.1. What is Hepatitis?

Hepatitis is an inflammation of the liver which is the consequence of a viral infection or noninfectious agents. Noninfectious hepatitis occurs as a secondary outcome of obesity, autoimmune diseases or consuming alcohol, toxins and medications. Viral infection accounts for the majority of hepatitis incidence, resulting in various liver-related issues, many of which can be lethal. There are 5 hepatitis viruses that have in common their predominant or exclusive hepatotropism: hepatitis A, B, C, D, and E virus. Although these viral infections all lead to liver inflammation and associated diseases, they differ in important aspects such as route of transmission, disease severity, and preventive measures (Table 1). It is estimated that ~354 million people worldwide live with hepatitis B or C, and for most, chronic hepatitis B and C are the most common causes of liver steatosis, cirrhosis, liver cancer, and viral hepatitis-related mortality [1]. Nevertheless, diagnosis and treatment are not readily available for most people, especially for those in low- and middle-income areas.

Table 1. Characteristics of Hepatitis viruses

	Hepatitis A virus (HAV)	Hepatitis B virus (HBV)	Hepatitis C virus (HCV)	Hepatitis D virus (HDV)	Hepatitis E virus (HEV)
Classification (family	Picornaviridae	Hepadnaviridae	Flaviviridae	Kolmioviridae	Hepeviridae
/ genus)	Hepatovirus	Orthohepadnavirus	Hepacivirus	Deltavirus	Orthohepevirus
Virus structure	Non-enveloped	Non-enveloped & enveloped	Enveloped	Enveloped (from HBV)	Non-enveloped & "quasienveloped"
Genome	ssRNA (+)	dsDNA	ssRNA (+)	ssRNA (-)	ssRNA (+)
Source of Transmission	fecal & oral	parenteral, neonatal, sexual	parenteral, neonatal, sexual	parenteral, neonatal, sexual	fecal & oral
Severity	mild, rarely severe	occasionally severe	usually acute asymptomatic, occasionally chronic severe	faster progression of severity than HBV alone	mild, occasionally severe, especially in pregnant women
Chronicity	acute	acute & chronic	acute & chronic (70%)	HBV/HDV coinfection	acute & chronic
Cure	no specific treatment for hepatitis A	no specific treatment for acute hepatitis B	direct-acting antivirals >95%	first drug has been approved by European Commission	no specific treatment for acute hepatitis E
Vaccination	effective vaccine	effective vaccine	no vaccine	vaccination against HBV	vaccination in China
Morbidity / Mortality (WHO)	7134 deaths (2016)	296 million / 820,000 (2019)	58 million / 290,000 (2019)	5% of people who have a chronic HBV infection	44,000 deaths (2015)

1.2. Hepatitis C

Hepatitis C is an inflammation of the liver as a result of hepatitis C virus infection. HCV causes both acute and, more often, chronic hepatitis, which varies from mild illnesses to severe and life-threatening conditions such as liver cirrhosis and hepatocellular carcinoma (primary liver cancer). Infection by HCV occurs primarily through contaminated blood exposure from inappropriate injection practices, untested blood transfusions, sexual engagement and, especially in high-prevalence countries, mother-to-child transmission. Approximately 58 million people worldwide have chronic hepatitis C, and 1.5 million new cases are reported annually. According to WHO, about 290,000 people died in 2019 due to liver failure caused by HCV infection. It is well established that direct-acting antivirals can cure more than 95% of infected patients suffering from hepatitis C, yet diagnosis and treatment are far from being universally available. Unfortunately, at the moment no vaccine that is effective against hepatitis C [1].

1.3. Molecular biology of HCV

1.3.1. Structure of the HCV particle (virion)

HCV is an enveloped virus harboring a single-strand RNA genome. The particle production of HCV is tightly regulated in association with the host cellular lipoproteins and lipids, resulting in its heterogeneous morphologies and biophysical characteristics depending on the host cells in which the virus is generated. In particular, HCV particles isolated from hepatitis C patients (lipoviroparticle) and *in vitro* cultured cells (HCVcc) differ in the level of 'imprinting' of cellular lipid components affecting density and specific infectivity of the produced particles [2]. HCV particles grown in cell culture (HCVcc) studied by cryo-electron tomography show spherical shapes with spike-like projections. Their diameters range from 40-100nm. The morphologies of HCV particles are briefly described in Figure 1.
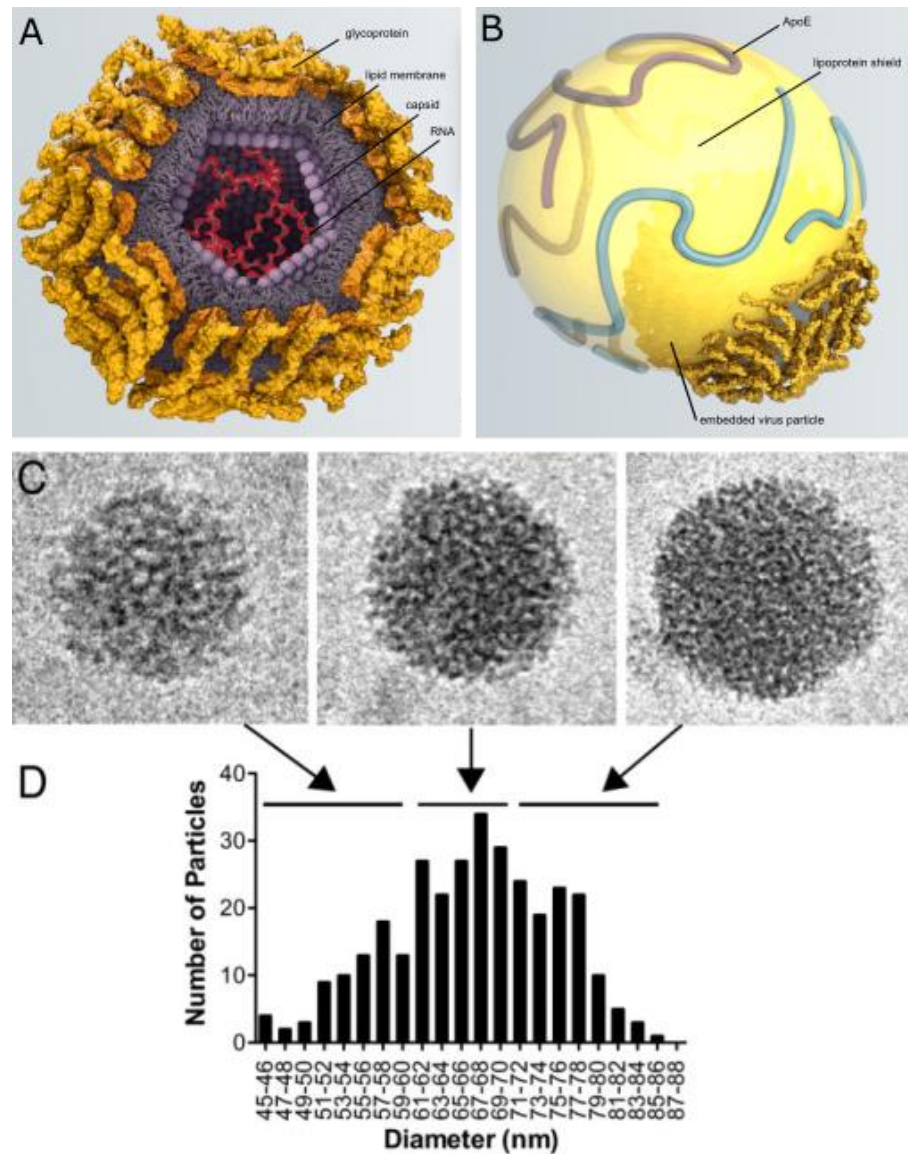
Figure 1. Structure of the HCV particle

(A) A cross-section of the model of HCV particle. (Adapted from [3]).
(B) Association of HCV particle with lipoprotein. (Adapted from [3]).
(C) and (D) Morphology of purified cell-culture grown HCV particles with different sizes (Adapted from [4]).

1.3.2. HCV genome organization

HCV belongs to the genus Hepacivirus of the family *Flaviviridae* [5]. The virus genome contains a positive-sense RNA harboring a single long ORF flanked by highly structured non-translated regions (NTRs), which are required for RNA replication (Figure 2). RNA genome translation is directed by a type III internal ribosome entry site (IRES) in the 5′ NTR

that does not require the capping of the viral RNA. The ORF encodes a ~3000 amino-acid otein, which is subsequently cleaved into 10 distinct proteins, all of which are associated with intracellular membranes. The 5 first proteins of the amino-terminal part of the ORF function as the "assembly module" that modulates HCV particle formation. HCV structural protein Core (C), envelope E1, E2 constitute the capsid and envelope of the virus whereas p7 and NS2 assist the virion assembly while not being packaged into the virion [2]. The remaining proteins NS3-NS5B are sufficient for viral RNA replication [6], which is grouped to the "replication module" (Figure 2).
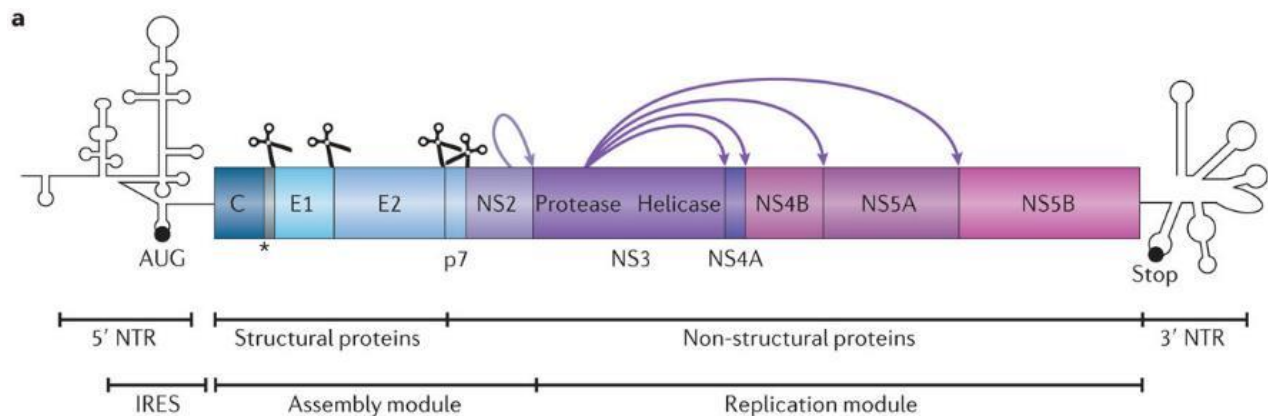
Figure 2. HCV genome organization

HCV RNA (~9,600 nucleotide bases in length) is flanked by the 5′ and 3′ non-translated regions (NTRs) which are highly structured with stem loops. The start (AUG) and stop codon positions for the initiation and termination of the polyprotein translation are indicated. The internal ribosome entry site (IRES) within the 5′ NTRs regulates HCV translation. Overall, HCV-coding region is subdivided into two groups: "assembly module" and "replication module". The former includes structural proteins C, E1, E2, p7 and a non-structural protein NS2. The remaining portion of the genome encodes for the nonstructural proteins NS3-NS5B contributing to the replication module. (Adapted from [7]).

The HCV polyprotein cleavage products with membrane topologies and major functions are briefly summarized in Figure 3.
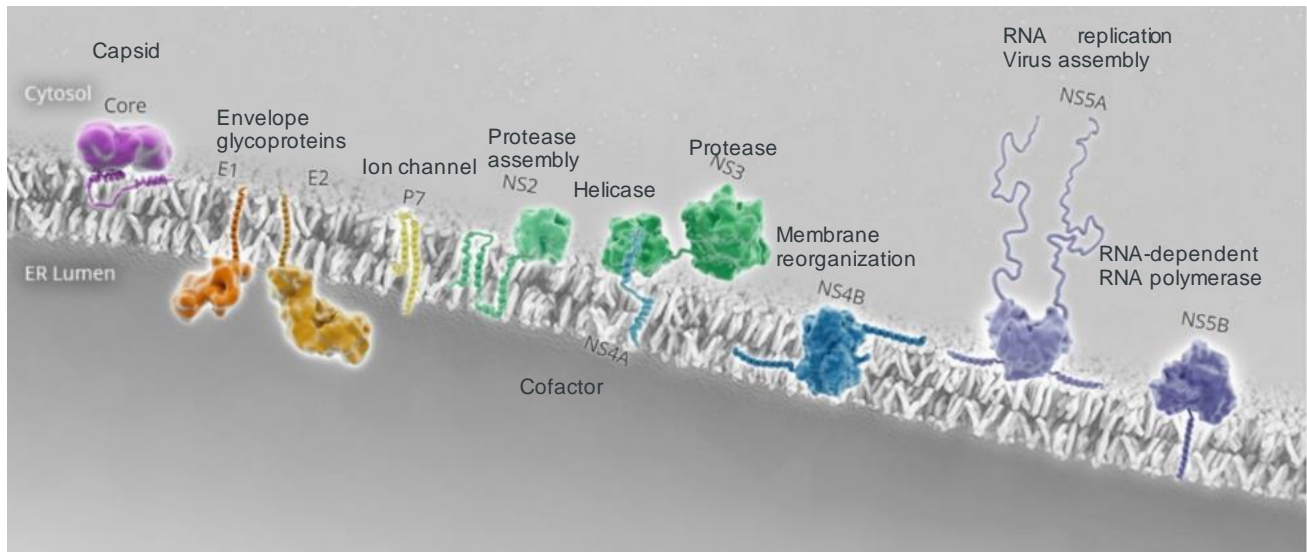
Figure 3. The association of HCV proteins with the ER and their major function

HCV proteins after translation are tethered to the ER or other intracellular membranes. The membrane interplay is mediated by amphipathic α-helices (core, NS3, NS5A), transmembrane domains (E1, E2, p7, NS2, NS4A, NS4B, and NS5B). Note that NS3 membrane attachment is also mediated by its cofactor NS4A and NS5A is exhibited as a homodimer. The main function of each protein is shown next to the depicted proteins. (Adapted from [3, 7]).

1.3.3. The life cycle of HCV
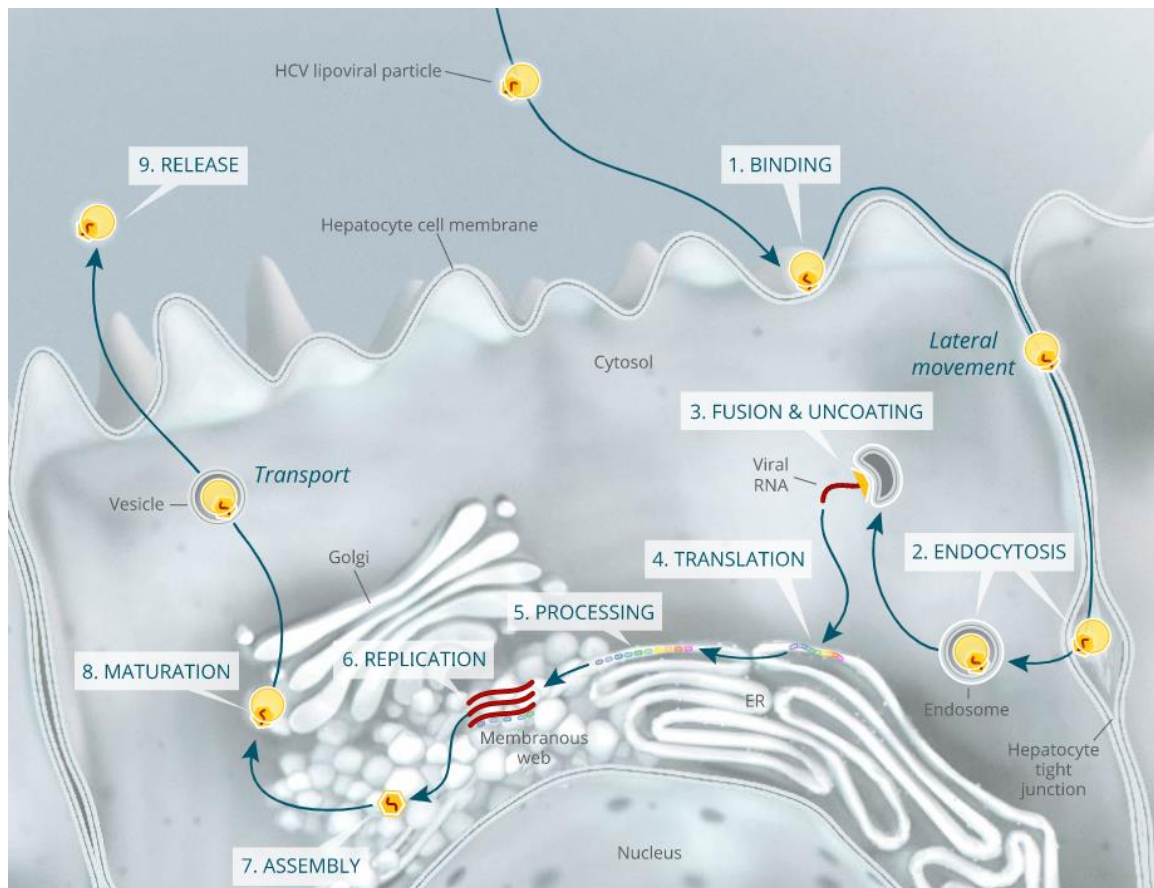
Figure 4. Summary of the HCV life cycle

HCV enters the hepatocytes by 1) binding to cell surface receptors and 2) endocytosis. The virus particle is then 3) uncoated by virus-endosome membrane fusion to release its genome. This genome is further 4) translated and 5) processed at the ER membrane and the RNA replication machinery is formed (5). The newly synthesized genome is subsequently 7) assembled into a new virus particle which further undergoes a 8) maturation step to 9) release extracellularly. (Adapted from [3]).

Step 1: Binding

HCV lipoviroparticle begins its life cycle when it binds to host ApoE-specific receptors on the surface of a hepatocyte: the low density lipoprotein receptor (LDLR) and the heparin sulfate proteoglycans (HSPGs). Following this initial interaction, the HCV E1-E2 glycoprotein heterodimers of the particle are promoted to interact with the scavenger receptor B1 (SR-B1) and

the tetraspanin protein CD81, inducing a wave in the host lipid membrane. As a result, this wave further propels the HCV particle to a tight junction connecting two hepatocytes [8-11].

Step 2: Endocytosis

Upon reaching the tight junction, CD81 binds to claudin-1 (CLDN1), causing inward folding of the viral particle and associated cell membrane into a clathrin-coated pit. The host cell membrane coats the virus particle within an endosome, which is enclosed in a clathrin cage [11-13].

Step 3: Fusion and uncoating

After the dispersal of the clathrin cage, by which the endosome is released into the cytosol, the low pH-driven endosomal fusion between the viral envelope and the host membrane occurs. It is thought that the HCV nucleocapsid is released into the cytoplasm for subsequent uncoating, perhaps triggered by ribosome binding to the RNA to initiate RNA translation [11][14, 15].

Step 4: RNA Translation

HCV RNA translation is directed by the internal ribosome entry site (IRES) within the 5' NTR which has a strong affinity with ribosomal 40S subunit. A mixed variety of the host canonical translation initiation factors (eIFs) including eIF3, eIF2, eIF1A, eIF5, and eIF5B are involved in HCV RNA translation. In addition, a part of the HCV core protein sequence, the HCV 3´NTR and the host microRNA-122 (miR-122) are also important for the regulation of this process. A polyprotein of approximately 3,000 amino acids is created as a result of translation [16].

Step 5: Proteolytic processing

The polyprotein is proteolytically processed by a combination of cellular and viral enzymes within the endoplasmic reticulum to yield 10 different mature proteins (Figure 5). The host signal peptide peptidase and signal peptidase cleave the N-terminal polyprotein to create the core, E1, E2 and p7. The NS2/NS3 junction is cleaved by a cysteine-autoprotease

encoded within NS2 and the N-terminus of NS3. Last, NS3 protease domain and its cofactor NS4A form the heterodimeric complex, which processes the remaining downstream polyprotein to yield NS3, NS4A, NS4B, NS5A and NS5B [17-19].
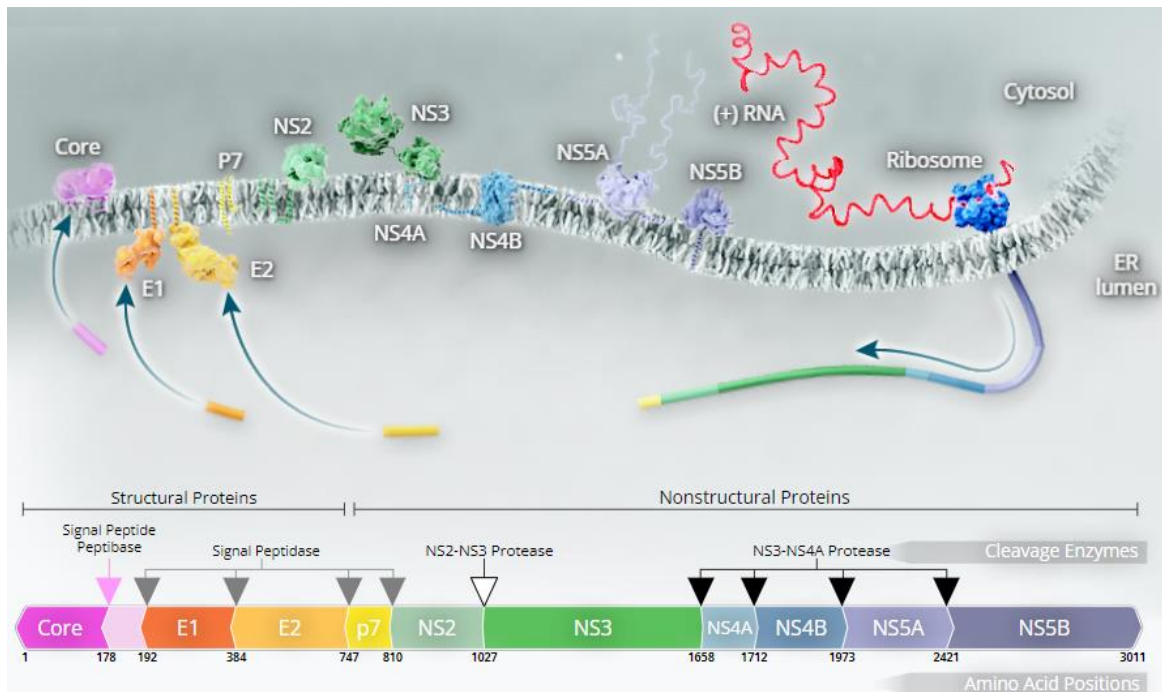
Figure 5. Proteolytic processing of HCV polyprotein

HCV polyprotein is cleaved by both cellular and viral proteases (bottom schematic). Signal peptidase cleaves at core-E1, E1-E2, and E2-p7 junctions. Signal peptide peptidase cleaves immature core for at aa178 for core maturation. NS2-NS3 auto-protease cleaves NS2 and NS3. NS3-NS4A cleaves at NS3-NS4A, NS4A-NS4B, NS4B-NS5B, and NS5A-NS5B junction. The 10 mature protein products in association with the ER membrane is shown on the top. (Adapted from [3]).

Step 6: RNA replication

Among 10 mature HCV proteins, HCV nonstructural proteins NS3-NS5B are sufficient for building up the HCV RNA replication sites. These viral proteins, in conjunction with cellular factors, induce the membrane rearrangement of the infected cell to form the "membranous web" comprised of many double-/multi-membrane vesicles. In these sites, the viral RNA is used as the template for the synthesis of a negative-sense RNA intermediate, which is later used to generate

multiple copies of progeny positive-sense genome. The newly synthesized RNA is either transported to the nearby assembly site (Figure 6) for the packaging of the new virus particles or used for a next translation/replication cycle [20-24].

Step 7: Virion assembly

HCV possibly coordinates HCV RNA replication and virion assembly by coupling these two processes in juxtaposition. The newly formed particle is believed to bud into the lumen of the ER, which wraps around a lipid droplet and contains many putative replication organelles, possibly DMVs [21] (Figure 6). A newly synthesized RNA from the replication site is transported to the assembly site, packaged in the core protein multimer-nucleocapsid and enveloped with the membrane containing E1, E2 glycoproteins. Later, the nascent luminal HCV particle fuses with a luminal lipid droplet to form a high-density particle that further enters the maturation process. Spatiotemporal control of HCV assembly requires multiple viral factors including HCV core, p7, NS2, E1, E2, and NS5A, as well as cellular components such as diacylglycerol acetyltransferase-1 (DGAT1) and microsomal triglyceride transfer protein (MTTP) [2, 21, 25-28].

Although the past years have seen substantial growth into the insights of HCV assembly events, neither the assembly of intracellular HCV particles nor topologically convincing HCV budding events have been visualized. In fact, all understanding about this step of the HCV life cycle is based on indirect evidence. This might be due to the pleiomorphic nature of the virus particles, the scarcity of the assembly events that preclude monitoring virus formation in real-time, and the ultrastructural deformation of the virus particles during the sample preparation process for TEM. Moreover, HCV particles have no unique protein markers in HCV-replicating cells that could be topologically assigned to them. Finally, attempts to enrich intracellular viral particles by using brefeldin A treatment and highly assembly-competent HCV, as well as to label HCV with immuno-EM failed [21].
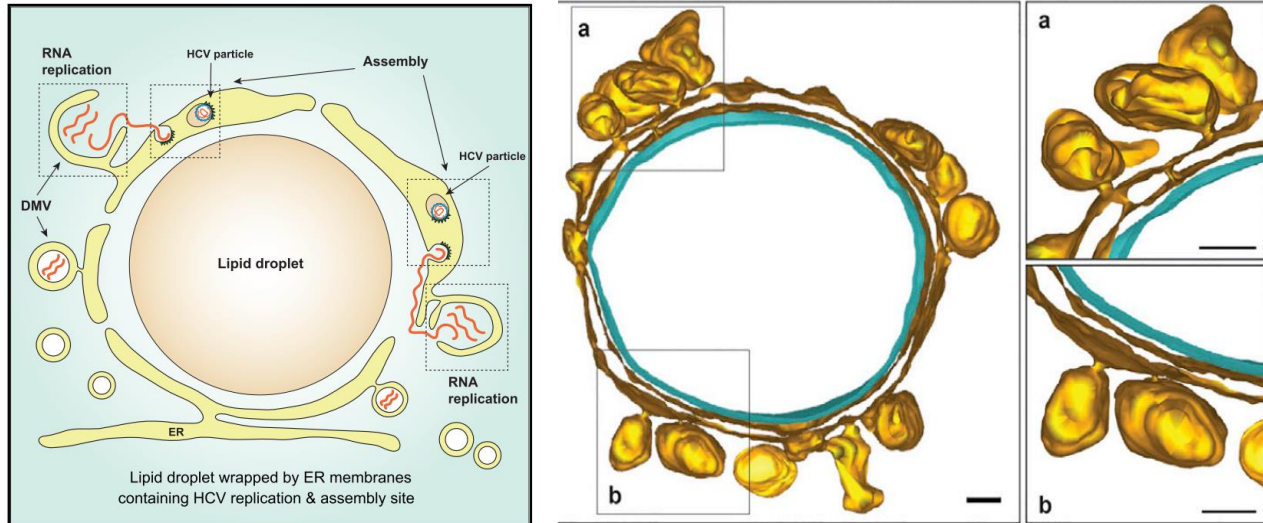
Figure 6. Cellular landscape of HCV RNA replication and putative assembly sites

HCV RNA replication is suggested to be tightly regulated with virus particle assembly. Study by Lee *et a*l., 2019 showed that HCV infection resulted in the DMV-connected ER that wrapped around a lipid droplet containing assembly platforms. The immediate vicinity of the assembly sites to the RNA replication factories favor the RNA encapsidation of newly synthesized RNA. (Adapted from [21]).

Step 8: Maturation

HCV particles are transported from the ER in COPII vesicles to the Golgi apparatus. In this compartment, the high-density viral particle is believed to fuse with a very low density lipoprotein (VLDL) to generate the lipoviroparticle. Of note, apolipoprotein E (ApoE) is critically involved in the maturation of HCV particles. These low-density particles further exit the trans-Golgi network and enter another organelle, namely multivesicular body (late endosome) by the endosomal-sorting complex required for transport (ESCRT) proteins [28-30].

Step 9: Release

Upon trafficking of the multivesicular bodies containing HCV lipoviroparticles to the cell surface, they fuse with the plasma membrane and release HCV particles to the extracellular compartments. It is believed that the secretion of HCV is coupled to the V(LDL) secretion pathway [28-30].

2. HCV NS5A protein structure and function

NS5A is an essential component of the viral RNA replication-coupled assembly platform of HCV. During the course of HCV infection, NS5A-containing "replication module" of HCV induces drastic changes in E2 distribution, forming NS5A-E2 positive foci, the hallmark of HCV assembly. Moreover, NS5A might also be a part of HCV-produced extracellular vesicles, specifically exosomes, making it a major candidate for my Ph.D. research project.

2.1. Structure

HCV NS5A is a membrane-associated RNA and zinc-binding phosphoprotein containing 448 amino acids. The overall structure of NS5A in relation to the associated membrane is described in Figure 7. It is composed of a N-terminal amphipathic helix (AH), a structural domain (D1), two intrinsically disordered domains (D2 and D3), and two interspersed low complexity sequences (LCS1 and LCS2). The AH anchors NS5A to the surface of intracellular membranes, including the cytoplasmic side of the endoplasmic reticulum membrane [31, 32]. There are multiple phospho-variants of NS5A, designated p56 and p58. Basal unphosphorylated NS5A (p56) shows variability of intrinsic conformations in different HCV genotypes. Furthermore, phosphorylation confers more conformers to NS5A structure (p58) without changing the disordered nature of D2 and D3 domains [33].
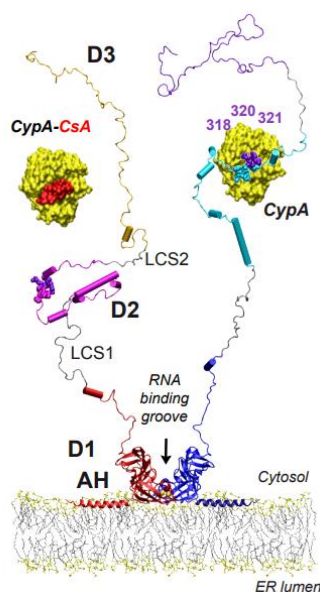
Figure 7. HCV NS5A structure model

"The structures and the membrane bilayer are shown at the same scale. NS5A domain 1 dimer (PDB entry 1ZH1 [34], subunits colored in red and blue) and the N-terminal amphipathic α-helix in-plane membrane anchor (PDB entry 1R7E [32], helices colored in red and blue) are shown in relative position to a phospholipid. The low-complexity sequences (LCS, [35]) connecting D1 to D2 (LCS1) and D2 to D3 (LCS2) are colored in grey. A surface representation of cyclophilin A (CYPA) in complex with cyclosporin A (CsA) is shown on the upper left (PDB accession 1CWA). A putative structure for CYPA and its main binding site in NS5A D2 is shown on the upper right". (Adapted from [33]).

2.2. **Function**

NS5A is an integral part of the HCV RNA replication complex and particle assembly mediator. It is post-translationally modified by host kinases including casein kinases [36-38] and Polo-like kinase 1 [39] to generate multiple phospho-variants, contributing to its various functions. It coordinates HCV RNA replication and assembly via the interaction with viral RNA, other viral and host replication-specific factors (e.g HCV NS4B, HCV NS5A, CypA, PI4KIIIα …), and assembly-specific factors (e.g. ApoE, HCV core…). The functions of NS5A domains are briefly summarized in Table 2.

Table 2. Function of NS5A domains

Domains	Functions	Reference
Amphipathic α-helix	anchors NS5A to membrane	[31, 32]
Domain I	interacts with ApoE and regulates HCV assembly	[40-42]
	regulates DMVs formation	[43]
	forms dimers, interacts with viral RNA and coordinates RNA replication	[34]
	interacts with phosphatidylinositol-4 kinase III alpha (PI4KIIIα) and regulates RNA replication	[44]
	is the target of the highly potent inhibitor Daclatasvir	[45]
Domain II	interacts with CypA and regulates RNA replication	[33]
	is the target of the cyclophilin inhibitors	[46]
Domain III	targets NS5A and core to cytosolic lipid droples and regulates HCV assembly	[47]
	interacts with core to facilitate HCV assembly	[26]

In addition to its roles in the regulation of the HCV life cycle, NS5A is the key driving force of HCV-mediated cell signaling pathways, virus response to interferon, virus persistence, and HCV-induced pathogenesis [48-50].

3. NS5A-ApoE interaction is important for HCV assembly

3.1. What is lipoprotein?

Because lipids are not soluble in water, they are transported in extracellular fluids such as blood plasma by means of transport vehicles, referred to as lipoproteins. A lipoprotein is a water-soluble assembly of macromolecules comprising lipids (triglycerides, cholesteryl esters) that are surrounded by a hydrophilic phospholipid external shell. The shell is often decorated with specific proteins, called apolipoproteins (ApoB, ApoE…) which stabilize the bound lipoprotein and determine the functional identity of their roles [51]. Lipoproteins are separated into numerous classes according to their density, size, electrophoretic mobility, or affinity chromatography. Human plasma lipoproteins are categorized into 6 major classes including: high density lipoprotein (HDL), low density lipoprotein (LDL), intermediate density lipoprotein (IDL), very low density lipoprotein (VLDL), chylomicron and chylomicron remnant. The lipoprotein composition exemplified by a very low density lipoprotein (VLDL) and a low density lipoprotein (LDL) is depicted in Figure 8.
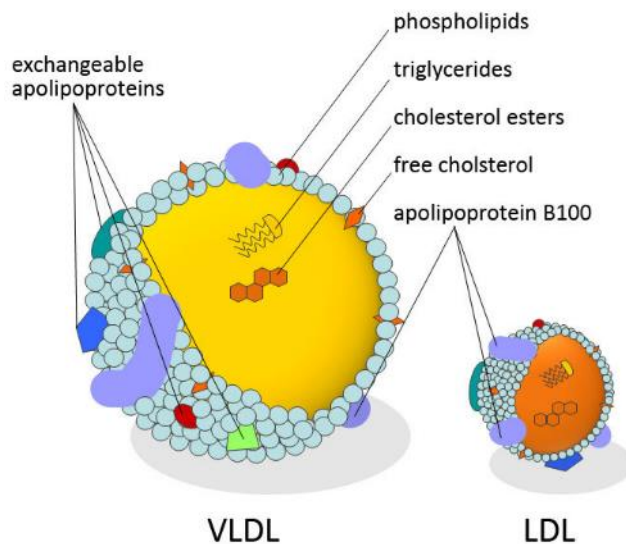
Figure 8. Composition of lipoproteins

Lipoprotein is constituted by a shell of phospholipid monolayer encapsulating neutral lipids including triglycerides and cholesteryl esters in its core. Apolipoproteins located on the shell (ApoE, ApoB, ApoA…) stabilize the assembly of lipoprotein structure and determine the binding of lipoproteins with their counterparts. VLDL (left): very low density lipoprotein; LDL (right): low density lipoprotein. (Adapted from [52]).

3.2. Apolipoprotein E

Apolipoprotein E is a constituent of the outer coat of lipoproteins. ApoE is primarily synthesized in the liver. In addition, macrophages have been shown to produce this protein in large quantities. Peripheral tissues including the brain, adrenal, spleen, ovary, kidney, and muscle account for about 10 to 20% of the circulating ApoE [51].

3.2.1. Structure

ApoE exhibits a complex isoform pattern because of the presence of three genetically determined alleles at a single locus and the post-translational sialylation of the produced protein [53, 54]. The nascent protein contains an 18 amino acid signal peptide that is cleaved during the translation process [55]. ApoE as well as other apolipoproteins has a high degree of ordered structure, and changes configuration upon binding to lipids. The structure of lipid-free and lipid-bound ApoE isoform 3 is described in Figure 9.
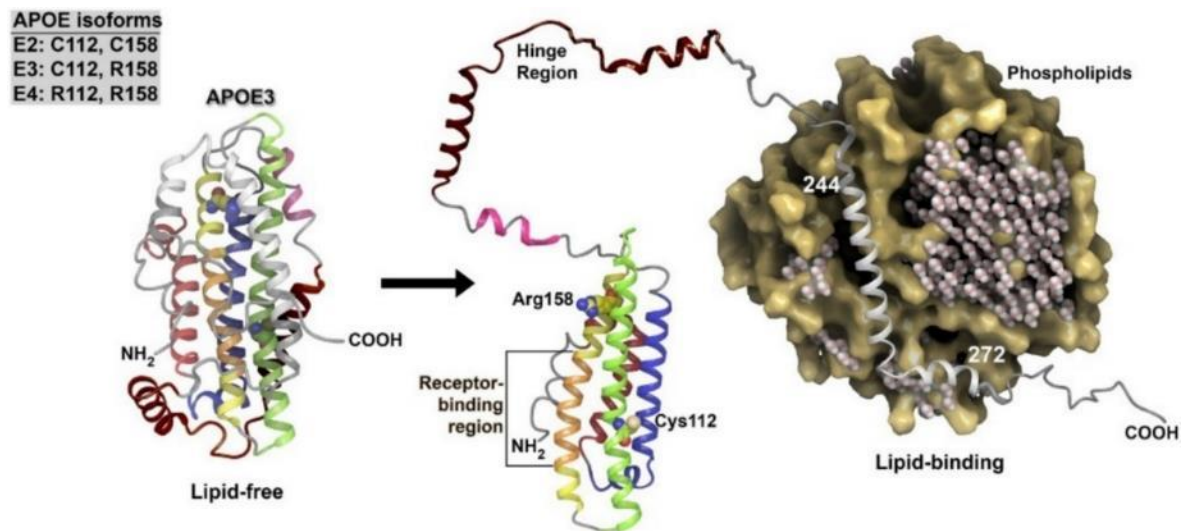
Figure 9. Putative structures of ApoE with and without lipid interaction

The structure of lipid-free and lipid-bound ApoE3 isoform is shown on the left and right, respectively. ApoE protein comprises multiple helices: a N-terminal 4-helix bundle (1: red, 2: blue, 3: green, 4: yellow and orange), hinge helices (pink and brown), and C-terminal helices (gray). The receptor binding region is in the N-terminal helix 4 (orange) and the critical lipid binding region is in the C terminus (residue 244-272). Upon lipid binding, ApoE undergoes a conformational change, releasing the lipid-binding and the hinge regions, and exposing the receptor binding region. (Adapted from [56]).

3.2.2. Universal function of ApoE under physiological conditions

Among all apolipoproteins, ApoE is the most extensively studied and appears to have various important functions. Structurally, like ApoB and other lipoproteins, it stabilizes the micellar structure of the lipoproteins and, in association with the phospholipids, confers the hydrophilic property of the micellar surface. ApoE-containing plasma lipoproteins transport lipids among cells of different organs, most notably, the liver and the brain, and within specific tissues. The function of ApoE relies on its affinity to ApoE-specific receptors expressed on the cell surface, leading to the receptor-mediated uptake of ApoE-containing lipoproteins [51, 57]. Low-density lipoprotein receptors (LDLRs) and lipoprotein receptor-related protein 1 (LRP1) are examples of ApoE-specific receptors. Therefore, ApoE is essential for the plasma clearance of the ApoE-containing lipoproteins. Abnormal function of ApoE was found in patients with type III hyperlipoproteinemia which is a disorder with high levels of triglycerides and cholesterol in the blood [58, 59]. In addition, ApoE also mediates the reverse cholesterol transport, called cholesterol efflux, in the autocrine and paracrine manner [60-62]. At least 18 distinct diseases including Alzheimer's and cardiovascular diseases are found in strong association with APOE genotypes [63].

3.2.3. Functional importance of NS5A-ApoE interaction in HCV assembly

The transmission of HCV is tightly linked to the host cellular lipids in which ApoE plays multiple roles in the HCV life cycle [64-67]. Of note, a long-standing conundrum in HCV biology is the tight association between ApoE and HCV NS5A, originally identified by yeast-two-hybrid screening by Evans *et al.*, 2004 [68]. Subsequent studies by other groups suggested the critical function of NS5A-ApoE interaction in HCV assembly [41, 42]. Nevertheless, it is not understandable of where and how ApoE and NS5A colocalize and interact in HCV-infected cells since ER lumen-residing ApoE [69] is unlikely interact with cytoplasm-facing ER-residing NS5A [31].

4. Extracellular vesicles as an alternative way of HCV transmission

4.1. What are extracellular vesicles?

EVs are cell-released membrane-encapsulated particles exploited by both host cells and viruses to transmit signaling molecules including DNAs, RNAs, proteins, lipids and metabolites [70-76]. They were originally thought as a selective means used by cells to get rid of unwanted cellular components. Although the term EV is currently used to describe all the secreted membrane vesicles, they are actually heterogeneous in their properties and functions. Transmission and immunoelectron microscopy, as well as biochemical methods, have provided insights into the biogenesis of secreted vesicles, leading to the classification of EVs into 2 main categories: exosomes and microvesicles [75]. The latter are formed by outward budding and fission of the plasma membrane, and are released into the extracellular space [77].

4.2. Exosome biogenesis

Exosome is a subclass of EV that plays significant roles in cell-cell communication. The constituents of exosomes are membrane-bound proteins including members of the tetraspanin family (CD63, CD81, CD9…), ESCRT proteins (TSG101, Alix…), cell adhesion molecules (integrin, lactadherin…), as well as luminal components such as heat shock proteins (HSP90, HSP70…) and nucleic acids (DNA, mRNA, miRNA…). Cell type-specific proteins (HSPG, MHC, CXCR4…) and lipids (cholesterol, ceramides, sphingomyelin…) are also detected in exosomes [78]. The biogenesis of exosomes occurs within the endosomal system which requires the sorting, internalization, and subsequent loading of exosome components into the intraluminal vesicles (IVs) of these endosomes. The endosomes containing IVs later fuse with the plasma membrane to release IVs as exosomes (Figure 10).
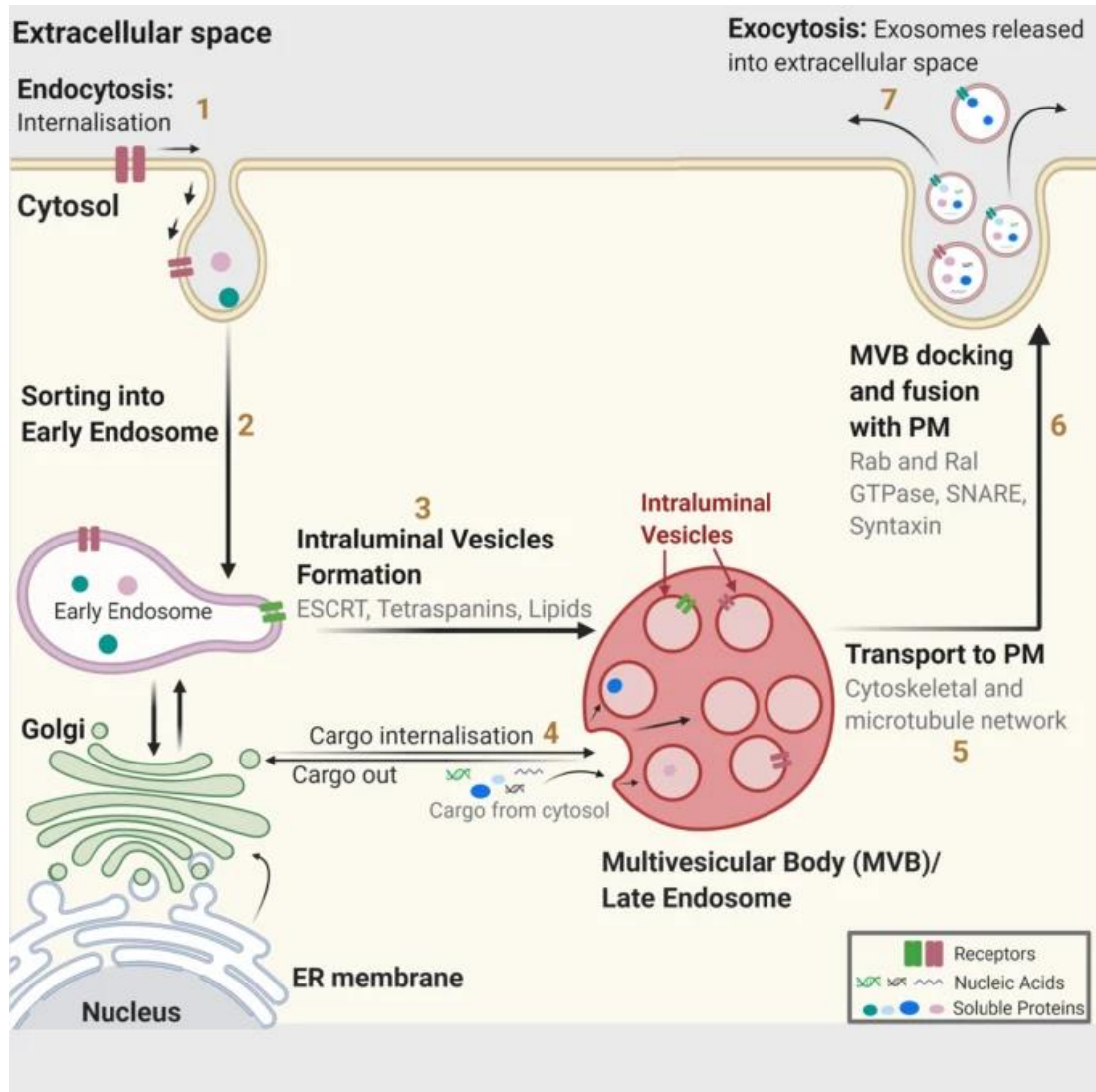
Figure 10. The biogenesis of exosome

Exosome is formed within the cellular endosomal system. Constituents that are derived from the extracellular space 1) internalized or from the Golgi are 2) loaded into the lumen of the early endosomes. Early endosomes undergo maturation forming late endosomes which involves the intraluminal vesicle (IV) formation step 3) or 4) loading of cargo from either the cytosol or the Golgi vesicles. Late endosomes are subsequently 5) transported to the plasma membrane (PM) in a microtubule-dependent manner and are 7) docked on the PM. Endosome-PM fusion triggered the release of IVs into the extracellular space as exosomes. (Adapted from [78]).

4.3. EV-mediated cell-to-cell communication under physiological conditions

In addition to the direct cell-cell contact, cells can communicate from a distance through secreted factors such as cytokines, hormone, and EVs. EVs secreted by the donor cells can enter

target cells through different mechanisms, leading to changes in the behaviors and characteristics of the target cells. The pleiotropic functions induced by EVs are briefly described in Figure 11.
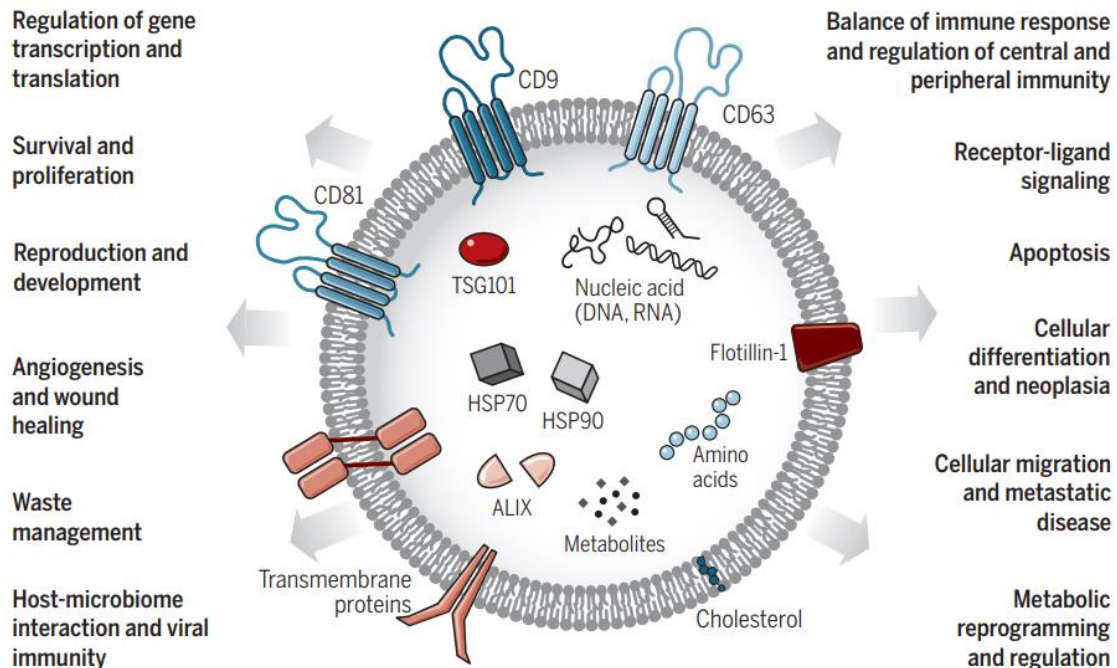
Figure 11. Structure of an exosome and possible roles in intercellular communication

Exosomes transmit various types of signaling molecules such as nucleic acids, proteins, lipids…resulting in changes of various signaling of the target cells including receptor-ligand signaling, apoptosis, cell differentiation, cell migration and metastasis…(Adapted from [76]).

4.4. EV-mediated cell-to-cell communication under pathological conditions

Fungi, protozoa, and bacteria might produce certain types of EVs that spread the infection and evade the host immunity [79]. For intracellular pathogens such as viruses, even more complex functions can be attributed to EVs, as the viral biogenesis pathway may overlap with EV pathways in many ways, producing a mixed variety of EVs (Figure 12) [70, 71, 80]. The molecular signature of EVs produced by virus-infected cells might share many similar features or differ significantly from healthy cells. In addition to the production of the classical complete virus particles, virus infection can lead to the generation of vesicles containing infective viral genomes,

virus-like particles with quasi-envelopes, and non-infectious vesicles containing viral components…that are secreted into the extracellular space. These EVs can have different effects on recipient cells. On the one hand, aside from directly infecting cells, they can also prime neighboring cells to become more vulnerable to infection, counteract antiviral pathways, and trigger virus-induced pathogenesis. For example, the human immunodeficiency virus (HIV) infection produces transactivation response (TAR) element RNA-bearing exosomes promoting tumor growth and cancer progression [81]. In contrast, these EVs could serve as the anti-viral mechanism employed by the host cells to combat infection by providing the neighboring cells with cytokines and antiviral-signaling molecules. However, in certain cases, this protective mechanism can result in traumatized clinical consequences due to the massive inflammation triggered by the EVs. For instance, exosomes isolated from COVID-19 patients contain severe acute respiratory syndrome coronavirus type 2 (SARS-CoV2) RNA as well as various components of the host inflammation, coagulation, immune response and the complement signaling [82]. The anti-or pro-viral effects sometimes can be seen in infections by the same viruses and vary vastly from different viral infections [71].
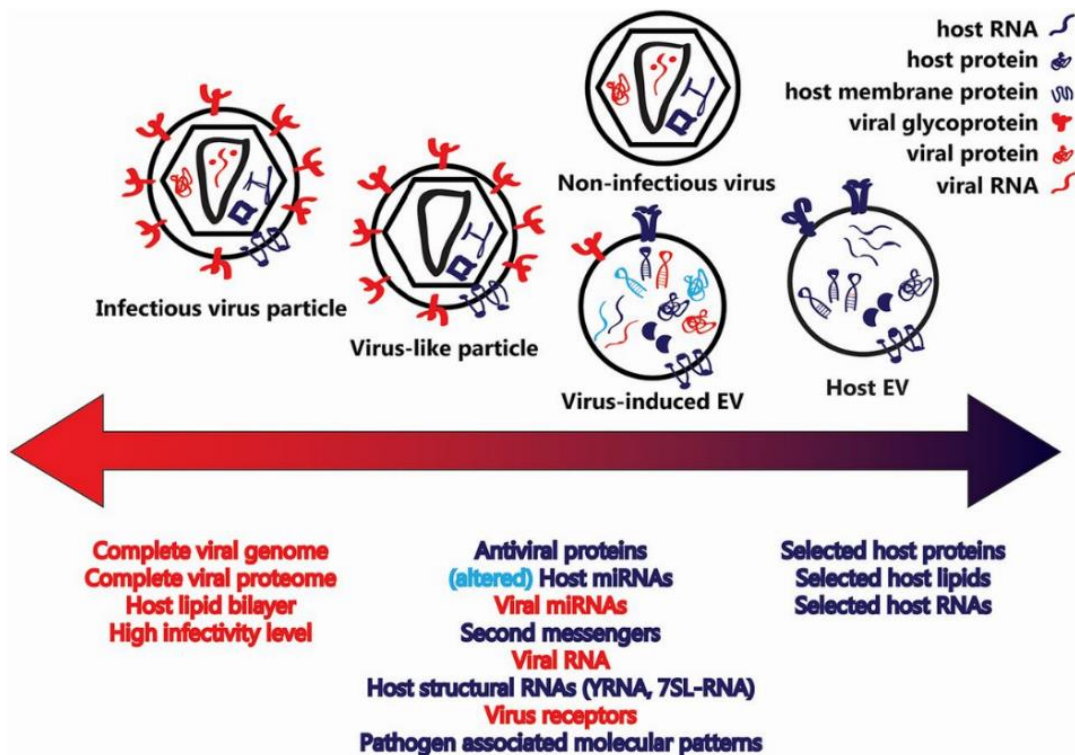
Figure 12. Structural parallelism between EVs and classical virus particles

In addition to the fully infectious virus particle production, infected cells release a mixed variety of EVs that might carry both host (deep blue color, right extreme) and virus-specific factors (red color, left extreme, mostly viral glycoproteins, viral proteins, and viral nucleic acids), or modified factors derived from the host or virus (light blue, middle). The complexity of EV species challenge researchers who really want to elucidate the function of each respective type of vesicle. (Adapted from [70]).

4.5. NS5A might be a component of HCV-induced extracellular vesicles that facilitates HCV RNA transmission

HCV RNA transmission is mediated by both virion-dependent and EV-mediated routes. Virion-independent transmission of HCV RNA via CD63-positive EVs has been reported by several research groups [83-86]. Although EV-mediated HCV RNA transmission seems to be relatively inefficient in the context of the subgenomic replicon, this model helps to exclude the virion-dependent process. Using this model, people also found that NS5A was readily secreted and detected in purified EV preparation [87, 88], indicating that HCV infection produced NS5A-positive EVs.

4.6. Possible interaction between extracellular vesicles and lipoproteins

Accumulating evidence has indirectly suggested the interaction between lipoproteins and EVs. First, various procedures of EV isolation and purification including size and density fractionation as well as CD63-positive selection did not give rise to lipoprotein-free EV preparations [89, 90]. Second, in vitro attachment of lipoproteins to purified EVs has also been reported, potentially affecting the lipid composition of the attached EVs [91, 92]. Third, pigment cell-derived ApoE associates with IVs/EVs and plays a role in the sorting of an interacting partner to IVs [93].

5. Objectives of the doctoral research project

The initial objective of my research project was to faithfully identify HCV assembly sites and to study formation of infectious virus particles. Lee *et al.*, 2019 [21] suggested that HCV possibly coordinates viral RNA replication and particle assembly at the DMV-connected ER, which wraps around lipid droplets and is enriched for NS5A and E2. Given the role of ApoE in HCV assembly, I included this host cell protein as an additional marker for HCV assembly sites and aimed to establish a multi-color live-cell imaging system in order to examine the formation of HCV particles. My plan was to establish an intact and fully functional FP-tagged ApoE along with engineered HCV genomes encoding FP-tagged NS5A and E2. Given the difficulties of unambiguously detecting assembling HCV particles, I shifted the focus of my project. Taking advantage of the observation I made in the course of these studies that ApoE accumulates in late endosomes and extensively associates with NS5A, I investigated the role of this association in viral processes that are not linked to HCV particle assembly. Taking into account that ApoE associates with lipoproteins and HCV-replicating cells release EVs, I studied the association and genuine cell-to-cell transmission of hepatic ApoE-containing lipoproteins and EVs using HCV-produced NS5A-containing EVs. Depending on obtained results, I wanted to expand these studies to non-infected hepatocytes in order to decipher EV production and intercellular transmission in dependency on ApoE.

The following parts of this thesis incorporate certain adapted parts from a manuscript that I have written by myself and that is in review with a cell biology journal.

II. MATERIALS and METHODS

1. Materials

The text from the following parts: "cell lines, plasmids, antibodies, key reagents, RT-qPCR probes and primers" has been adapted from the manuscript in preparation originally written by myself.

1.1. Cell lines

In this work, I used various cell lines that were previously produced and multiple cell lines that had been generated by myself (Table 3).

Table 3. Cell lines used in this study

Number	Cell lines	Reference	Identifier
1	HEK293T	[94]	RRID:CVCL_0063
2	HEK293T-miR122	[95]	N/A
3	HEK293T-miR122/empty_vector	This study	N/A
4	HEK293T-miR122/ApoE^{wt}	This study	N/A
5	HEK293T-miR122/ApoE^{mT2}	This study	N/A
6	Huh7.5	[96]	RRID:CVCL_7927
7	Hela Kyoto	N/A	N/A
8	Huh7-Lunet/CD81H (Lunet)	[14]	N/A
9	Huh7-Lunet/CD81H/ApoE-KD (Lunet/ApoE-KD)	[64]	N/A
10	Huh7-Lunet/CD81H/ApoE-KD/ApoE^{mT2} (Lunet-ApoE^{mT2})	This study	N/A
11	Huh7-LunetCD81H/ApoE-KD/ApoE^{SNAPf} (Lunet-ApoE^{SNAPf})	This study	N/A
12	Lunet-ApoE^{mT2}/Core-NS2/E2^{eYFP}	This study	N/A
13	Lunet-ApoE^{mT2}/Core-p7/E2^{eYFP}	This study	N/A
14	Lunet-ApoE^{mT2}/CD63^{mCherry} (HCV negative donor)	This study	N/A
15	Lunet-ApoE^{mT2}/CD63^{mCherry}/sgNeo-JFH1 (sgHCV donor)	This study	N/A
16	Huh7-LunetCD81H/$^{eYFP-CaaX}$ (recipient)	This study	N/A

Remarks of selected cell lines with the most important features:

- Cell line #5: mTurquoise2-tagged ApoE expressing HEK293T-miR122 cells. These cells are permissive to HCV replication and virion production.

- Cell line #10: mTurquoised2-tagged ApoE expressing Lunet cells. These cells are permissive to HCV RNA replication and production, and are well suitable for live-cell imaging and CLEM experiment.

- Cell line #11: SNAPf-tagged ApoE expressing Lunet cells. This cell line is used for the study of ApoE by super-resolution imaging including STED.

- Cell line #12: Lunet cells expressing HCV "assembly module" with eYFP-tagged E2. This cell line can be used for the production of HCV trans-complementation particles (TCP) by transfecting the "replication module" RNA (NS3-NS5B).

- Cell line #13: Lunet cells expressing HCV "assembly module" with eYFP-tagged E2 but lacking NS2. This cell line does not support HCV TCP production upon "replication module" RNA transfection.

- Cell line #14: Lunet cells expressing mTurquoise2-tagged ApoE and mCherry-tagged CD63. This cell line can be used for the study of lipoprotein-IV/EV association.

- Cell line #15: Lunet cells harboring HCV JFH1 subgenomic replicon and expressing mTurquoise2-tagged ApoE and mCherry-tagged CD63. This cell line can be used for the study of lipoprotein-IV/EV association in the context of active HCV RNA replication.

- Cell line #16: Lunet cells containing eYFP-anchored plasma and intracellular membranes. CaaX is a farnesylation signal from human HRAS protein. This cell line is well suitable for live-cell imaging with the purpose of membrane visualization.

1.2. Plasmids

In this work, I generated numerous new plasmid constructs. Important DNA plasmids used in this study are listed in Table 4.

Table 4. Plasmids used in this study

Number	Plasmids	Reference
1	pWPI-ApoE3	[65]
2	pWPI-ApoE3^{mTurquoise2}	This study
3	pWPI_ApoE^{SNAPf}	This study

4	pWPI-ApoE3^{mCherry}	This study
5	pWPI-ApoE3$^{mScarlet-C1}$	This study
6	pWPI-ApoE3$^{mScarlet-H}$	This study
7	pWPI-ApoE3^{mKate2}	This study
8	pWPI-ApoE3$^{Tag-RFP}$	This study
9	pWPI-ApoE3^{eYFP}	This study
10	pWPI-CD63^{mCherry}	This study
11	pWPI_eYFP-CaaX	This study
12	pFK_Jc1	[97]
13	pFK_JcR2a	[44]
14	pFK_I389neoNS3-3'_dg_JFH1_NS5A-aa2359_mCherry_NS3-K1402Q (sgNeo/JFH1/NS5A^{mcherry})	[98]
15	pFK_I389neoNs3-3'_dg_JFH1_NS5A-aa2359_CLIPf_NS3-K1402Q (sgNeo/JFH1/NS5A^{CLIPf})	This study
16	pFK_I389HygNS3-3'_dg_JFH1_NS3-K1402Q (sgHyg/JFH1)	This study
17	pFK_I389HygNS3-3'_dg_JFH1_NS5A-aa2359_APK99AAA_NS3-K1402Q (sgHyg/JFH1/NS5A^{APK99AAA})	This study
18	pFK_I389HygNS3-3'_dg_JFH1_NS5A-aa2359-NLuc-NS3-K1402Q (sgHyg/JFH1/NS5A^{NLuc})	This study
19	pCDNA3$^+$ NS5A-myc	This study
20	pCDNA3$^+$ NS5A-APK99AAA-myc	This study
21	pWPI-Core-NS2/E2^{eYFP}	This study
22	pWPI-Core-p7/E2^{eYFP}	This study
23	pWPI-CD63_M153R-pHluorin	This study

Remarks of selected DNA constructs with the most important features:

- Plasmid #2: A lentiviral construct encoding for mTurquoise2-tagged ApoE

- Plasmid #3: A lentiviral construct encoding for SNAPf-tagged ApoE.

- Plasmid #11: A lentiviral construct encoding for eYFP-tagged membrane anchor signal CaaX from human HRAS protein

- Plasmid #15: HCV JFH1 subgenomic replicon with the Neo-resistance gene and CLIPf-tagged NS5A. NS5A can be visualized by microscopy by the addition of cell-permeable dyes such as CLIP-ATTO590.

- Plasmid #16: HCV JFH1 subgenomic replicon with the Hyg-resistance gene. This replicon can be stably selected by culturing cells in Hygromycin B-containing medium.

- Plasmid #17: HCV JFH1 subgenomic replicon with the Neo-resistance gene and ApoE-binding defective NS5A.

- Plasmid #18: HCV JFH1 subgenomic replicon with the Hyg-resistance gene and Nanoluciferase-tagged NS5A. This construct is well suitable for the measurement of HCV RNA replication and a sensitive detection of NS5A secretion into the culture supernatant.

- Plasmid #19: A CMV promoter-based myc-tagged HCV NS5A expression construct. NS5A can be pulldown efficiently by myc-specific antibody.

- Plasmid #21: A lentiviral construct encoding the "assembly module" of HCV with eYFP-tagged NS5A.

- Plasmid #22: A lentiviral construct encoding the "assembly module" of HCV with eYFP-tagged NS5A but lacking NS2, an essential factor for the assembly of HCV.

- Plasmid #23: A lentiviral construct encoding a pH-sensitive green fluorescent protein pHluorin that is fused to the first extracellular loop of CD63-M153R. This fusion protein can be used as the endosome-plasma membrane sensor.

1.3. Antibodies

The key antibodies used in this study are listed in Table 5.

Table 5. Antibodies and sources

Number	Antibodies	Source	Identifier
1	goat polyclonal anti-ApoE	Chemicon	AB947
2	normal goat IgG	Santa Cruz Biotechnology	sc-2028
3	mouse monoclonal anti-NS5A (9E10)	Gift from C. M. Rice	N/A
4	mouse monoclonal anti-CD63 (MX-49.129.5)	Santa Cruz Biotechnology	sc-5275
5	mouse monoclonal anti-CD63 Alexa Fluor® 488 (MX-49.129.5)	Santa Cruz Biotechnology	sc-5275
6	rabbit polyclonal anti-PDI	Sigma Aldrich	P7496
7	rabbit monoclonal anti-GM130 (D6B1) XP®	Cell Signalling	12480S
8	rabbit polyclonal anti-ApoB	Abcam	ab20737
9	rabbit polyclonal anti c-Myc	Santa Cruz Biotechnology	sc-789
10	mouse monoclonal anti c-Myc (9E10)	ThermoFisher Scientific	MA1-980
11	rabbit polyclonal anti-HA	ThermoFisher Scientific	PA1-985
12	mouse monoclonal anti-HA (HA-7)	Sigma Aldrich	H3663
13	mouse monoclonal anti-β-Actin	Sigma Aldrich	A5441
14	mouse monoclonal anti-α-tubulin	Hoelzel-biotech	A01410
15	rabbit polyclonal anti-goat HRP	Sigma Aldrich	A5420

16	goat polyclonal anti-mouse HRP	Sigma Aldrich	A0168
17	goat polyclonal anti-rabbit HRP	Sigma Aldrich	A0545
18	Alexa Fluor® 488, donkey anti-goat	ThermoFisher Scientific	A-11055
19	Alexa Fluor® 568, donkey anti-goat	ThermoFisher Scientific	A-11057
20	Alexa Fluor® 647 donkey anti-rabbit	ThermoFisher Scientific	A-31573
21	Alexa Fluor® 647 donkey anti-mouse	ThermoFisher Scientific	A-31571
22	rabbit anti-goat	Dianova	305-001-003
23	rabbit anti-mouse	Rockland	800-656-7625
24	protein A coupled to 10-nm gold particles	Cell Microscopy Center, Utrecht, The Netherlands	N/A

1.4. Key reagents and kits

Key reagents and kits used in this study are listed in Table 6.

Table 6. Key reagents and kits

Number	Key reagents and kits	Source	Identifier
1	DAPI (4',6-Diamidino-2- Phenylindole, Dihydrochloride)	ThermoFisher Scientific	D1306
2	TransIT®-LT1 Transfection Reagent	Mirus Biology	MIR2306
3	NucleoSpin RNA extraction kit	Machery-Nagel	740955
4	HCS LipidTOX	ThermoFisher Scientific	H34477
5	Optiprep	Sigma Aldrich	D1556
6	Benzonase Nuclease	EMD-Millipore	70664
7	Nano-Glo® Luciferase Assay System	Promega	N1110
8	Coelenterazine	PJKBiotech	102172
9	Hulu probe	PixelBiotech	N/A
10	ProLong™ Gold Antifade Mountant	ThermoFisher Scientific	N/A
11	SNAP-Cell® 647-SiR	New England BioLabs	S9102S
12	CLIP-ATTO590	N/A	N/A

1.5. RT-qPCR probes and primers

HCV RNA is quantified by RT-qPCR using primers and probes listed in Table 7.

Table 7. Probes and primers used for HCV RNA RT-qPCR

Number	RT-qPCR probes and primers	Source	Identifier
1	HCV probe: 5' - 6-FAM - AAA GGA CCC AGT CTT CCC GGC AAT T - TAMRA	Merck, Darmstadt, Germany	N/A

2	HCV qPCR primer (sense) S-146: 5'-TCT GCG GAA CCG GTG AGT A-3'	Merck, Darmstadt, Germany	N/A
3	HCV qPCR primer (antisense) A-219: 5'-GGG CAT AGA GTG GGT TTA TCC A-3'	Merck, Darmstadt, Germany	N/A
4	GAPDH probe: 5´- 6-VIC -CAA GCT TCC CGT TCT CAG CCT- TAMRA	Merck, Darmstadt, Germany	N/A
5	GAPDH primer (sense) S-GAPDH: 5´-GAA GGT GAA GGT CGG AGT C-3´	Merck, Darmstadt, Germany	N/A
6	GAPDH primer (antisense) A-GAPDH: 5´-GAA GAT GGT GAT GGG ATT TC-3´	Merck, Darmstadt, Germany	N/A

1.6. Buffers

The buffers and corresponding recipes classified based on the name of experiments are listed in Table 8.

Table 8. Buffers and recipes

Classification	Name of solution	Composition
Cell culture	DMEM complete (cplt)	DMEM supplemented with 2 mM L-glutamine, 1x non-essential amino acid, 100 µg/ml streptomycin, 10% fetal calf serum (heat inactivated), 100 U/ml penicillin
	Trypsin-EDTA solution	0.05 % trypsin, 0.02 % (w/v) EDTA
	10x PBS (cell culture)	80 mM Na_2HPO4, 20 mM NaH_2PO4, 1.4 M NaCl
	G418 stock	100 mg/ml
	Blasticidin stock	5 mg/ml
	Zeocin stock	100 mg/ml
	Hygromycin stock	50 mg/ml
	Puromycin stock	1 mg/ml
SDS-PAGE	Sample buffer (5x) without DTT	250 mM TrisHCl [pH6.8], 10% w/v SDS, 30% v/v Glycerol, 0.02% bromophenol blue
	Sample buffer (5x) with DTT	250 mM TrisHCl [pH6.8], 10% w/v SDS, 30% v/v Glycerol, 0.02% bromophenol blue, freshly added 50µM DTT
	Phosphate buffered saline (PBS) (molecular)	8 mM Na_2HPO_4, 2 mM NaH_2PO_4, 140 mM NaCl, 2.7 mM KCl, 0.176 mM K_2HPO_4
	TGS running buffer (10x)	150 mM Tris, 1.92M glycine, 1% (w/v) SDS
	Protein sample buffer (2x)	120 mM Tris-HCl [pH 6.8], 60 mM SDS, 100 mM DTT, 1.75% glycerol, 0.1% bromophenol blue
	SDS-PAGE resolving gel buffer	1.5 M Tris-HCL [pH 8.8], 0.4% (w/v) SDS
	SDS-PAGE stacking gel buffer	1 M Tris-HCl [6.8], 0.8% (w/v) SDS
	Semi-dry transfer buffer	25 mM Tris [pH 8.3], 150 mM glycine, 10% (v/v) methanol
	Wet-blot transfer buffer	25 mM Tris [pH 8.3], 192 mM Glycine, 20% (v/v) methanol
	APS solution	saturated ammonium persulfate in H_2O
	PBS-T	PBS with 0.5% (v/v) Tween-20
	Blocking buffer	5% (w/v) skim milk in PBS-T

Electroporation	Cytomix	120 mM KCl, 0.15 mM CaCl$_2$, 10 mM potassium phosphate buffer, 2 mM EGTA, 5 mM MgCl$_2$, 25 mM HEPES [pH 7.6], freshly added 2 mM ATP and 5 mM glutathione
In vitro transcription	rNTP mix for IVT	25 mM ATP, 25 mM UTP, 25 mM CTP, 12.5 mM GTP in ddH$_2$O
Bacteria culture	Luria-Berthani (LB) medium	10 g Bacto-Trypton, 5 g Yeast Extract, 2.5 g NaCl dissolved in 1 l ddH$_2$O and sterilized
	LB-agar medium	20 g Agar in 1 l LB medium, sterilized
	Ampicillin stock (1000x)	100 mg/ml ampicillin in H2Odd, filtered through 0.22 µm pore
	Kanamycin stock (1000x)	30 mg/ml kanamycin sulfate in H2Odd, filtered through 0.22 µm pore
Immunofluorescent assay	Blocking buffer	3% BSA (w/v) in PBS
	Fixation	4% paraformaldehyde in PBS
	Permeabilization	0.1% Triton X-100 in PBS
	Selective permeabilization	5 µg/ml digitonin in PBS
Agarose gel electrolphoresis	50x TAE buffer	2 M Tris [pH 8.3], 2 M acetic acid, 50 mM EDTA
Luciferase assay	Coelenterazine stock solution	0.043 % (w/v) coelenterazine dissolved in methanol, stored at -80°C
	Luciferine stock solution	1 mM luciferine, 25 mm glycyl-glycin, stored at -80°C
	Luciferase lysis buffer	1 % (v/v) Triton X-100, 10 % (v/v) glycerol, 25 mM glycine-glycine [pH 7.8], 15 mM MgSO4, 4 mM EGTA, stored at 4°C freshly add 1 mM DTT
	Firefly luciferase assay buffer	25 mM glycine-glycine [pH 7.8], 15 mM potassium phosphate buffer [pH 7.8], 15 mM MgSO4, 4 mM EGTA, freshly add 1 mM DTT and 2 mM ATP
	Renilla luciferase assay buffer	25 mM glycine-glycine [pH 7.8], 15 mM potassium phosphate buffer [pH 7.8], 15 mM MgSO4, 4 mM EGTA
TCID50	TCID50 detection substrate, solution 1	0.32 % (w/v) carbazole dissolved in N,N-dimethylformamide, storage at 4°C in the dark
	TCID50 detection substrate, solution 2	37.5 mM sodium acetate, 15 mM acetic acid, storage at 4°C
	0.5% Triton X-100 stock solution	0.5% (v/v) Triton X-100 in 1x PBS
CLEM	CLEM fixative	4% PFA and 0.2% glutaraldehyde in PBS
	EM fixative	50 mM cacodylate buffer [pH 7,2] containing 2.5% glutaraldehyde, 2.6 mM MgCl$_2$, 2.6 mM CaCl$_2$, 50 mM KCl, 2% sucrose
	2% OsO$_4$	2% OsO$_4$ in 50mM cacodylate buffer
	Contrasting solution 1	3% uranyl acetate in 70% methanol
	Contrasting solution 2	2% lead citrate in H$_2$O
	ImmunoEM blocking buffer	0.8% (w/v) BSA, 0.1% fish skin gelatin, 50 mM glycine in PBS
	ImmunoEM fixative	1% glutaraldehyde in PBS
Imunnoprecipitation	Lysis buffer	50mM Tris-HCl, pH 7.5, 150mM NaCl, 1% Triton X-100, 1mM EDTA, 10% Glycerol, 1x Protease Inhibitor Cocktail (Roche)
	Washing buffer	50mM Tris-HCl, pH 7.5, 150mM NaCl, 1% Triton X-100, 1mM EDTA
FISH	HuluHyb solution	2xSSC, 2M Urea, 10% dextran sulfate, 5x Denhardt's solution
	HuluWash	2xSSC, 2M Urea

1.7. Software

The main software packages used in this study are listed in Table 9.

Table 9. Software for data processing and analysis

Number	Software	Source (cat #)	Identifier
1	FIJI	open-source	https://imagej.nih.gov/ij/
2	GraphPad Prism 8.0	LaJolla, CA, USA N/A	https://graphstats.net
3	Huygens Professional version s19.10	Scientific Volume Imaging, The Netherlands	http://svi.nl
4	Ilastik	ilastik: interactive machine learning for (bio)image analysis	https://doi.org/10.1038/s41592-019-0582-9
5	ColocQuant	Biomedical Computer Vision Group, IPMB, Univeristy of Heidelberg, Germany	http://www.bioquant.uni-heidelberg.de/index.php?id=322
6	ColocJ	Biomedical Computer Vision Group, IPMB, Univeristy of Heidelberg, Germany	http://www.bioquant.uni-heidelberg.de/index.php?id=322

1.8. Other materials

The common materials used in this study are listed in Table 10.

Table 10. Other materials used in this study

Other resourses	Source	Identifier
Acrylamide: Bisacrylamide mix (29:1) 40%	Sigma Aldrich, St. Louis, USA	A7802
Agarose	Thermo Fisher Scientific, Waltham, USA	16500100
Ammonium Persulfate	Sigma Aldrich, St. Louis, USA	248614
Ampicillin	Roche, Mannheim, Germany	68-53-4
Blasticidin	Thermo Fisher Scientific, Waltham, USA	R21001
BSA	Sigma Aldrich, St. Louis, USA	A1933
CellTiter-Glo® Luminescent Cell Viability Assay	Promega, Madison, USA	G7571
Cellview cell culture dish, PS, 35/10 mm, 4 compartments	Greiner bio-one, Solingen, Germany	N/A
Coelenterazine	PJK, Kleinblittersdorf, Germany	102171
DAPI (4',6-Diamidino-2-Phenylindole, Dihydrochloride)	Thermo Fisher Scientific, Waltham, USA	D1306
Digitonin	Sigma Aldrich, St. Louis, USA	N/A
Dithiothreitol (DTT)	Sigma Aldrich, St. Louis, USA	D0632
D-Luciferin	PJK, Kleinblittersdorf, Germany	102142

DMSO	Sigma Aldrich, St. Louis, USA	D8418
dNTPs	Sigma Aldrich, St. Louis, USA	R0191
ECL Plus Western Blot Detection System	Perkin-Elmer, Waltham, USA	NEL122001EA
EDTA	Merck, Darmstadt, Germany	324503
Ethanol	Sigma Aldrich, St. Louis, USA	493511
Fetal Calf Serum	PAA Laboratories, USA	G7041
Fish Skin Gelatin	Sigma Aldrich, St. Louis, USA	G7041
Fluoromount G	Southern Biotechnology Associates, Birmingham, USA	0100-01
G418 (Geneticin sulfate)	Thermo Fisher Scientific, Waltham, USA	11811023
GeneRuler 1 kb DNA Ladder	Thermo Fisher Scientific, Waltham, USA	SM1163
Glutaraldehyde	Science Services, Munich, Germany	E16200
Glycerol	Roth, Karlsruhe, Germany	3783
Glycyl-glycin	Sigma Aldrich, St. Louis, USA	702560
HEPES	Thermo Fisher Scientific, Waltham, USA	15630080
High precision glass coverslips	Deckgläser, Marienfeld	N/A
Hygromycin B	Sigma Aldrich, St. Louis, USA	I9516
Isopropanol	Thermo Fisher Scientific, Waltham, USA	25030081
L-Glutamine for cell culture	Invitrogen, Karlsruhe, Germany	H34477
LipidTox Deep Red Neutral Lipid Stain	Sigma Aldrich, St. Louis, USA	M6250
Lipofectamine® RNAiMAX Reagent	Thermo Fisher Scientific, Waltham, USA	13778
Matek dishes containing gridded coverslips	MatTek Corporation	34860
Methanol	Sigma Aldrich, St. Louis, USA	34860
Midori Green Direct (10x)	Nippon Genetics Europe, Dueren, Germany	MG06
Nitrocellulose western blot membrane	GE Healthcare, Germany	N/A
Non-essential amino acid	Thermo Fisher Scientific, Waltham, USA	11140050
NucleoBond PC500	Macherey-Nagel	740574
NucleoSpin Extract II	Macherey-Nagel	740609
NucleoSpin Plasmid	Macherey-Nagel	740588
NucleoSpin RNA	Macherey-Nagel	740955
Opti-MEM	Thermo Fisher Scientific, Waltham, USA	N/A
Osmium tetroxide	Electron Microscopy Sciences, Hatfield, USA	N/A
Paraformaldehyde	Science Services, Munich, Germany	E15700
PEI	Polysciences Inc, Warrington, USA	N/A
Penicillin-Streptomycin	Thermo Fisher Scientific, Waltham, USA	15140122
Prestained protein marker	New England Biolabs, Frankfurt, Germany	P7719L
ProLong™ Gold Antifade Mountant	Sigma Aldrich, St. Louis, USA	P8833
Puromycin	Perkin-Elmer, Waltham, USA	N/A
PVDF western blot membrane	MedChemExpress, NJ, USA	HY-104077
Phenol-Red Free DMEM		N/A
Quick CIP	New England Biolabs, Frankfurt, Germany	M0525
RNasin RNase inhibitor	Promega, Madison, USA	N2511
RQ1 RNase free DNase	Promega, Madison, USA	M6101
Skim milk	Serva, Heidelberg, Germany	N/A

Sodium cacodylate	Thermo Fisher Scientific, Waltham, USA	28365
Sodium dodecysulfate (SDS)	Sigma Aldrich, St. Louis, USA	S2626
Spermidine	Roth, Karlsruhe, Germany	N/A
Sucrose	Applichem, Darmstadt, Germany	A1148
TEMED	Merck, Darmstadt, Germany	112298
Tween 20	Roth, Karlsruhe, Germany	9127.1
Triton X-100	Electron Microscopy Sciences, Hatfield, USA	N/A
Uranyl acetate	Thermo Fisher Scientific, Waltham, USA	R25001
Zeocin	Thermo Fisher Scientific, Waltham, USA	10687010
β-Mercaptoethanol	Thermo Fisher Scientific, Waltham, USA	P10144

1.9. Instruments

Important instruments used in this study are listed in Table 11.

Table 11. Key instruments used in this study

Equipments	Source
Beckman Coulter Optima XE-90 Ultracentrifuge	Beckman Coulter, Indiana, USA
Biometra TOne Gradient 96 Thermal Cycler	Biometra GmbH, Göttingen, Germany
Biometra TPersonal Combi PCR Thermal Cycler	Biometra GmbH, Göttingen, Germany
Centrifuge 5424 R - Eppendorf	Eppendorf, Hamburg, Germany
CO_2 Incubator C200 - Labotect	Labotect, Rosdorf, Germany
ChemoCam Imager 3.2	Intas Science Imaging Instruments, Göttingen, Germany
Eppendorf Thermomixer Compact	Eppendorf, Hamburg, Germany
Gene Pulser II	Bio-Rad Laboratories, Hercules, USA
GFL Shaking Water Bath 1083	GFP, Hannover, Germany
Jeol JEM-1400 transmission electron microscope	JEOL, Akishima, Japan
Leica SP8 inverted confocal microscope	Leica, Heidelberg, Germany
Mini-PROTEAN Tetra Cell	Bio-Rad, Hercules, CA, USA
Mithras LB 940 plate luminometer	Berthold Technologies, Bad Wildbad, Germany
NanoDrop Lite Spectrophotometer	ThermoFisher Scientific
PerkinElmer UltraVIEW Vox Spinning Disc	PerkinElmer, Waltham, USA
Sorvall Lynx 6000 centrifuge	ThermoFisher Scientific
TC20 Automated Cell Counter	Bio-Rad Laboratories, Hercules, USA
Tecan Fluor4	Tecan, Wiesbaden, Germany
Trans-Blot Semi-Dry Transfer Cell	Bio-Rad Laboratories, Hercules, USA

2. Methods

The text from the following parts: "Cell culture conditions, DNA plasmid constructs, production of lentiviruses, Western blot analysis, immunofluorescent staining and confocal microscopy, super-resolution microscopy, HCV RNA staining by Hulu probes, immunoprecipitation, iodixanol density gradient centrifugation, luciferase reporter assay, immunocapture of extracellular ApoE-associated structures and immunogold labeling, quantification and statistical analysis" has been adapted from the manuscript in preparation originally written by myself with modifications.

2.1. Cell culture

2.1.1. Cell culture conditions

All cells used in this study were cultured in Dulbecco's modified Eagle medium (DMEM, Thermo Fisher Scientific), supplemented with 2 mM L-glutamine, nonessential amino acids, 100 U/ml of penicillin, 100 µg/ml of streptomycin, 10% fetal calf serum (DMEMcplt) and given concentrations of antibiotics to select for stable expression of genes of interest. Huh7-Lunet/CD81H cells (750 µg/ml G418) derived from the Huh7 subclone Huh7-Lunet [99] and expressing high levels of the HCV entry receptor CD81, and Huh7-LunetCD81H/ApoE-KD cells (5 µg/ml puromycin) with a stable knockdown of ApoE have been described earlier [14, 64]. For reasons of simplicity, in this study Huh7-Lunet/CD81H cells are designated Lunet cells. HEK293T-miR122 cells (2 µg/ml puromycin), kindly provided by Thomas Pietschmann, have been reported elsewhere [95]. Huh7.5 and HEK293T cells have been described elsewhere [94, 96]. HEK293T-miR122, Hela Kyoto, and Lunet/ApoE-KD cells were used to generate ApoE^{mT2} expressing cells by lentiviral transduction and stable selection with 10 µg/ml blasticidin. For the production of HCV-like transcomplemented particles (HCV$_{TCP}$), Lunet/ApoE-KD/ApoE^{mT2} cells (designated Lunet-ApoE^{mT2} in this study for reasons of simplicity) were transduced with lentiviruses encoding the HCV structural proteins (C-E1-E2^{eYFP}-p7-NS2 or C-E1-E2^{eYFP}-p7), selected with 500 µg/ml Zeocin and maintained in 50 ug/ml Zeocin-containing DMEMcplt. To obtain cells with stably replicating subgenomic replicon of the HCV strain JFH1 and used for the coculture experiment, Lunet-ApoE^{mT2}/CD63^{mCherry} cells were electroporated with *in vitro* transcripts of the construct sgHyg/JFH1. To monitor HCV RNA secretion in the context of an ApoE-binding defective NS5A

mutant or wildtype NS5A, Lunet cells were electroporated with *in vitro* transcripts of the construct sgHyg/JFH1/NS5A^{APK99AAA} or sgHyg/JFH1, respectively. Stable cells were selected in a medium containing 400 µg/ml hygromycin and maintained in 150 µg/ml hygromycin-containing DMEMcplt. FCS devoid of EVs was prepared as previously described [88]. The full names of constructs used in this study are given in the Materials and Methods.

2.1.2. Cell stock preparation for long-term storage and thawing of cells

For long-term storage, cells were frozen at -80°C or in the liquid nitrogen. Typically, 6-7 aliquots were prepared from a confluent cell monolayer that had been cultured in a 15-cm dish. For this purpose, cells were detached by trypsinization, resuspended in DMEMcplt, and subsequently pelleted by centrifugation at 700 rpm for 5 min. Cells were then resuspended in the the cryo solution (90 % FCS + 10 % DMSO), and divided into 1.5 ml aliquots in cryotubes (Nunc). Cells were then immediately frozen at -80°C, and were transferred to the liquid nitrogen tank if necessary.

For thawing a frozen cell stock, the aliquot was incubated shortly in a water bath at 37°C and transferred to a conical tube containing 10ml DMEMcplt. Cells were then suspended and pelleted by centrifugation at 700 rpm for 5 min. After the aspiration of the supernatant, cells were resuspended again in 10ml DMEMcplt and transferred to a 10-cm cell culture dish.

2.1.3. Cell counting

The number of cells in suspension was quantified automatically using the TC20 automated cell counter (Biorad). Briefly, 10 µl of cell suspension was applied onto the cell counting-slide and inserted into the cell counter.

2.2. Molecular biological methods

2.2.1. DNA plasmid constructs

The lentiviral construct pWPI_ApoE encoding human ApoE3 was described previously [65]. To generate pWPI_ApoEFP and pWPI_ApoESNAPf constructs, the FP- and the SNAPf-

coding sequences were amplified by PCR using the corresponding plasmids as templates (see Key Resources Table) and inserted at the 3' end of the ApoE-coding sequence via the linker sequence SGGRGG. Construct pWPI_CD63[mCherry] encodes a fusion protein of human CD63 and C-terminal mCherry. To generate the construct pWPI_eYFP-CaaX, the eYFP-coding sequence was extended at the 3' end by the CaaX coding sequence derived from the human HRAS protein and inserted into the lentiviral vector pWPI. To generate pWPI_CD63_M153R_pHluorin, the CD63-pHluorin coding sequence contained in plasmid pCMV-Sport6-CD63-pHluorin [100] was amplified by PCR and inserted into the lentiviral vector pWPI. To stabilize pHluorin and increase signal intensity, I inserted the M153R mutation [101] by using PCR and primers carrying the desired nucleotide substitutions.

The full-length HCV constructs Jc1 and JcR2A have been described elsewhere [44, 97]. The lentiviral constructs encoding the HCV structural proteins Core-NS2/E2[eYFP] or Core-p7/E2eYFP were created by replacing the eGFP-coding sequence reported previously [21] by the eYFP-coding sequence. Plasmid pFK_I389neoNS3-3′_dg_JFH1_NS5A-aa2359_mCherry_NS3-K1402Q (designated sgNeo/JFH1/NS5Amcherry in this study) has been reported earlier [98]. To generate the subgenomic replicon encoding a CLIPf-tagged NS5A and the neomycin resistance gene (construct sgNeo/JFH1/NS5A[CLIPf]), the mCherry-coding sequence in construct sgNeo/JFH1/NS5Amcherry was replaced by the CLIPf-coding sequence. To allow selection with hygromycin, the neomycin resistance gene was replaced by the hygromycin resistance gene. To generate the subgenomic replicon construct encoding a NanoLuciferase-tagged NS5A (sgHyg/JFH1/NS5ANluc), the mCherry-coding sequence of construct sgHyg/JFH1/NS5A[mCherry] was replaced by the NanoLuciferase-coding sequence [102]. Mutations in NS5A interfering with ApoE interaction APK99AAA and PPT102AAA [41, 103] were inserted into the replicon construct sgHyg/JFH1 by using PCR-based mutagenesis.

To generate plasmids encoding myc-tagged NS5A wildtype and the APK99AAA mutant corresponding plasmids were used as template for PCR using primers encoding the myc-tag sequence and NS5A sequences were inserted into the pCDNA3+ vector. Other plasmids used in this study are listed in the Materials and Methods.

2.2.2. Transformation of competent *E. coli*

The plasmid DNA was incubated with 50 µL home-made chemically competent *E. coli* DH5α for 10 min on ice. Then, the mixture was heat-shocked at 42°C for 1 min, followed by 2 min incubation on ice. Subsequently, transformed bacteria were then recovered by the addition of 500 µL of antibiotic-free LB and shaking at 37°C for 40 min. Bacteria were then plated on LB-agar plates containing the appropriate selective antibiotic for at least 12-16 hours at 37°C for colony formation.

2.2.3. Purification of plasmid DNA

Plasmid DNA was purified from *E. coli* cultures using the NucleoSpin Plasmid (miniprep) or NucleoBond PC 500 kit (maxiprep) (Macherey-Nagel), according to the manufacturer's protocol. DNA was eluted in milli-Q water and the concentration was determined using the NanoDrop Spectrophotometer (Thermo Scientific).

2.2.4. Polymerase chain reaction (PCR)

For the amplification of a specific DNA sequence, 0.5 µg DNA template was used and amplified using specific primers (Sigma Aldrich) with the Phusion® High-Fidelity PCR Master Mix (NEB, M0531). PCR was conducted using a TPersonal or TGradient thermocycler with the following thermo cycles: initial denaturation: 95°C for 2 min → amplification: 10 cycles [95°C for 30 sec (denaturation) → 60-68°C for 30 sec (annealing) → 68°C for 1 min per 1,000 bp (elongation)] → final elongation: 68°C for 5 min → storage: 4°C, ∞. The annealing temperatures were adjusted according to the primer melting temperatures (Tm) as calculated by the supplier (Sigma Aldrich) to prime specific binding of the primers to the DNA templates. Typically, the annealing temperatures were 5°C lower than the lowest Tm of a primer pair. PCR products were resolved by agarose gel electrophoresis and subsequently purified using the NucleoSpin Extract II Kit (Macherey-Nagel).

2.2.5. Site-directed mutagenesis

The mutations in the DNA plasmids were introduced using the overlap extension PCR. The primers carrying the designed mutation generally had at least 18 nucleotides overlap. PrimerX (bioinformatics.org) was used to design primers.

2.2.6. DNA digestion with restriction enzymes

All restriction endonucleases were purchased from New England Biolabs except FastDigest KflI (Thermo Fisher Scientific). Generally, plasmid DNA was digested with 5-10 units of restriction enzymes per one microgram of DNA in a reaction buffer according to the manufacturer's instructions. Double digestion conditions were recommended by Double digest Finder (NEBcloner). Digested products were visualized by agarose gel electrophoresis and extracted if necessary.

2.2.7. Ligation of DNA fragments

For ligation reactions, digested and dephosphorylated [by quick CIP (NEB)] DNA insert and backbone were mixed with a ratio of 3:1, and ligated using the T4 DNA Ligase. Typically, 50 ng of the backbone and the corresponding amount of insert were added in a reaction of 10 µl with 5U T4 ligase and T4 ligase buffer. The mixture was incubated at 37°C for 30 min or overnight at RT. Subsequently, the whole mixture was transformed into competent *E. coli* DH5α.

2.2.8. Agarose gel electrophoresis

DNA or RNA was mixed with Midori Green Direct (Genetics) and separated using 0.8-1.2% (w/v) agarose gels in the 1x TAE buffer. Samples were then visualized and imaged with a blue light illuminator chamber equipped with a gel imaging system.

2.2.9. Western blot analysis

Total protein from cells were extracted in 2x sample buffer (120 mM Tris-HCl [pH 6.8], 60 mM SDS, 100 mM DTT, 1.75% glycerol, 0.1% bromophenol blue) supplemented with 5mM $MgCl_2$ and 5U/ml Benzonase nuclease. Cell lysates were denatured at 95°C for 5 min. Proteins were separated by SDS-PAGE, transferred to a polyvinylidene difluoride (PVDF) membrane, and blocked in 5% skim milk-containing PBS-0.05% Tween 20, pH 7.4 (PBST) for 1h at RT. The membrane was then incubated with a primary antibody in 1% skim milk-containing PBST for either 1h at RT or overnight at 4°C, and subsequently incubated with a secondary antibody conjugated with horseradish peroxidase (HRP) for 1h at RT. Immunodetection was performed using the Western Lightning Plus-ECL reagent (PerkinElmer) and signals were visualized by using the Intas ChemoCam Imager 3.2 (Intas).

2.3. Virological methods

2.3.1. Preparation of *in vitro* transcribed RNA and electroporation of HCV RNA

In vitro transcribed HCV RNA preparation and transfection using electroporation were described elsewhere [104]. In brief, DNA plasmids (10 µg) containing HCV JFH1 genomes were linearized using MluI-HF restriction enzyme (NEB) for 1h at 37°C according to the manufacturer's instruction, and were purified using the NucleoSpin Extract II Kit (Macherey-Nagel) with the PCR protocol. RNA transcripts were synthesized via *in vitro* transcription using T7 RNA polymerase in the 100 µl-reaction mixtures [80 mM HEPES (pH 7.5), 12 mM $MgCl_2$, 2 mM spermidine, 40 mM dithiothreitol, 3.125 mM of each rNTP, 1 U/µl RNasin (Promega), 0.6 U/µl T7 RNA polymerase, and the respective linearized DNA template]. Reaction was performed at 37°C for total 4 h. After 2 h incubation, 0.3 U/µl T7 RNA polymerase was supplemented to the reaction mixture to maintain high efficiency of RNA transcription. DNA template was then digested for 45 min at 37°C by the addition of 2 U of RNase-free DNase (Promega) per µg DNA. Transcribed RNA was further purified with acidic phenol-chloroform method, precipitated with isopropanol, and dissolved in RNase-free water. The integrity and concentration of RNA were evaluated using agarose gel electrophoresis and nanodrop.

For the electroporation, confluent cell monolayers were trypsinized, pelleted, and washed with 1x PBS and resuspened in Cytomix solution [120 mM KCl, 0.15 mM $CaCl_2$, 10 mM potassium phosphate buffer, 25 mM HEPES (pH 7.6), 2 mM EGTA, and 5 mM $MgCl_2$] [105] containing 2 mM ATP and 5 mM glutathione ($1-2x10^7$ cells/ml). *In vitro* transcribed RNA (5 µg) was mixed with 200 µl of the cell suspension by pipetting. Electroporation was performed at 975 µF and 166 V using the Gene Pulser system (Bio-Rad) and a cuvette with a gap width of 2 mm (Bio-Rad). For a larger scale electroporation, 10 µg of *in vitro* transcribed RNA was mixed with 400 µl of the cell suspension by pipetting. Electroporation was performed at 975 µF and 270 V using a cuvette with a gap width of 4 mm. Cells were then transferred immediately to the DMEMcplt and seeded to the desired cell culture dishes for downstream experiments.

2.3.2. Quantitative detection of HCV RNA by RT-qPCR

Intracellular total RNA from cell lysates and extracellular total RNA in cell culture supernatant were extracted using a NucleoSpin RNA extraction kit (Macherey-Nagel) according to the manufacturer's instruction. The HCV RNA copies in extracted samples were quantified with HCV specific primers and a probe using the Quanta BioSciences qScript XLT One-Step RT-qPCR KIT (Quanta Biosciences, Gaithersburg, MD) according to the manufacturer's instructions [88]. The primers and probes are listed in Table 6. Briefly, 15 µL of reaction mixture comprises of 7.5 µL 2x enzyme/buffer mix, 1 µM of each JFH1-specific primer, 0.27 µM HCV-specific probe, 3 µL template RNA and RNase-free water. Reactions were performed using the following setting: 50°C for 10 min, 95°C for 60 sec, and 40 cycles as follows: 95°C for 10 sec, 60°C for 60 sec. Serially diluted *in vitro* transcribed HCV RNA were included in parallel for the calculation of HCV RNA copy numbers in the RT-qPCR analysis.

2.3.3. Determination of HCV Core protein amount

HCV core protein amount were quantified using a commercial Chemiluminescent Microparticle Immunoassay (CMIA) (6L47, ARCHITECT HCV Ag Reagent Kit, Abbott Diagnostics) according to the manufacturer's instructions as reported earlier [21]. To determine the intracellular core amounts, cells were lysed using the luciferase lysis buffer (1% Triton X-100, 10% glycerol, 25 mM glycylglycine, 15 mM $MgSO_4$, 4 mM EGTA, and 1 mM DTT) for 15 min at RT. For extracellular core detection, HCV-containing supernatants were also inactivated with Triton X-100 (0.5% Triton X-100 final dilution) prior to the quantification.

2.3.4. Production of lentiviruses

Lentiviruses containing genes of interest were produced as described earlier [106]. In brief, HEK-293T cells were co-transfected with the human immunodeficiency virus-Gag packaging plasmid pCMV-dR8.91, the vesicular stomatitis virus-G expressing plasmid pMD2.G, and the pWPI construct containing a gene of interest using polyethylenimine (Polysciences Inc.). Lentivirus-containing supernatants were harvested at about 48 hours post-transfection and filtered through a 0.45 µm pore-size filter (MF-Millipore).

2.4. Imaging methods

2.4.1. Immunofluorescence staining and confocal microscopy

Immunofluorescence (IF) staining was performed as previously described [64]. Briefly, cells seeded onto coverslips were fixed with 4% paraformaldehyde (PFA) in PBS for 10 min at RT and permeabilized with 0.1% Triton X-100 in PBS for 10 min at RT. After blocking with 3% (w/v) bovine serum albumin (BSA) in PBS for 20 min at RT, cells were incubated with a diluted primary antibody in 1% BSA/PBS for 1 h at RT or overnight at 4°C. Cells were further incubated with a diluted secondary antibody conjugated with an Alexa fluorophore (1:1000) in 1% BSA/PBS (Molecular Probes) for 1h in dark condition at RT. If required, cell nuclei were counterstained with DAPI (1:3000) (Molecular Probes). During each step in between, washing was performed at least 3 times with 1x PBS. Unless otherwise stated, coverslips were mounted with Fluoromount-G mounting medium (Electron Microscopy Sciences, Ft. Washington, USA) overnight at 4°C. For selective permeabilization assay, cells were permeabilized in 5 µg/ml digitonin dissolved in PBS for 15 min at 4°C. IF images were generated with a Leica TCS SP8 (Leica Microsystems) or Spinning disc confocal microscope (PerkinElmer).

2.4.2. Live-cell time-lapse confocal imaging

Cells were seeded on either 4-compartment (CELLview, Greiner BIO-ONE) or 1-compartment (MatTek Corporation) 35 mm glass-bottom imaging dishes. Prior to imaging, cells were washed twice and cultured in phenol red-free DMEMcplt. Live-cell time-lapse confocal imaging was performed in the humidified incubation chamber at 37°C and 5% CO_2 with the PerkinElmer UltraVIEW Vox Spinning Disc CSU-X1 with Nikon TiE which is equipped with the EM-CCD Hamamatsu ImageEM X2 camera and an automated Nikon perfect focus system. The imaging medium of pHluorin-tagged CD63 expressing cells was supplemented with 25mM Hepes for the stabilization of neutral pH. The imaging of different channels was recorded sequentially with different time intervals as indicated in the figure legends.

2.4.3. Super-resolution microscopy

Lunet-ApoE[SNAPf] stable cells were electroporated with *in vitro* transcribed RNA of HCV sgJFH1/NS5A[CLIPf] and grown on high precision glass coverslips (Deckgläser, Marienfeld). At 48 h post-electroporation, cells were sequentially incubated with CLIP[ATTO590] (1:2500) and 5 µM SNAP[SiR647] in DMEMcplt for 1 h. Cells were then washed intensively at least 3 times with DMEMcplt and cultured further for 15 min. Thereafter, cells were washed 3 times with PBS, fixed with 4% PFA in PBS for 10 min at RT, and subjected to immunofluorescent staining to label CD63 with anti-CD63 conjugated to Alexa Fluor 488 antibody (Santa Cruz). Cells were later mounted with ProLong Gold Antifade Mountant overnight at RT (ThermoFisher Scientific). STED imaging was performed using the Abberior STED Super resolution microscopy equipped with 488 nm, 594 nm, 640 nm and 775 STED lasers, spatial Light Modulator 2D/3D, Adaptive illumination (RESCue, DyMIN), and Hardware-based autofocus. Images were deconvoluted with Huygens (Scientific Volume Imaging).

2.4.4. Live-cell imaging coupled to correlative light electron microscopy (CLEM)

Cells were cultured on 35-mm glass-bottom culture dishes containing gridded coverslips (MatTek Corporation). Live-cell time-lapse confocal imaging were performed with the PerkinElmer Spinning Disc as described above. Cells were then fixed on stage immediately after live-cell imaging for 30 min at RT with the CLEM fixative containing 0.2% GA and 4% PFA. The coordinates of cells or interest were captured with the 20x objective using transmitted light with differential interference contrast (DIC). Thereafter, cells were washed 3 times with PBS to remove the fixative. Cells were then subjected to fixed-cell imaging using an oil immersion 60x objective, covering the ~2.8 µm cell thickness with 0.2 µM spacing between optical planes before and after the addition of LipidTox™ Deep Red Neutral Lipid Stain (Invitrogen). After that, cells were further fixed with the EM fixative [2.5% GA, 2% sucrose, 50 mM sodium cacodylate (Caco), 50 mM KCl, 2.6 mM $MgCl_2$, and 2.6 mM $CaCl_2$] for 30 min or overnight at 4°C. After 3 washes with 50mM CaCo buffer, cells were incubated with 2% osmium tetroxide in 50 mM CaCo for 40 min on ice, washed 3 times with milli-Q water, and incubated with 0.5% uranyl acetate in water at 4°C. Samples were washed again with water prior to the sequential dehydration of cells using a graded ethanol series from 50% to 100% at RT. Samples were then embedded in Epon 812 (Carl Roth) and incubated for at least 2 days at 60°C for the polymerization of Epon. Epon were furthered

detached from the glass coverslips by dipping several times into liquid nitrogen and hot water. Cells of interest were identified by the negative imprint of the gridded coverslips and cut into 70nm ultrathin sections using the ultramicrotome Leica EM UC6 (Leica Microsystems). Sections were then collected on grids (Science Services, GMBH) and counterstained sequentially by 3% uranyl acetate in 70% water for 5 min and lead citrate (Reynold's) for 5 min. Images were acquired by using the Jeol JEM-1400 (Jeol Ltd., Tokyo, Japan) transmission electron microscope (TEM) equipped with a 4k pixel digital camera (TemCam F416; TVIPS, Gauting, Germany) and the EM-Menu or Serial EM software [107]. Lipid droplets were used as fiducial markers to correlate the EM images to the IF images using the Landmark Correspondences plugin in the Fiji software package.

2.4.5. HCV RNA staining by Hulu probes

Intracellular HCV RNAs were visualized by smFISH with Hulu probes (PixelBiotech, Germany) according to the manufacturer's instruction with modifications. In brief, cells grown on glass coverslips were fixed with 4% paraformaldehyde (PFA) in PBS for 30 min at RT. Cells were then treated with 150mM Glycine in PBS to quench residual PFA, permeabilized with 0.1% TritonX-100 in PBS for 10 min, and treated with Proteinase K (1:4,000) (ViewRNA ISH Kit, ThermoFisher Scientific) in PBS for 5 min. HCV RNAs were then hybridized with Hulu probes targeting the positive strand of HCV NS3 RNA region spanning 1157 nucleotides (3733-4889, AB047639) in HuluHyb solution (2xSSC, 2M Urea, 10% dextran sulfate, 5x Denhardt's solution) in a humidified chamber at 30°C overnight. Cells were subsequently washed with HuluWash and coverslips were mounted on glasses with Prolong Gold Antifade Mountant overnight at RT (ThermoFisher Scientific).

2.5. Biochemical methods

2.5.1. Immunoprecipitation

HEK293T-miR122 cells were cotransfected with HA-tagged ApoE and either an empty vector, pCDNA3+ myc-tagged NS5A^{wt}, NS5A^{APK99AAA} or NS5A^{PPT102AAA}, respectively using TransIT-LT1 Transfection Reagent (Mirus Bio). At 30 h.p.t, cells were lysed in lysis buffer (50mM Tris-HCl, pH 7.5, 150mM NaCl, 1% Triton X-100, 1mM EDTA, 10% Glycerol, 1x Protease Inhibitor Cocktail (Roche)) on ice for 10 min. Cell lysates were then centrifuged at 15,000g for 15 min at 4°C. Supernatants were later precleared by protein G-magnetic bead slurry (Dynabeads,

ThermoFisher Scientific) for 30 min at 4°C, incubated with rabbit anti c-myc antibody at 4°C overnight, and immunoprecipitated with protein G bead slurry with rotation for 1h at 4°C. Thereafter, beads were washed 5 times with Glycerol-omit lysis buffer, eluted with 2x sample buffer, and denatured for 5 min at 95°C. Bound proteins were detected using mouse anti-HA antibody.

2.5.2. Iodixanol density gradient centrifugation

Cells were washed and cultured for 5 h in 1% FCS-containing DMEM. Thereafter, cell cultured supernatant was filtered with a 0.45 μm pore-size filter (MF-Millipore), loaded on top of a PBS-based 10-50% iodixanol gradient (Sigma Aldrich), and subjected to isopycnic centrifugation for 18h at 34,000 rpm (~120,000 x g) at 4°C using an SW60 rotor (Beckman Coulter, Inc.). Eleven fractions were then collected from top to bottom and subjected to density measurement by a refractometer (Krüss, AGS Scientific) and western blot analysis.

2.5.3. Luciferase reporter assay

HCV RNA replication kinetics were monitored by the HCV JcR2A reporter construct. Briefly, *in vitro* transcribed HCV RNA transfected cells were collected at 4, 24, 48 and 72 h post-electroporation. Cells were lysed in luciferase lysis buffer (1% Triton X-100, 10% glycerol, 25 mM glycylglycine, 15 mM $MgSO_4$, 4 mM EGTA, and 1 mM DTT) for 15 min at RT. Cells lysates were transferred to 96-well plates, injected with Coelenterazine-containing luciferase assay buffer (25 mM glycylglycine, 15 mM $MgSO_4$, 4 mM EGTA, 1 mM DTT, and 15 mM K_3PO_4, pH 7.8). Renilla luciferase activities were then measured using Mithras LB 940 plate luminometer (Berthold Technologies, Freiburg, Germany). The HCV RNA replication overtime were normalized to 4 h values to account for possible differences in transfected RNA inputs among samples. To measure the HCV transmission ability produced in cell culture supernatant, HCV-containing supernatants were inoculated into naïve Huh7.5 cells. At 72 h post-inoculation, cells were lysed and subjected to luciferase measurement.

NanoLuciferase (Nluc) activity was measured using Nano-Glo Luciferase Assay System (Promega) according to the manufacturer's instruction with modifications. Briefly, 50 μl of samples were mixed with 50 μl NLuc substrate (1:1,000) in the assay buffer. NLuc activities were then measured using Mithras LB 940 plate luminometer (Berthold Technologies, Freiburg, Germany).

2.5.4. Immunocapture of extracellular ApoE-associated structures and immunogold labeling

Supernatants of cells cultured in EV-free DMEM were collected, filtered through a 0.45 µm pore-size filter (MF-Millipore), and incubated with anti-ApoE antibody for 3 hours at 4°C. ApoE-associated structures were further precipitated with protein G-magnetic beads (Dynabeads, ThermoFisher Scientific) overnight at 4°C, washed 5 times with cold PBS, eluted with 0.1M Glycine, pH 2.5 for 10 min at RT and neutralized with 1M Tris, pH 7.5. To visualize eluted structures, samples were applied on freshly glow-discharged carbon- and pioloform-coated 300-mesh copper grids (Science Services GmbH, Munich, Germany) and subjected to negative staining with 3% uranyl acetate for 5 min at RT.

Immunogold labeling of ApoE-associated structures followed the protocol as reported elsewhere [108] with modifications. All of the incubation and washing steps were conducted by floating the grids on top of drops at RT. Washing were performed at least 2-min 5 times with PBS in between steps. In brief, absorbed samples on copper grids were blocked with blocking solution (0.8% BSA [Roth, Karlsruhe, Germany], 0.1% fish skin gelatin [Sigma-Aldrich], 50 mM glycine in PBS). For ApoE and CD63 labeling, grids were incubated with goat anti-ApoE antibody (1:100) and mouse anti-CD63 antibody (1:100) in blocking solution, respectively for 30 min. Grids were further incubated with rabbit anti-goat- or anti-mouse-bridging antibody (1:150) in blocking solution for 20 min. Bound antibodies were detected with protein A conjugated to 10-nm gold particles diluted 1:50 in blocking buffer for 30 min. Thereafter, grids were fixed with 1% glutaraldehyde in PBS for 5 min, washed 7 times with H_2O, briefly rinsed with 3% uranyl acetate, and negatively stained again with 3% uranyl acetate for at least 5 min.

2.6. Imaging analysis

This part was done in collaboration with Christian Ritter, BioQuant Center, Biomedical Computer Vision Group, Heidelberg University, Heidelberg, Germany. The text is originally written by Christian Ritter and Karl Roth and modified by myself.

2.6.1. Automated particle tracking in fluorescence microscopy images

Particle tracking in fluorescence microscopy images was performed by using a probabilistic particle tracking approach that is based on Bayesian filtering and multi-sensor data

fusion [109]. This approach combines Kalman filtering and particle filtering and integrates multiple measurements by separate sensor models as well as sequential multi-sensor data fusion. The sensor models determine detection-based and prediction-based measurements via elliptical sampling [110] and take into account different uncertainties. In addition, the tracking approach exploits motion information by integrating displacements in the cost function for correspondence finding. Particles are detected by the spot-enhancing filter (SEF) [111] consisting of a Laplacian-of-Gaussian (LoG) filter followed by intensity thresholding of the filtered image and determination of local maxima.

2.6.2. Motility analysis of ApoE^{mT2} and CD63^{mCherry}

The motility of CD63 and ApoE was quantified by a mean squared displacement (MSD) analysis [112] using the computed trajectories. For each trajectory with a minimum of 10 time points (corresponding to a time duration of 32.5 s), he computed the MSD as a function of the time interval Δt. All MSD curves corresponding to each of the HCV associated proteins were averaged to obtain MSD curves for CD63 and ApoE. To quantify the motility, he fitted the anomalous diffusion model $MSD(\Delta t) = 4\,\Gamma\,\Delta t^{\alpha}$ to the MSD values and obtained the anomalous diffusion exponent α for motion classification and the transport coefficient Γ [$\mu m^2 s^{-\alpha}$]. The motion of CD63 and ApoE was classified into confined diffusion ($\alpha \leq 0.1$), obstructed diffusion ($0.1 < \alpha <$ 0.9), normal diffusion ($0.9 \leq \alpha < 1.1$), and directed motion ($\alpha \geq 1.1$) [113]. To quantify the diffusion coefficient D [$\mu m^2 s^{-1}$], he fitted the normal diffusion model $MSD(\Delta t) = 4\,\Gamma\,\Delta t$ to the MSD values.

2.6.3. Colocalization analysis of ApoE^{mT2} and CD63^{mCherry}

To quantify interactions between ApoE and CD63, automatic colocalization was performed using the computed trajectories with a minimum of 10 time points (corresponding to a time duration of 32.5 s). For each time point, colocalization was determined using a graph-based k-d-tree approach which efficiently computes a nearest neighbor query based on Euclidean distances. An ApoE particle is considered to be colocalized with a CD63 particle, if the ApoE particle has a nearest CD63 particle within a maximum distance for at least a minimum number of consecutive frames. Otherwise, the ApoE particle is considered as non-colocalized with a CD63 particle. He used a maximum distance of 5 pixels (corresponding to 0.449 μm) and a minimum number of four consecutive frames (corresponding to 13 s). The computed colocalization information was visualized by color representations, and the motility of colocalized and non-colocalized ApoE was quantified by a MSD analysis.

2.6.4. Analysis of directed motion of ApoE colocalized with CD63

To quantify the directed motion of colocalized ApoE, he performed a MSD analysis [112] using the computed colocalized trajectories of ApoE and CD63. To robustly classify the motion type into directed and non-directed motion of colocalized ApoE, he fitted for each trajectory the anomalous diffusion model $MSD(\Delta t) = 4\,\Gamma\,\Delta t^{\alpha}$ to the MSD values in two intervals from $\Delta t = 0$ s to 25 s and from $\Delta t = 0$ s to 60 s. Directed motion is considered if for one of the intervals he has $\alpha \geq 1.1$, otherwise non-directed motion is considered. For the classified trajectories, the MSD curves were averaged to obtain a MSD curve for colocalized ApoE with directed and non-directed motion, and the motion was quantified by the transport coefficient Γ [$\mu m^2 s^{-\alpha}$], the diffusion coefficient D [$\mu m^2 s^{-1}$], and the anomalous diffusion exponent α.

2.7. Quantification and statistical analysis

Unless otherwise stated, differences between sample populations were evaluated using a two-tailed, unpaired Student's t-test provided in the GraphPad Prism 8 software package. Differences with P-values less than 0.05 are considered to be significant and shown on the graph. The sample size of each experiment is specified in the corresponding figure legend.

III. RESULTS

1.   Identification of HCV assembly sites

The first chapter of the RESULTS section describes my attempts to faithfully identify HCV assembly sites. These studies were performed mainly during May 2018 - May 2020. I established an intact and fully functional FP-tagged ApoE along with engineered HCV genomes encoding FP-tagged NS5A and E2. I used these to employ live-cell imaging with the aim to observe the convergence of these three assembly factors, and CLEM to characterize the ultrastructure at the sites of these converged signals in HCV-replicating cells.

1.1.   Rationale and approach to identify HCV particle assembly events

Since the discovery of HCV in 1989, a lot of effort has been made by numerous groups to visualize HCV virions and assembly sites, but no conclusive results were obtained. In 2019, Lee *et al.*, suggested that HCV assembly might take place at the DMV-connected ER in apposition to lipid droplets where NS5A and E2 co-localize [21]. I hypothesized that luminal ApoE should come close to the budding virions at the NS5A-E2 double-positive puncta because several lines of evidence indicated that HCV particles acquire ApoE-containing lipoproteins intracellularly. Therefore, I employed live-cell confocal imaging to visualize ApoE-NS5A-E2 triple-positive signals and CLEM to examine the subcellular structure at these sites. This working hypothesis is summarized in Figure 13.
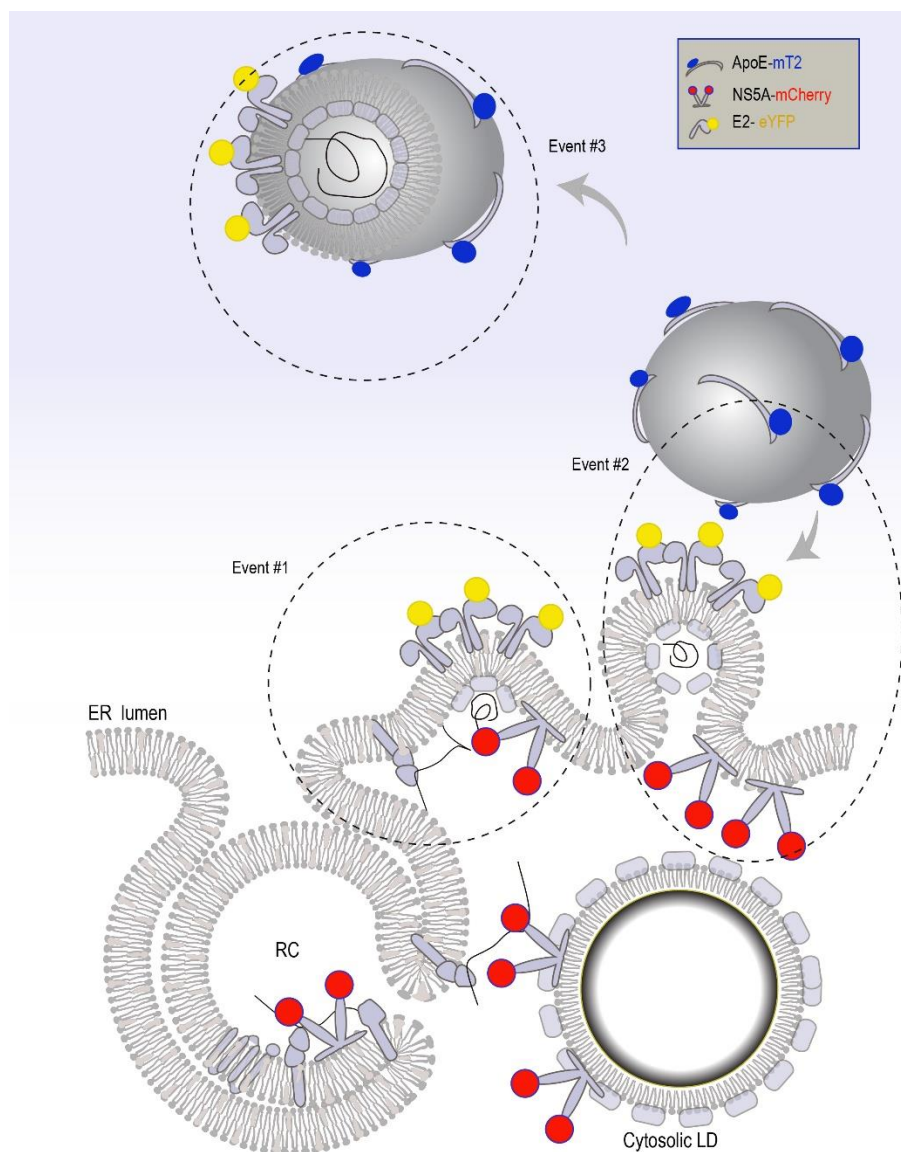
Figure 13. Working hypothesis and visualization of HCV particle assembly events

Spatial-temporal regulation of HCV assembly events and visualization by time-lapse confocal imaging. Event #1: formation of nascent HCV particles at NS5A-E2 localizing ER adjacent to a NS5A-localizing cytosolic lipid droplet and a replication complex (E2-NS5A positive structure). Event #2: budding of the HCV particle into the ER lumen coupled to ApoE-coating of the particles (E2-NS5A-ApoE positive structure). By CLEM, I aimed to identify HCV particles at this site. Event #3: maturation of HCV particles. The ApoE-coated HCV particle leaves the budding site to enter the maturation process (E2-ApoE positive structure). RC: replication complex.

1.2. Establishment of fully functional fluorescently tagged ApoE

Live-cell imaging of ApoE requires a suitable fluorescent protein tag that preserves the integrity of the fusion protein as well as its normal function. GFP was previously selected for ApoE labeling but ApoE-GFP fusion protein showed significant fragmentation and was not fully functional [114]. Therefore, I aimed to seek for an alternative tag, originally red fluorescent proteins (RFPs). Endogenously expressed ApoE of Lunet cells was stably knocked down by an

ApoE shRNA [64] and these cells were further stably reconstituted with different RFP variants-tagged ApoE (Figure 14).
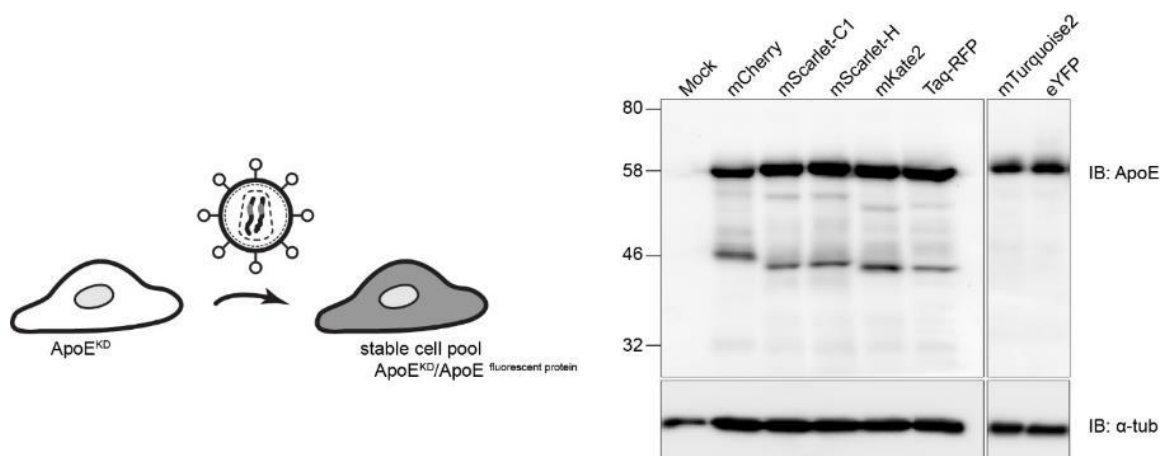
Figure 14. Intact labeling of ApoE with mTurquoise2 and eYFP

[Left] Illustration of the experimental design.
[Right] Lunet/ApoE-KD cells were transduced with lentiviruses containing different fluorescent protein tagged-ApoE variants as indicated and stably selected. Cell lysates were immunoblotted with anti-ApoE antibody. α tubulin antibody was used as a loading control.

In addition to the major full-length forms (~58-kDa bands) which were detected by anti-ApoE antibody (upper, left), ApoE-RFPs were also partially truncated into smaller ~46 kDa fragments. This was probably due to the hydrolysis of the N-acylimine group of the DsRed-like chromophores in these fluorescent proteins, especially under the acidic condition of late endosomes that I expect ApoE might reside therein. ApoE was then labeled with mTurquoise2 and eYFP. As expected, ApoE^{mT2} and ApoE-eYFP showed no fragmentation of the fusion proteins (upper, right). Because mTurquoise2 is a cyan rapidly-maturing monomer with very low acid sensitivity (pkA=3.1) [115], I selected this protein for subsequent characterization. Importantly, ApoE^{mT2} showed normal secretion into cell culture supernatant (Figure 15).
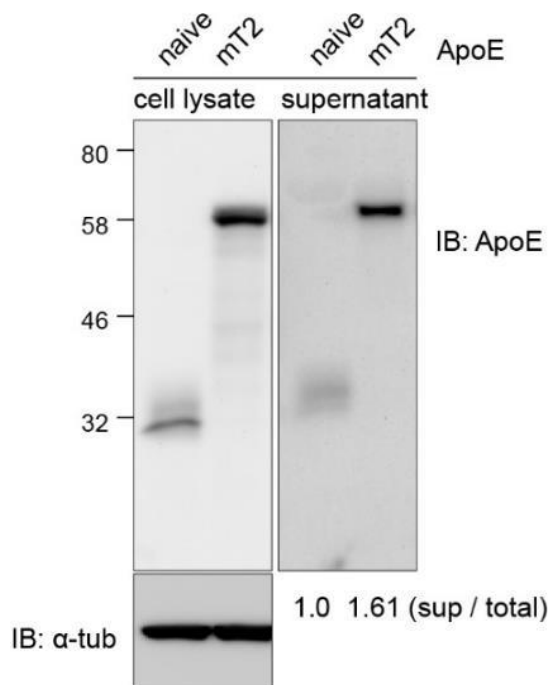
Figure 15. Normal secretion of ApoE^{mT2}

Lunet/ApoE-KD cells were transduced with lentiviruses containing mTurquoise2-tagged ApoE and stably selected. Cell lysate and cell culture supernatant were immunoblotted with anti-ApoE antibody and anti-α-tubulin antibody.

Secreted ApoE^{mT2} was fractionated by a sucrose density gradient to examine its lipid-binding property (Figure 16). Extracellular ApoE^{mT2} showed a marginal shift in density (peaked at 1.05 g/ml) as compared to wild-type ApoE of naïve cells (1.04 g/ml), indicating the maintenance of its lipoprotein binding property.
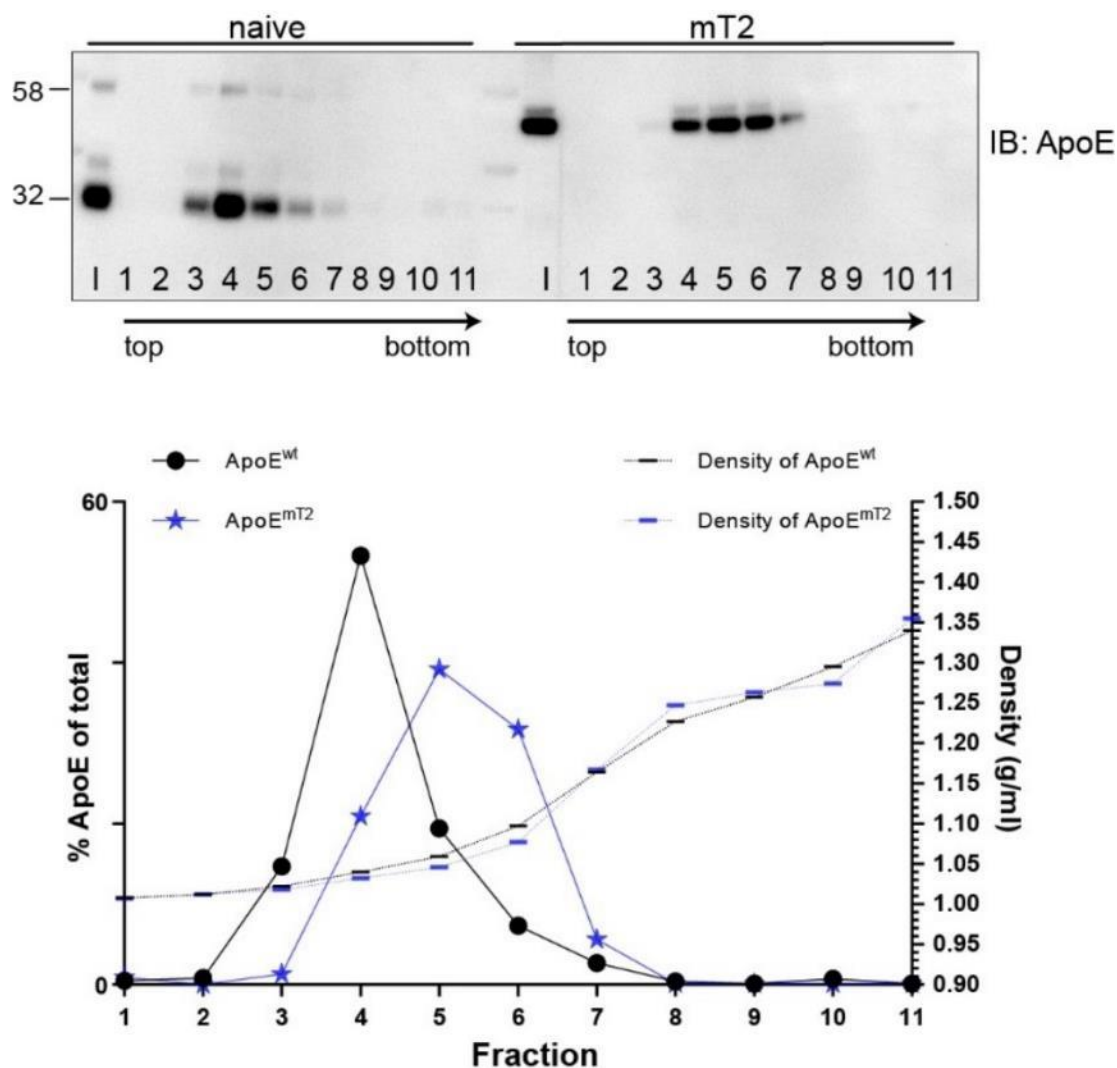
Figure 16. Density of secreted ApoE^{mT2}

Conditioned media of ApoE^{wt} and ApoE^{mT2} reconstituted cells from (Figure 15) were subjected to 10-50% iodixanol isopycnic centrifugation and fractionated into 11 fractions from top to bottom.
[Upper] Inputs and collected fractions were immunoblotted with anti-ApoE antibody.
[Lower] ApoE intensity from the upper panel was quantified. Percent ApoE of total and density of each fraction (g/ml) are shown. Data are from a representative experiment (n=2).

In addition to weak diffuse fluorescent pattern, ApoE^{mT2} showed strong dotted signals overlapping well with endogenously expressed ApoB (Figure 17, arrowheads). This further confirmed its normal lipoprotein affinity. Of note, although ApoE could be generally detected by anti-ApoE antibody staining in fixed conditions, dotted ApoE structures are very dim and not well visualized by this method. In contrast, dotted mTurquoise2 signals of mTurquoise2-tagged ApoE are much brighter, allowing more informative detection of ApoE, especially in the live-cell imaging condition.
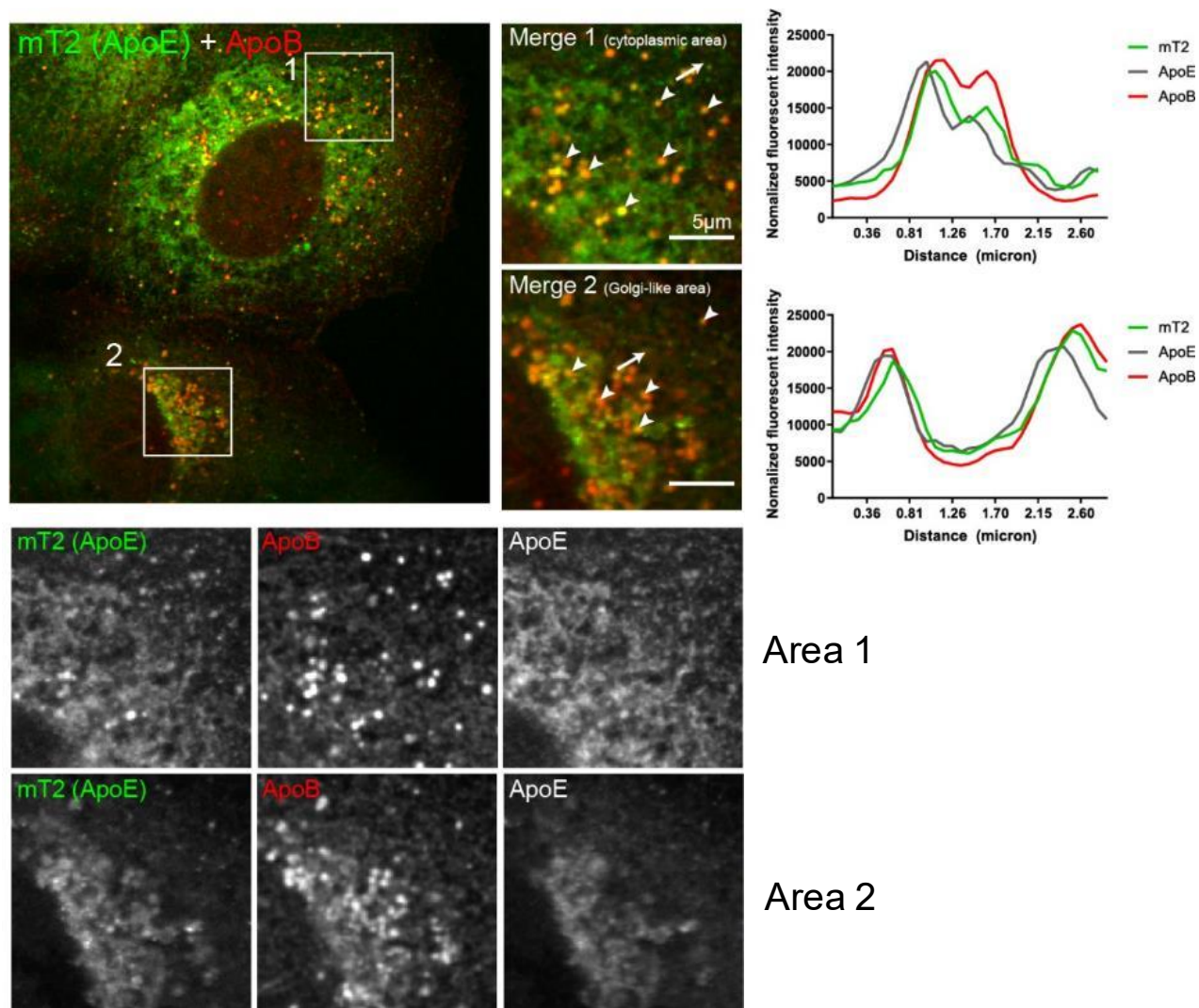
Figure 17. Normal lipid binding property of ApoE^{mT2}

Immunofluorescent staining of ApoE^{mT2} in ApoE^{mT2} -reconstituted Lunet/ApoE-KD cells with anti-ApoE antibody and anti-ApoB antibody. Note that ApoB is a marker of lipoproteins.
[Upper] The overview image is shown on the left (ApoE staining by ApoE-specific antibody is not shown for a reason of simplicity). Merge 1 and 2 are magnified views of two selected areas in the overview image. Arrowheads: overlapped signals of ApoE^{mT2} and ApoB in cropped images. Plot profiles on the upper right panels are from white arrows in Merge 1 and 2 images.
[Lower] Split channels of Merge 1 and Merge 2 images.

I further investigated how ApoE^{mT2} signals look like in ApoE-empty cell lines including HEK293T and Hela when ApoE was ectopically expressed. As expected, ApoE^{mT2} showed remarkably strong dotted signals in both cell lines, suggesting the formation of ApoE-containing lipoproteins (Figure 18).
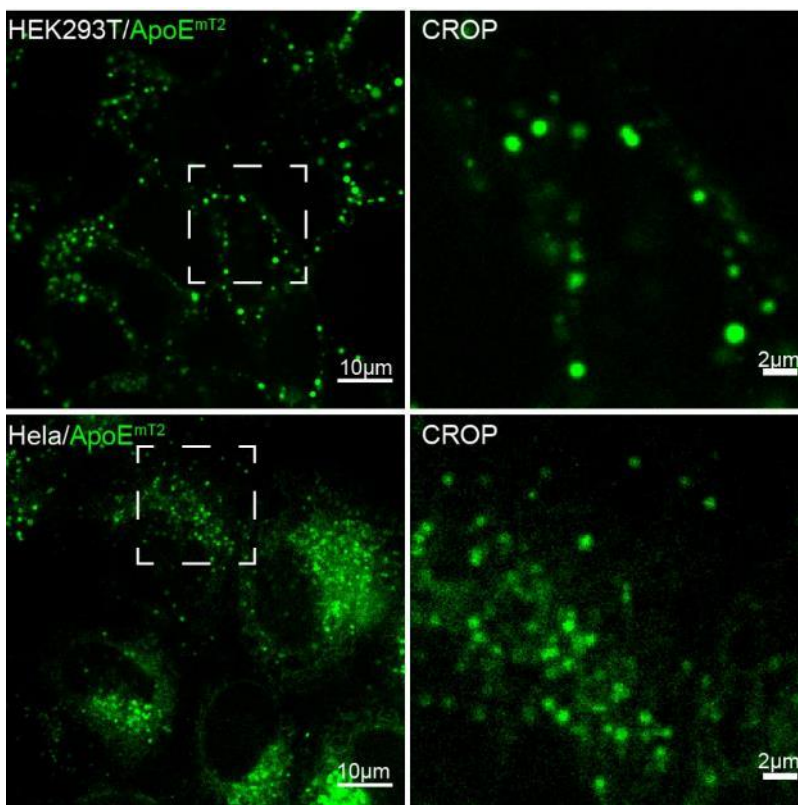
Figure 18. Subcellular distribution of ApoE^{mT2} in HEK293T and Hela cells

HEK293T and Hela cells were transduced with lentiviruses containing ApoE^{mT2} and stably selected. Cells were further subjected to live-cell confocal microscopy. Boxed areas in the left panels are shown as enlarged views in the panels on the right of each row.

Given that mTurquoise2 is suitable for ApoE labeling, I subsequently validated the functional contribution of ApoE^{mT2} to HCV production. To this end, I employed HCV Renilla luciferase reporter virus JcR2a [44], and firstly used the lipoprotein-empty HEK293T-miR122 cell line that supports HCV RNA replication but does not render HCV particle formation. Importantly, solely ectopic expression of ApoE can act as a "switch" that turns on HCV particle production [95]. ApoE^{mT2} constituted HEK293T-miR122 cells showed a similar trend in HCV RNA replication kinetics after electroporation of HCV RNA as compared to ApoE^{wt} (Appendix Figure 2). As expected, empty vector reconstituted control cells showed no or marginal HCV core secretion, indicating no virus production in ApoE-free cells (Figure 19, left). By contrast, ApoE^{mT2} and ApoE^{wt} expressing cells similarly exhibited high level of core secretion demonstrating the detrimental contribution of ApoE to HCV production as well as the functional maintenance of mTurquoise2 tagging. I further inoculated the conditioned media of these cells to naïve Huh7.5 cells to examine the transmission ability of produced HCV (Figure 19, right). Consistently, extracellular HCV produced in ApoE^{mT2} expressing cells showed normal virus infectivity.
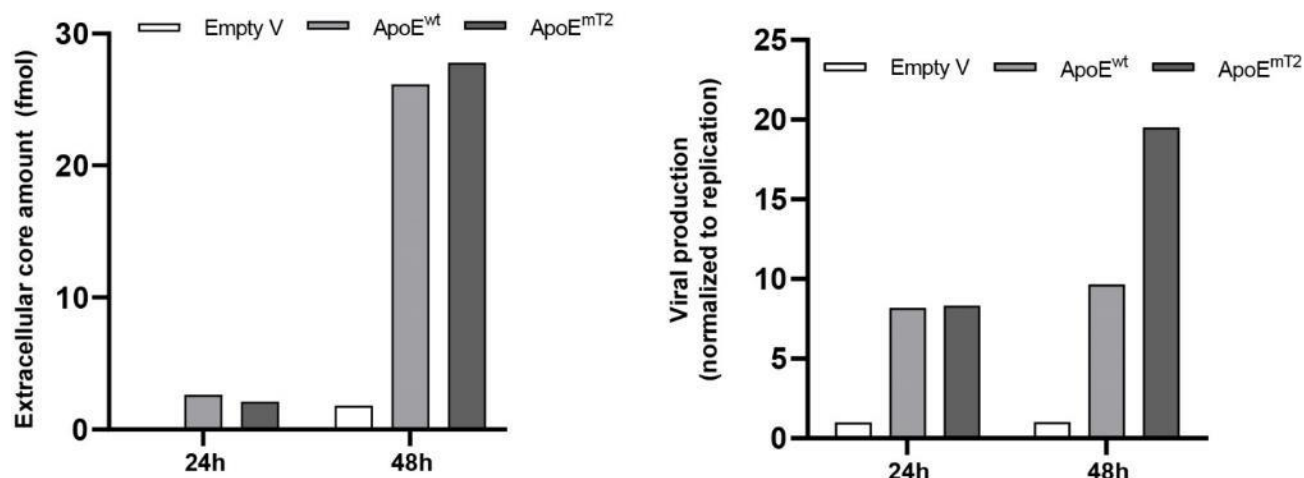
Figure 19. Functional validation of ApoE in HCV transmission

[Left] HEK293T-miR122 cells were transduced with either an empty vector (Empty V), ApoE^{wt}, or ApoE^{mT2}, respectively. Cells were then electroporated with *in vitro*-transcribed Renilla luciferase (RLU)-reporter HCV-JcR2a RNA. The amounts of extracellular core protein (fmol) detected in culture supernatant at 24 and 48 h post-electroporation by core CMIA for a representative experiment (n=2) are shown.
[Right] Infectivity of HCV produced in HEK293T-miR122/ApoE^{mT2} cells. HCV-containing supernatants harvested at indicated time points were used to inoculate naïve Huh7.5 cells. HCV infectivity measured by RLU activity at 72 h after inoculation normalized to HCV RNA replication are shown. Data are means for a representative experiment (n=2).

Taken together, these data clearly demonstrate that ApoE^{mT2} fully supports HCV production. Furthermore, since HCV has hepatotropism under physiological conditions, I further validated the functional complementation of ApoE^{mT2} in stable ApoE-knockdown Lunet cells. As a result, I observed that ApoE^{mT2} contributed to HCV production and infectivity although the experimental window was not very impressive (Figure 20). This is probably because of the functional redundancy of a mixed variety of apolipoproteins expressed in the Huh7-based cell line [116, 117].

During this course of my doctoral research, I also characterized multiple other ApoE mutants including ApoE with defects in secretion (ApoE-KDEL; KDEL: ER-retention signal), lipid binding (ApoE C-terminal deletion), and ApoE with normal secretion but abnormal monomer-tetramer equilibrium (ApoE-CRAC mutants; CRAC: cholesterol recognition/interaction amino acid consensus sequence). All these types of ApoE mutants did not favor the production of infectious HCV, indicating that the normal secretion, lipid binding, and equilibrium are crucial for the

maintenance of its contribution to HCV production (refer to the chapter 1 of the APPENDIX section).
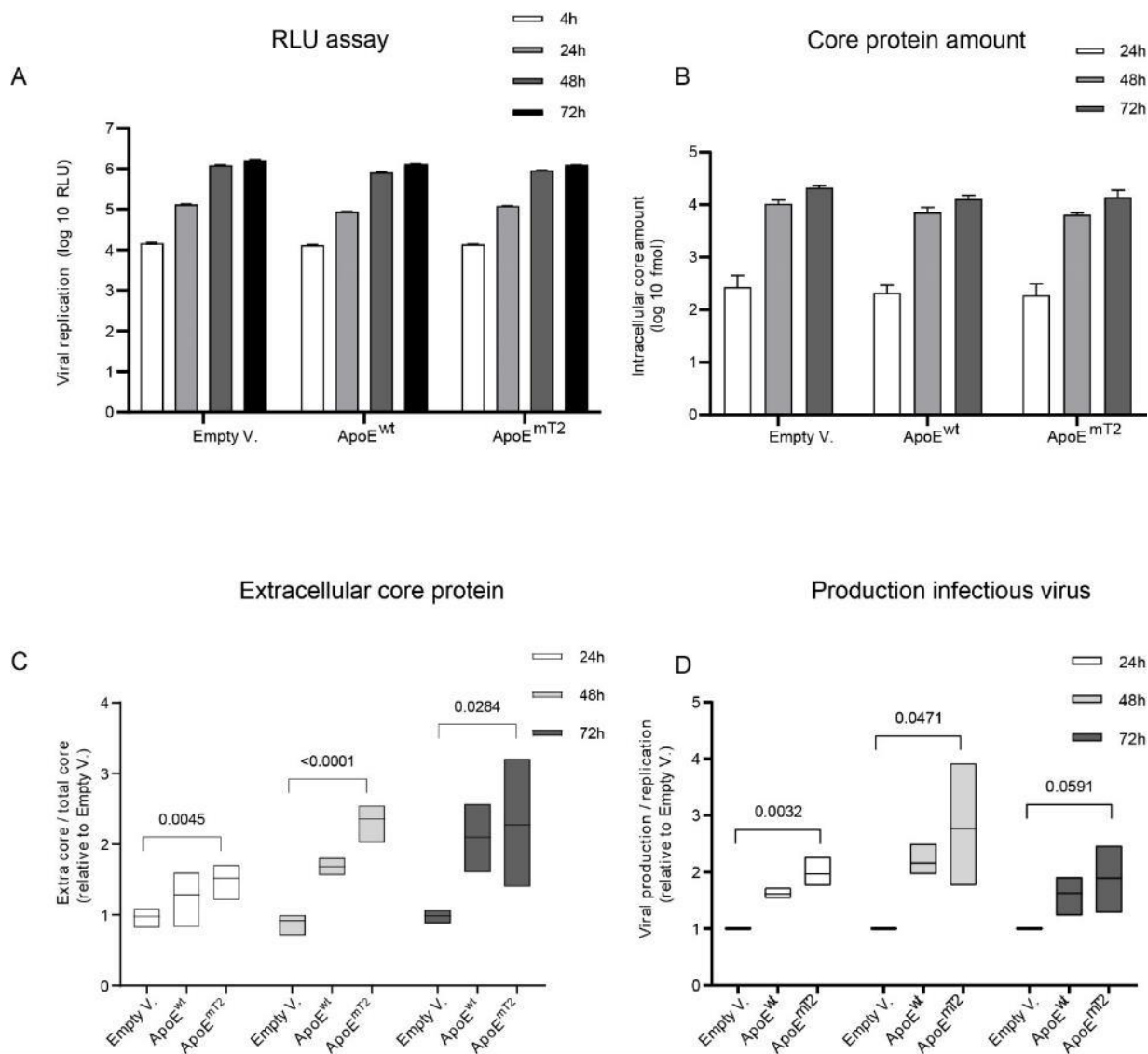
Figure 20. Functional validation of ApoE^{mT2} in HCV transmission in Lunet/ApoE-KD cells

A) Lunet/ApoE-KD cells were transduced with either an empty vector (Empty V.), ApoE^{wt} or ApoE^{mT2}, respectively and electroporated with *in vitro*-transcribed Renilla luciferase (RLU)-reporter HCV-JcR2a RNA. The replication of HCV at indicated time points were measured by RLU activity.
B) The amounts of intracellular core protein (fmol) from A at indicated time points were measured by Core CMIA.
C) The amounts of extracellular core protein detected in culture supernatant from A at indicated time points were measured by Core CMIA. Ratios of extracellular core to total core are shown. Data are medians (range) from three independent experiments. P-value was determined using unpaired Student's *t*-test.
D) Infectivity of HCV produced in Lunet/ApoE^{mT2} cells

HCV-containing supernatants harvested at indicated time points were inoculated into naïve Huh7.5 cells. HCV infectivity was measured by RLU activity at 72 h after inoculation. HCV infectivity normalized to HCV RNA replication is shown. Data are medians (range) from three independent experiments. P-value was determined using unpaired Student's *t*-test.

1.3. Ultrastructure of co-trafficking ApoE, NS5A and E2 puncta and dependency on virus assembly competence

Given that mTurquoise 2 tagging retains full functionality of ApoE, I labeled NS5A and E2 with two other FPs harboring the spectrally distinct or barely overlapping excitation/emission spectra. Therefore, I selected mCherry and eYFP for the labeling of NS5A and E2, respectively and created the HCV trans-complementation particle (TCP) system based on a previous report [21], splitting the HCV genome into an "assembly module" and a "replication module", allowing the live-cell imaging under biosafety level 2. The schematics of the FP-labeled HCV assembly factors are shown in Figure 21, upper panel.
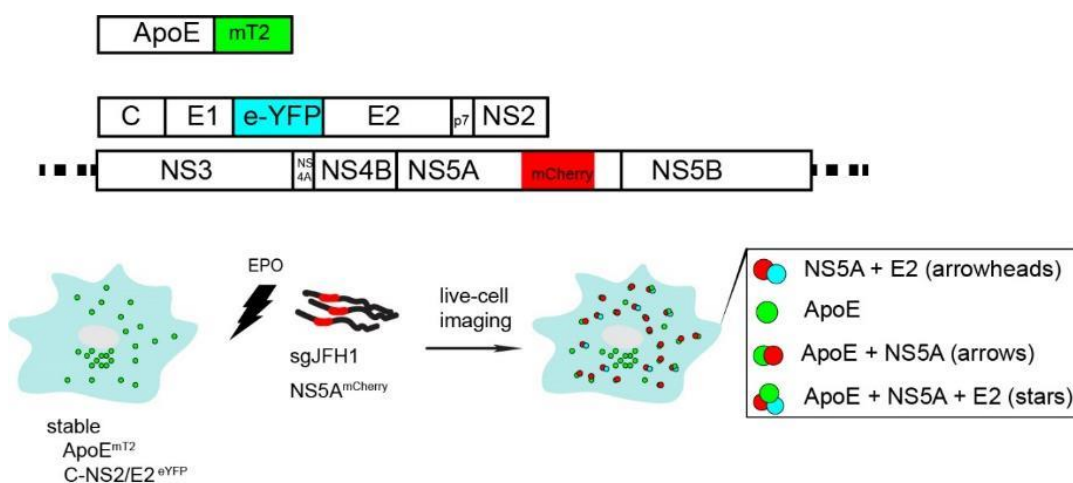
Figure 21. Illustration of the experimental approach to monitor ApoE, NS5A and E2 co-trafficking

[Upper] Schematic representation of ApoE tagging and HCV E2 and NS5A tagging of the trans-complemented HCV genome with indicated fluorescent proteins.
[Lower] Schematic representation of the experimental procedure to monitor ApoE, NS5A, and E2 positive structures and their co-trafficking.

The experimental approach to visualize ApoE, NS5A and E2 trafficking with the expected overlapping signals is described in Figure 21, lower panel. I examined a) the formation of NS5A-E2 foci as described previously [21] and b) ApoE-NS5A-E2 triple-positive as well as ApoE-exclusive or ApoE-NS5A double-positive signals according to my hypothesis summarized in Figure 13. For this purpose, I electroporated the HCV "replication module" RNA harboring NS5A^{mCherry} coding sequence into the cells stably expressing ApoE^{mT2} and HCV "assembly module" with eYFP-tagged E2.

Initially, to have the overall impression of how ApoE, NS5A and E2 behave during the course of HCV infection, I acquired live-cell time-lapse images with the confocal spinning disc microscope every 30 min from early infection to late infection (5 to 54 h post-electroporation) with minimum laser exposure to avoid phototoxicity. Prior to the electroporation of *in vitro*-transcribed RNA of the nonstructural part, E2 showed a weak reticular ER-like pattern. Upon electroporation, at early infection (~24 h.p.e), NS5A induced changes in E2 distribution and formed NS5A-E2 foci as expected (Figure 22, arrowheads, movie 1). ApoE-NS5A-E2 foci were formed at a later time point but the number of events was very low (Figure 22, stars).
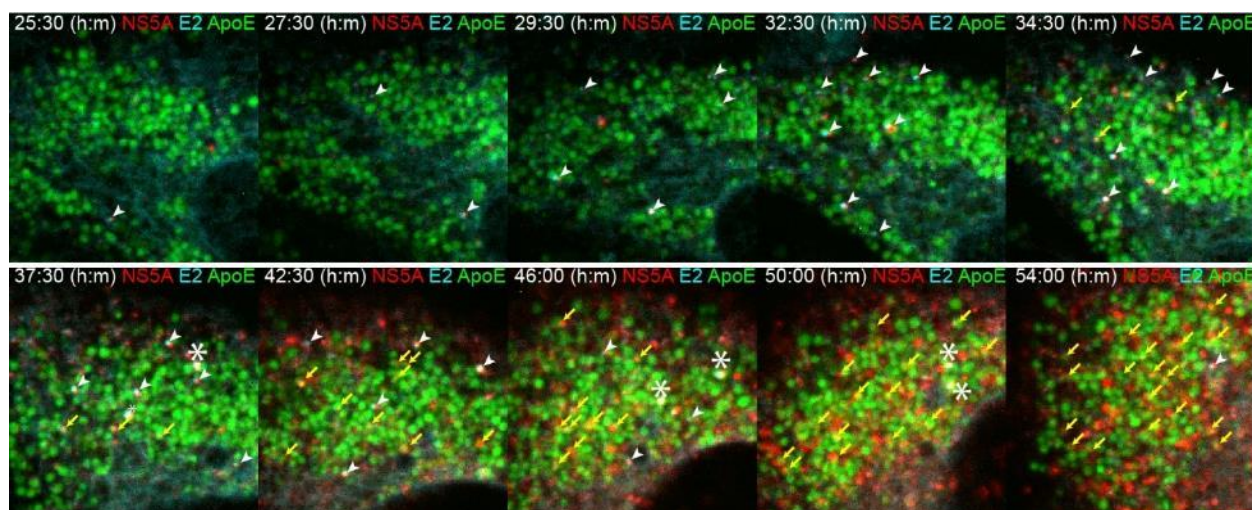
Figure 22. Co-trafficking of HCV-assembly factors ApoE, NS5A, and E2 in HCV-replicating cell

Lunet/ApoE^{mT2} cells harboring HCV Core-NS2/E2^{eYFP} were electroporated with *in vitro*-transcribed sgJFH1/NS5A^{mCherry} RNA. Cells were subjected to live-cell confocal imaging from 5 to 54h.p.e (30 min/frame) to observe ApoE, NS5A and E2 signals. Extracted time points from early infection (at 25.5 h.p.e) to late high HCV infection (at 54 h.p.e) are shown. Arrow heads: NS5A-E2 foci; arrows: ApoE-NS5A positive signals; stars: ApoE-NS5A-E2 positive signals.

Thereafter, I further confirmed the relatively high number of NS5A-E2 foci and the scarcity of ApoE-NS5A-E2 foci at late infection by live-cell imaging with a stronger laser exposure and shorter time interval (10 sec/frame) setting. Of note, triple-colocalizing dots of ApoE-NS5A-E2 existed for many minutes after forming. An example of the convergence of ApoE signal with NS5A-E2 puncta and its subsequent separation therefrom is shown in Figure 23 and movie 2.
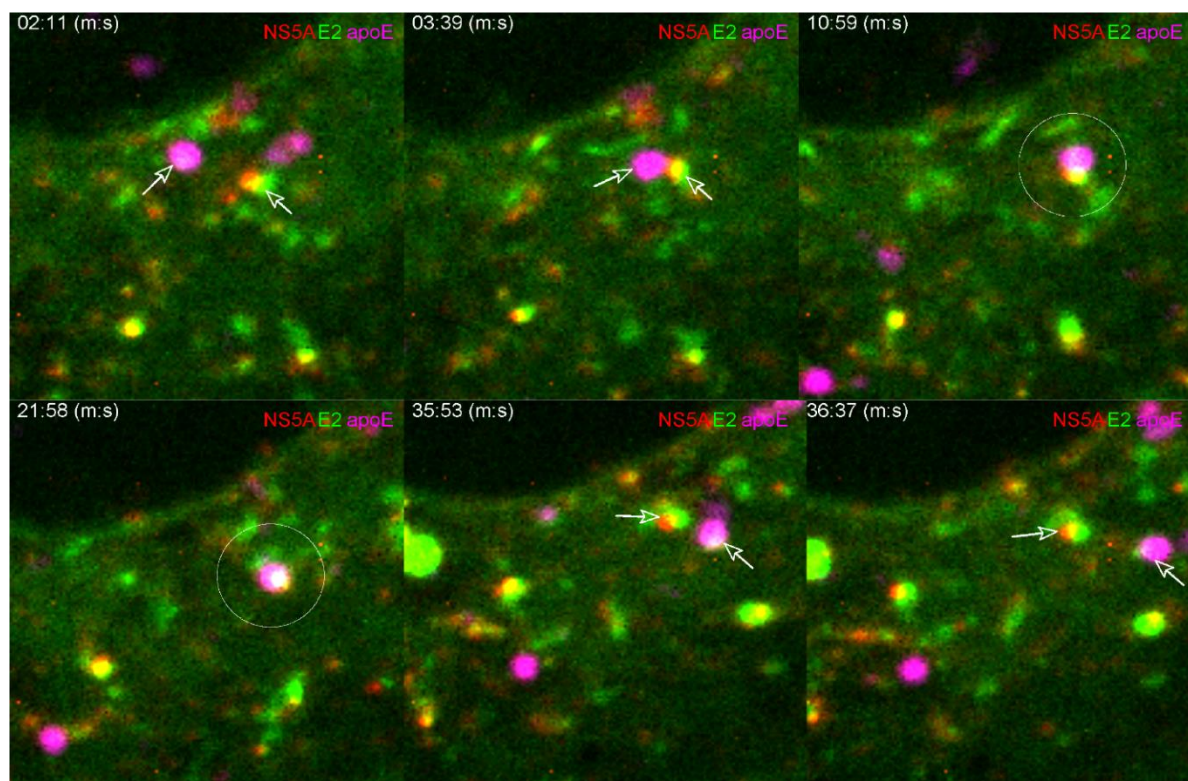
Figure 23. Spatio-temporal convergence and divergence of ApoE and NS5A-E2 double-positive signals

Lunet-ApoE^{mT2} cells harboring HCV "assembly module" Core-NS2/E2^{eYFP} were electroporated with *in vitro*-transcribed sgJFH1/NS5A^{mCherry} RNA. Cells were subjected to live-cell confocal imaging at 36 h.p.e (10 sec/frame) to observe ApoE, NS5A, and E2 signals. Circles: converged ApoE-NS5A-E2 signals.

Next, I combined CLEM with live-cell imaging to figure out the ultrastructure behind the converging ApoE-NS5A-E2 signals. For this purpose, I recorded IF images of these structures for 10 min with short-term interval setting (e.g 5 sec/frame). Thereafter, cells were fixed immediately on the imaging stage with 0.2% glutaraldehyde-containing fixative that preserves the IF signals and incubated with LipidTox for subsequent imaging of lipid droplets that were later used as fiducial markers for the correlation of the IF and EM micrographs. Cells were further fixed with the EM

fixative and processed for EM imaging. Thereafter, I analyzed the IF data and searched for the ApoE-NS5A-E2 foci and acquired high-resolution EM images at these sites to find the assembling HCV particles. The schematic of the experimental approach is summarized in Figure 24. Unfortunately, in spite of many efforts, I did not observe any distinct structures that could be unambiguously assigned to an HCV particle. Since later I found that ApoE is heavily enriched in late endosomes, my experimental strategy potentially identified endosome-ER contact sites established during HCV infection.
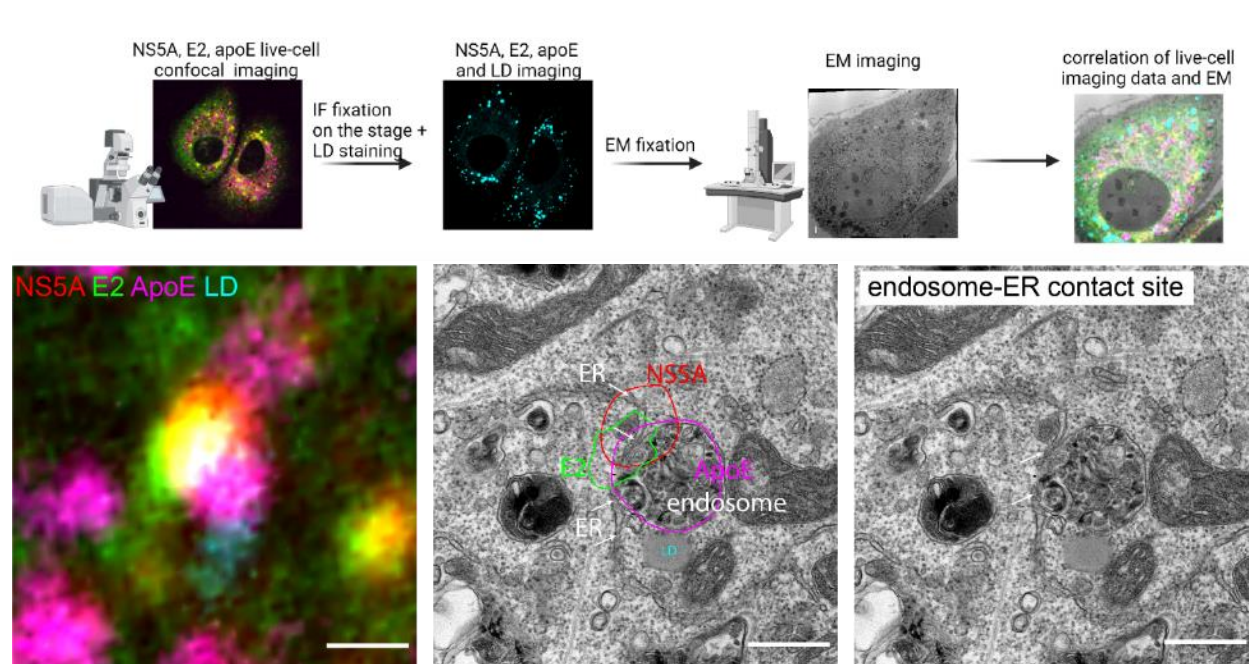
Figure 24. Integrative imaging approach to visualize HCV assembly at the sites correlating with ApoE-NS5A-E2 triple-positive structures

[Upper] Lunet-ApoE^{mT2} cells stably expressing Core-NS2/E2^{eYFP} were electroporated with *in vitro*-transcribed sgJFH1/NS5A^{mCherry} RNA. Cells were subjected to time-lapse live-cell confocal imaging at 36 h.p.e to observe ApoE-, NS5A- and E2-positive signals. Cells were further fixed immediately on the stage after live-cell imaging and stained with LipidTox to label lipid droplets. Thereafter, cells were subjected to EM preparation to visualize the ultrastructure at the sites of ApoE-NS5A-E2 triple-positive signals. Lipid droplets were used as fiducial markers for the correlation of light and electron micrographs.

[Lower] Example of the ultrastructure found at an ApoE-NS5A-E2 triple-positive site. Left, ApoE-NS5A-E2 triple-positive puncta. Middle, contours of converged signals shown in the left image on top of the EM image. Right, correlated electron microphraph (without contours) showing an endosome-ER contact site. Scale bar: 500nm.

2. Discovery of the intercellular transmission of HCV RNA by Apolipoprotein E-associated NS5A-containing extracellular vesicles

ApoE has been shown to predominantly interact with NS5A and the E2 glycoprotein [41, 42, 64, 68]. While the ApoE-NS5A interaction appears to be critical for HCV particle production, NS5A was also suggested to be released via EVs [87, 88] raising the question of whether ApoE might play a role also in this process. Taking advantage of my live-cell imaging system, I shifted the focus of my project towards the investigation the role of NS5A and ApoE in the formation of EVs released from HCV-replicating cells. Obtained results are described in the second chapter of this RESULTS section.

2.1. Accumulation of NS5A - ApoE double-positive structures independent of HCV assembly

As described above (Figure 22), ApoE-NS5A double-positive puncta appeared late during HCV infection (~34.5 h.p.e) and clearly exceeded the number of NS5A-E2 double-positive puncta, assumed to correspond to HCV assembly events (movie 3 and Figure 25).
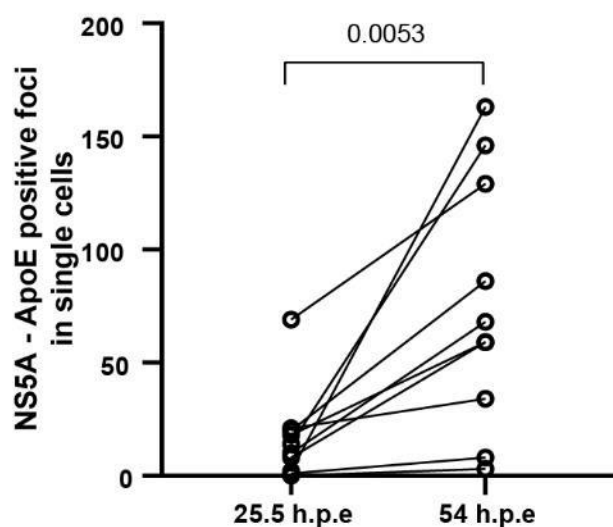
Figure 25. The number of NS5A-enriched ApoE-vesicular signals

The number of NS5A-ApoE foci quantified in single cells (10 cells) exemplarily shown in Figure 22 by using the Colocquant software package.

I then confirmed the colocalization of NS5A expressed from the full-length highly assembly-competent HCV Jc1 strain with ApoE in ApoE^{mT2} expressing cells. Partial permeabilization with digitonin prior to NS5A staining showed PDI-devoid NS5A signals overlapping with vesicular ApoE signals (Figure 26A and 26B) confirming that the trans-complementation system faithfully recapitulates assembly events occurring in natural infection.

A

B
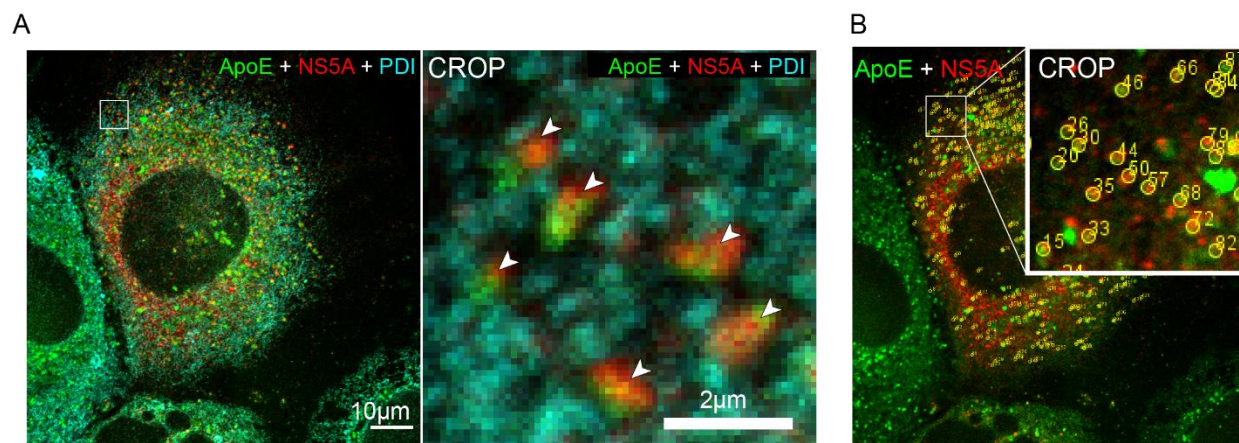
Figure 26. ApoE-NS5A colocalization in HCV Jc1-infected cells

A) ApoE-NS5A colocalization in HCV Jc1-infected cells
Lunet/ApoE^{mT2} cells were electroporated with *in vitro*-transcribed HCV Jc1 RNA. At 54 h.p.e cells were fixed and partially permeabilized with 5 µg/ml digitonin in PBS, and incubated with anti-NS5A and anti-PDI antibody for subsequent immunofluorescent staining, and were further imaged with confocal microscopy. Arrowheads point to PDI-devoid ApoE-NS5A signals.
B) An example of ApoE-NS5A dot detection and visualization by ColocQuant and ColocJ. ApoE-NS5A positive signals from A were detected by Colocquant and visualized by ColocJ.

I further demonstrated that NS5A deposition into vesicular ApoE sites was not linked to the formation of HCV particle assembly as I could detect time-dependent formation of NS5A-ApoE foci in cells unable to support HCV assembly conditions, e.g by using a mutant lacking the essential HCV assembly factor NS2 (Figure 27).

A

B
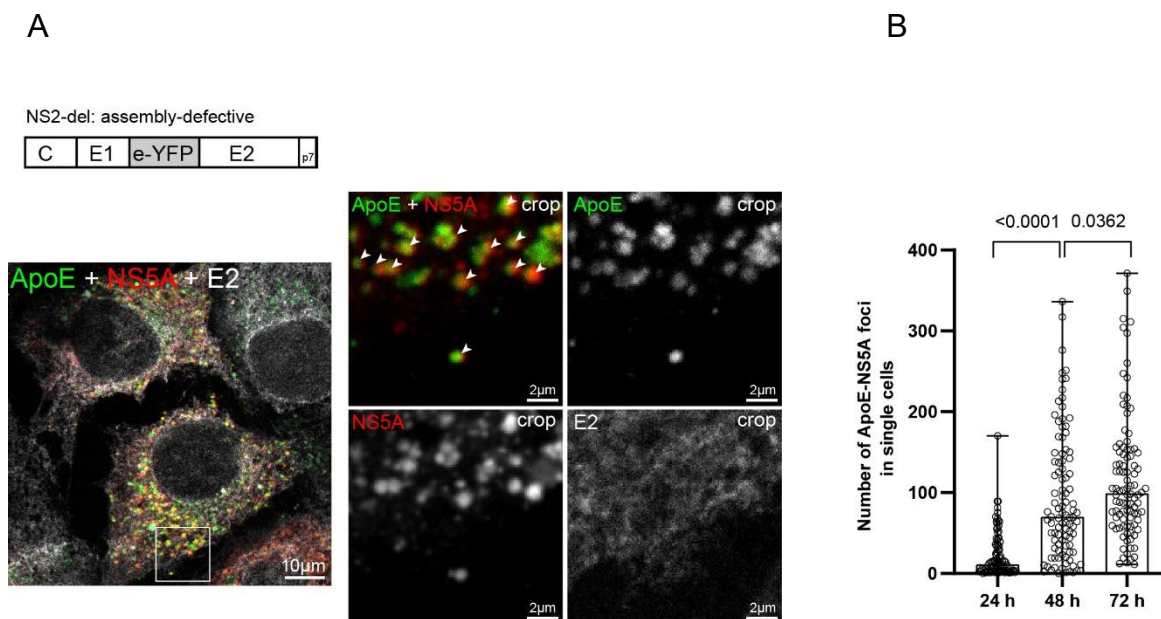
Figure 27. Assembly-independent enrichment of NS5A into ApoE vesicular signals

A) [Upper] Schematic representation of HCV "assembly module" lacking NS2
[Lower] Lunet-ApoE^{mT2} harboring HCV Core-P7/E2^{eYFP} (NS2-del) was electroporated with *in vitro*-transcribed sgJFH1/NS5A^{mCherry} RNA. At 72 h.p.e, cell were fixed and subjected confocal imaging to observe ApoE, NS5A, and E2 signals. Images on the right are magnified views from the selected area in the left overview image. Arrowheads: ApoE-NS5A positive signals

B) Quantification of the number of NS5A-ApoE foci at indicated time points. Each dot represent single cells. Data are medians (range) of the number of detected foci. P-value was determined using unpaired Student's *t*-test.

Taken together, I showed the massive enrichment of NS5A into dotted ApoE signals at a post-assembly time point of HCV infection; and this enrichment is not dependent on the formation of HCV virions.

2.2. ApoE and NS5A colocalize in regions enriched for endosomes containing intraluminal vesicles

By CLEM, I further demonstrated that NS5A-ApoE double-positive dots corresponded to endosomes (Figure 28A, overlay panel, dashed circles surrounding yellow signals).
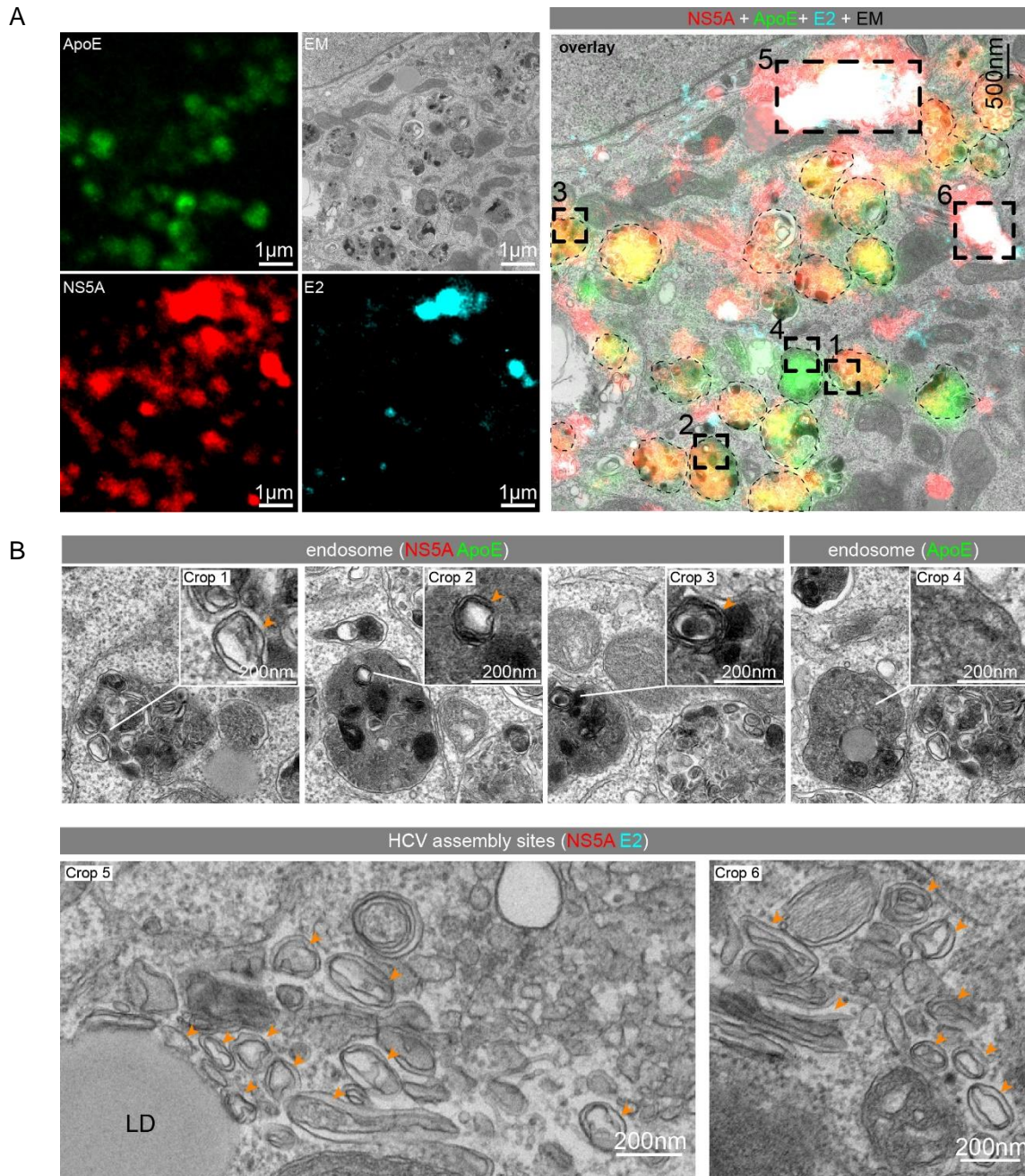
Figure 28. ApoE^{mT2} and NS5A colocalize in regions enriched for endosomes

A) Lunet-ApoE^{mT2} cells harboring HCV Core-NS2/E2^{eYFP} were electroporated with *in vitro*-transcribed sgJFH1/NS5A^{mCherry} RNA (refers to Figure 22). At 48 h.p.e cells were analyzed by a CLEM method to examine the ultrastructure at the sites of the ApoE-NS5A positive signals. Stained lipid droplets with lipidTox were used as fiducial markers for the correlation of IF and EM micrographs. Dashed circles in the overlay image correspond to ApoE-containing endosomes.

B) Magnified views of cropped regions indicated in A). Cropped 1, 2, 3: ApoE-NS5A positive endosomes; crop 4: a NS5A-negative endosome; crop 5 and 6: NS5A-E2 positive areas: putative HCV assembly sites.

66

Strikingly, inside these endosomes, I detected many intraluminal vesicles having double/multi-membranous structures (Figure 28B, crop 1, 2 and 3, arrowheads) which were mostly absent in NS5A-negative endosomes (crop 4). NS5A-E2 positive sites, (Figure 28B, dashed rectangles 5 and 6) correlated to typical membrane landscapes of HCV assembly sites consisting of double-membrane vesicles (DMVs) that are often in close proximity to a lipid droplet (Figure 28B, crop 5 and 6) [21].

2.3. Evidence for the formation of NS5A and CD63-positive intraluminal vesicles inside ApoE-containing late endosomes

So far, my data demonstrated the highly abundant formation of NS5A-ApoE double-positive structures which are formed independent from HCV assembly and possibly relevant to HCV-induced EV formation or release. Because HCV has been documented to transmit its RNA via virion-free CD63-positive exosomes, I investigated the association of ApoE-NS5A containing structures with the IV/endosomal marker CD63 by using super-resolution stimulated emission depletion (STED) microscopy. For this purpose, I replaced FP labels of ApoE and NS5A by SNAPf and CLIPf, respectively to allow observation of different combinations of overlapping signals as summarized in Figure 29.
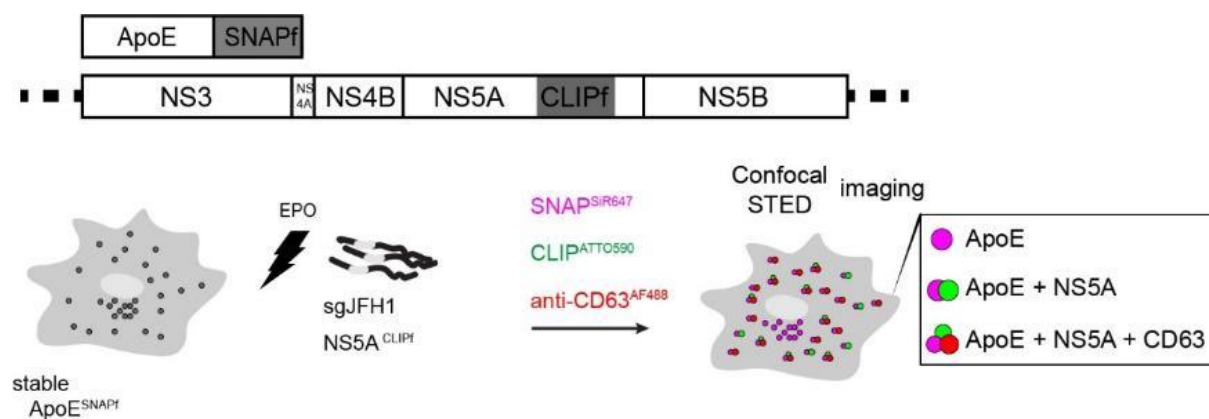
Figure 29. Experimental approach to visualize ApoE and NS5A double-positive structures by super-resolution microscopy

[Upper] Schematic representation of ApoE tagging and NS5A tagging of the HCV sgJFH1 with SNAPf and CLIPf, respectively.
[Lower] Schematic representation of experimental procedure to image ApoE and NS5A by STED microscopy.

ApoE^{SNAPf} fusion protein showed no fragmentation and was secreted efficiently into cell culture supernatant (Figure 30A) while NS5A^{CLIPf} did not severely affect the replication competence of the subgenomic replicon (Figure 30B).
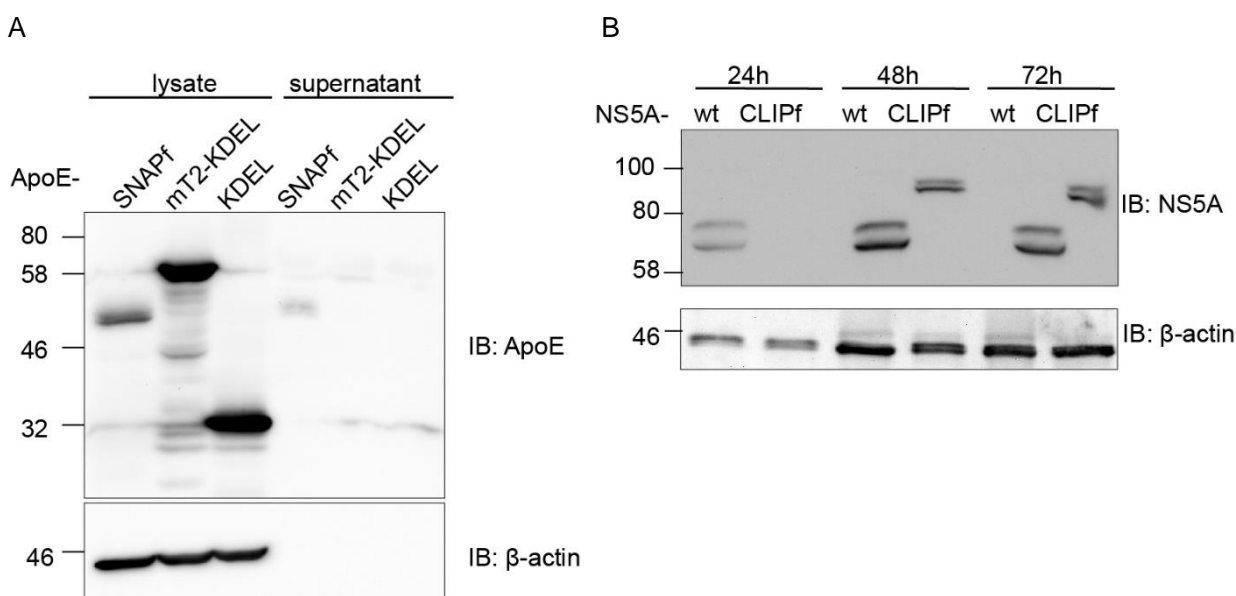
Figure 30. Normal secretion of SNAPf-tagged ApoE and unperturbed replication of CLIPf-tagged NS5A sgJFH1

A) Lunet/ApoE-KD cells were transduced with lentiviruses containing either ApoE^{SNAPf}, ApoE$^{mT2-KDEL}$ or ApoE^{KDEL}, respectively. Cell lysates and cell culture supernatants were immunoblotted with anti-ApoE antibody and anti-β-actin antibody.
B) Lunet cells were electroporated with either *in vitro*-transcribed sgJFH1/NS5A^{wt} or sgJFH1/NS5A^{CLIPf}, respectively. Cells were harvested at indicated time points and cell lysates at were immunoblotted with anti-NS5A antibody and anti-β-actin antibody.

These two fusion proteins were labeled with the synthetic cell-permeable fluorophores SNAP-SIR647 and CLIP-ATTO590. Confocal imaging showed specific labeling of ApoE and NS5A (Figure 31). Importantly, I could again observe the colocalization of vesicular ApoE and NS5A (arrowheads), which is consistent with my previous results with FP-tagged ApoE and NS5A.
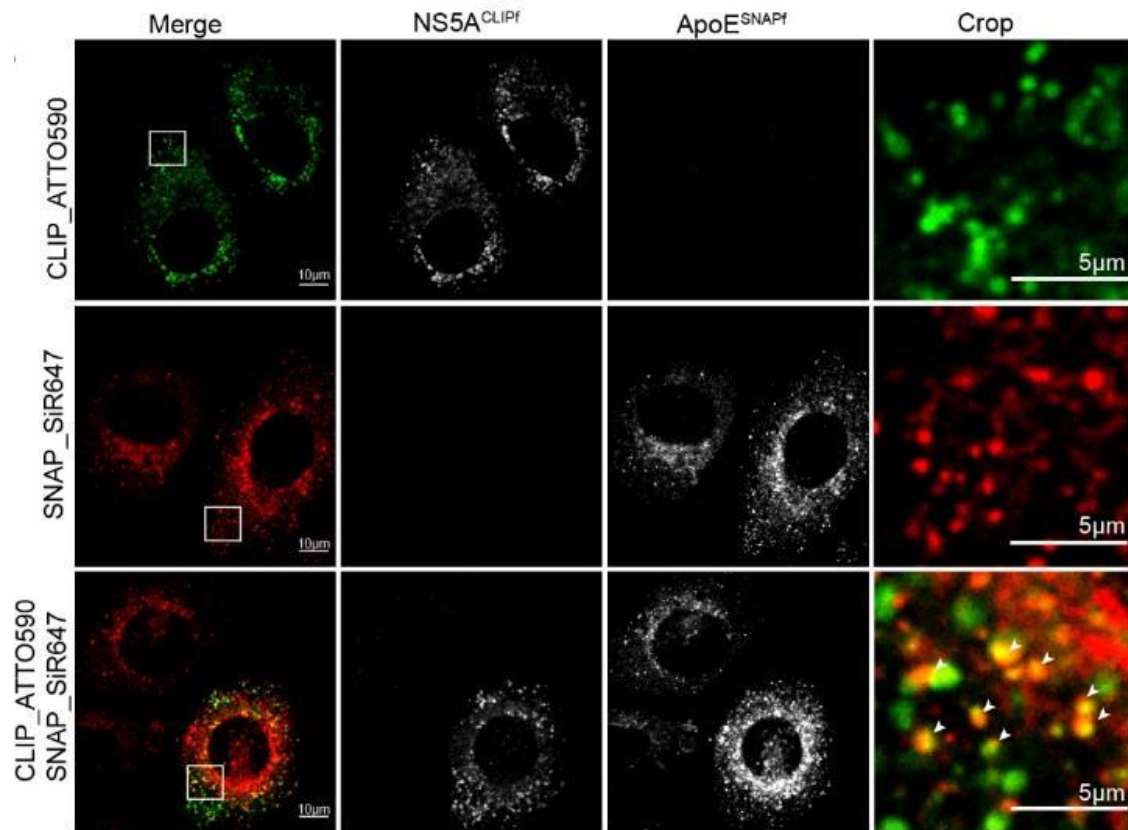
Figure 31. Detection of ApoE-SNAPf and NS5A-CLIPf with SNAP[SiR647] and CLIP[ATTO590] by super-resolution microscopy

Lunet-ApoE[SNAPf] cells were electroporated with *in vitro*-transcribed sgJFH1/NS5A[CLIPf] RNA. At 48 h.p.e cells were labeled with SNAP[SiR647] and CLIP[ATTO590] for 1 h, fixed, and subjected to confocal microscopy. Arrowheads: colocalized ApoE-NS5A signals.

Importantly, I demonstrated that approximately 50% of ApoE-NS5A foci are CD63-positive (Figure 32).
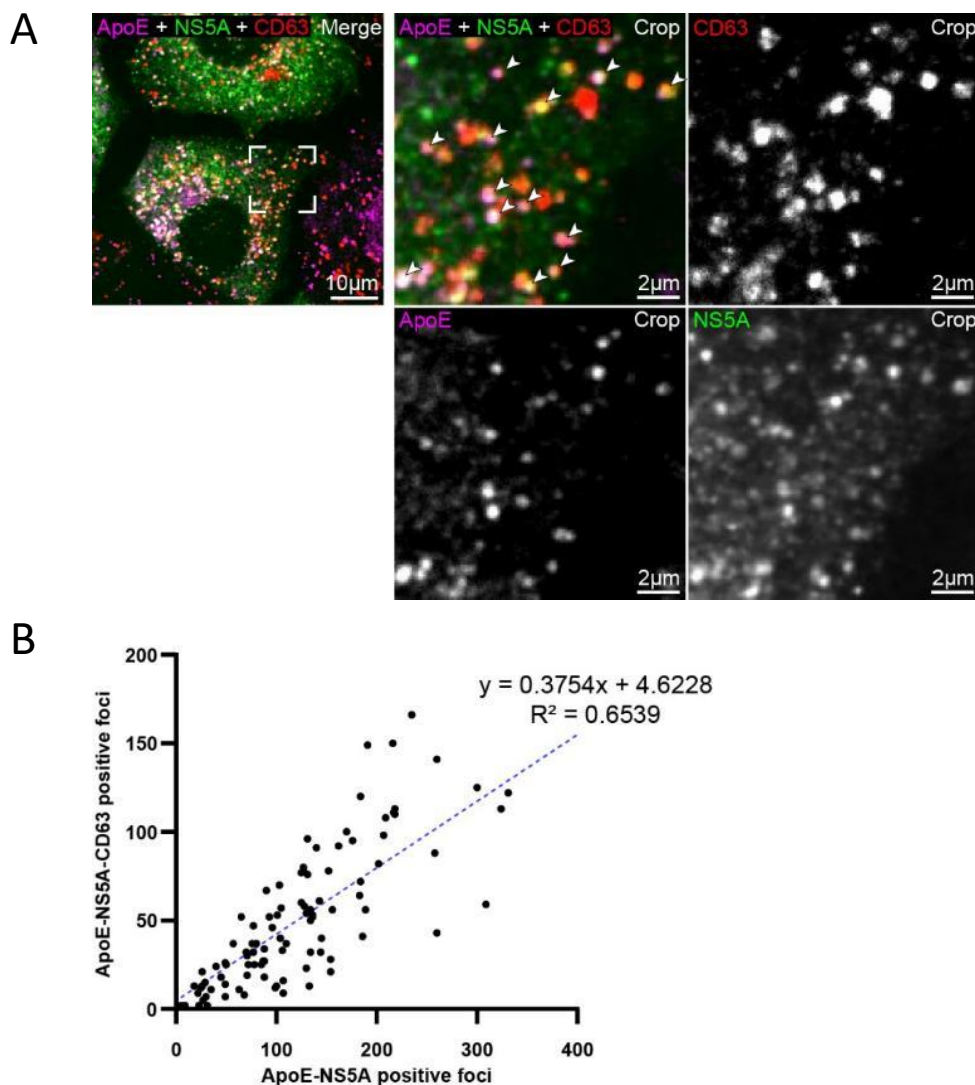
Figure 32. CD63-positive NS5A-ApoE foci formation in HCV-replicating cells

A) Lunet-ApoE^{SNAPf} cells were electroporated with the *in vitro* transcribed sgJFH1/NS5A^{CLIPf} RNA and after 72 h, cells were sequentially labeled with SNAP^{SiR647} and CLIP^{ATTO590} for 1 h, fixed, permeabilized, incubated with anti-CD63^{AF488} antibody. Cells were subjected to confocal microscopy. Images on the right show magnified views of the boxed area in the left overview image. Arrowheads: ApoE-NS5A-CD63 triple-positive foci.

B) Quantification of CD63-positive ApoE-NS5A positive foci of cells from (A) using Colocquant. Each dot represents the number of ApoE-NS5A double-positive foci (x-axis) and the number of CD63-ApoE-NS5A triple-positive foci (y-axis) of a single cell. The linear regression equation and R squared value are shown on the plot.

I further resolved the ApoE-NS5A signals using STED microscopy. Importantly, in addition to typical reticular ER and ring-like lipid droplet staining patterns (Figure 33, stars), I detected ~100-200nm diameter dotted NS5A structures that were decorated with ApoE signals at CD63-positive sites (Figure 33, arrows). I speculated that HCV produces NS5A-CD63-positive intraluminal vesicles (IVs) inside ApoE-containing late endosomes where ApoE and NS5A could interact.
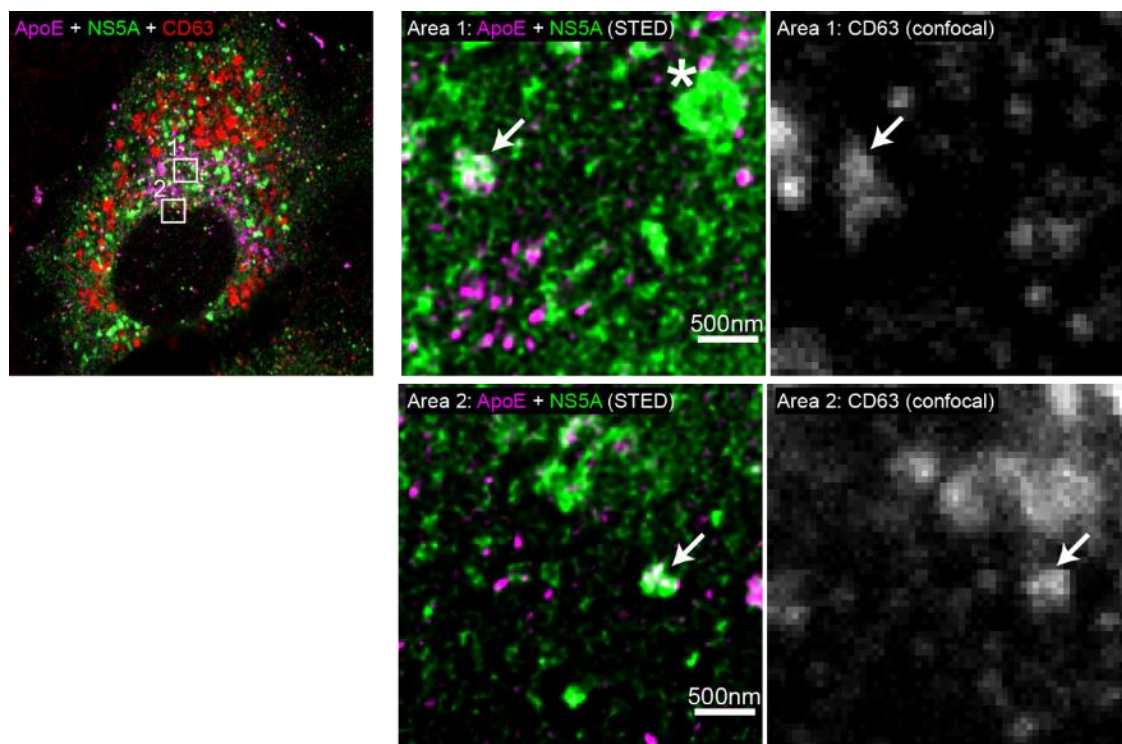
Figure 33. Resolved ApoE-NS5A structures by STED microscopy

Lunet-ApoE[SNAPf] was electroporated with *in vitro*-transcribed sgJFH1/NS5A[CLIPf] RNA. At 48 h.p.e, cells were labeled with SNAP[SiR647] and CLIP[ATTO590] for 1h, fixed, and incubated with anti-CD63[AF488] antibody. ApoE, NS5A and CD63 fluorescent signals were sequentially imaged with confocal microscopy and STED microscopy to achieve higher resolution of ApoE and NS5A. ApoE and NS5A signals were deconvoluted using Huygens. Arrows: ~100-200nm ApoE-NS5A-CD63 positive signals; star: a ~500nm ring-like NS5A signal.

2.4. Secretion of ApoE-associated NS5A-positive extracellular vesicles containing HCV RNA

I further investigated the possible relevance of ApoE as well as the ApoE-NS5A interaction beyond HCV assembly. Several lines of evidence suggest that HCV RNA can be transmitted from cell-to-cell via exosomes [84-86]. Moreover, NS5A was identified in exosomes purified from HCV-replicating cells [87, 88]. Given that ApoE associates with NS5A in regions of endosomes containing intraluminal double or multi-membrane vesicles and HCV suppresses the fusion of late endosomes with lysosomes [118], it is very likely that these IVs contain HCV RNA and are secreted out. To exclude the possibility of HCV transmission via HCV virions, I employed the HCV subgenomic model although HCV RNA transmission via EVs lacking HCV structural components seems to be relatively inefficient [84]. I initially tested if I could detect HCV RNA in ApoE-associated structures secreted in the conditioned media of stable HCV subgenomic replicon cells or parental control cells. As expected, I detected HCV RNA in immuno-captured ApoE preparation of HCV replicon samples indicating the association of extracellular ApoE with HCV RNAs (Figure 34).
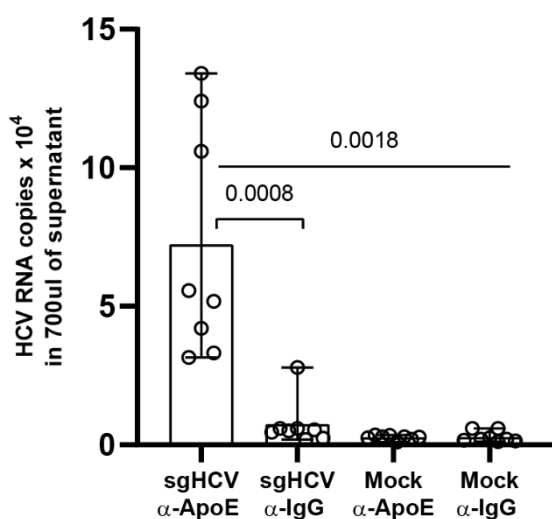
Figure 34. Association of secreted ApoE and HCV RNA

Huh7 cells harboring HCV JFH1 subgenomic replicon (NS3-NS5B) and the control Huh7 cells were cultured in 1% FCS media for 6 h. Cell-conditioned media were immunoprecipitated with either anti-ApoE antibody or anti-IgG control. Precipitated samples were subjected to RNA extraction and were subsequently examined for HCV RNA by qPCR. Data are means (range) from 2 independent experiments. P-values were determined using one-way ANOVA and unpaired Student's *t*-tests.

Next, I verified the association of extracellular ApoE with NS5A-positive EVs. To this end, I employed the Nanoluciferase (Nluc)-tagged NS5A subgenomic replicon for the sensitive detection of NS5A in the cell culture supernatant (Figure 35, upper panel). In agreement with a previous report, I observed marked secretion of NS5A-Nluc into cell culture supernatant [87] (data

not shown). Immuno-captured extracellular NS5A using NS5A-specific antibody revealed high Nluc activity and an appreciable amount of co-precipitated ApoE (Figure 35A, lane #4), indicating that NS5A is well accessible to NS5A-specific antibody and the association of secreted ApoE and NS5A, respectively. In addition, immunocaptured ApoE (Figure 35A, lane #2) also exhibited some Nluc activity (~3.6% of the IP-NS5A sample) suggesting that a subpopulation of ApoE-lipoprotein bind NS5A-containing structures. The specificity of the pulldown was confirmed by using Mock or irrelevant antibody TIA-1 (lane #1 and #3). Importantly, negative-staining of immunocaptured NS5A and ApoE confirmed the presence of EVs which were frequently detected in close association with lipoprotein-like structures of around 20 nm in diameters (Figure 35B, arrows). Taken together, my data suggest that secreted ApoE associated with a fraction of NS5A-positive EVs containing HCV RNA.
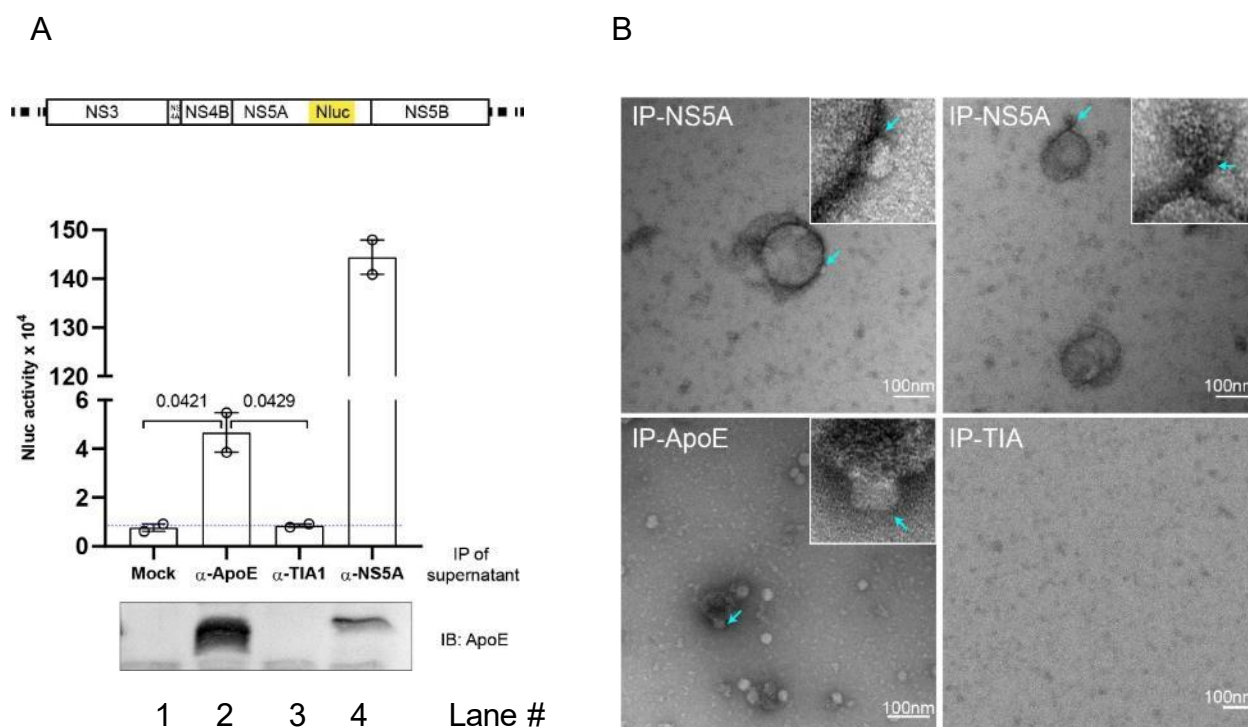
Figure 35. Association of secreted ApoE and NS5A-positive EVs

(A) [Top] Schematic representation of the Nanoluciferase (Nluc)-tagged NS5A subgenomic replicon construct. [Middle and bottom] Lunet cells were electroporated with the *in vitro* transcript of the subgenomic replicon encoding the Nluc-tagged NS5A. At 72 h.p.e, culture supernatant was precipitated using ApoE-, or NS5A-, or control TIA1-specific antibodies. The presence of NS5A contained in captured structures was inferred by the Nluc activity containing therein (middle panel).

Captured ApoE in samples was analyzed by Western blot analysis (bottom panel). Data are means (range) of two independent experiments. P-value was determined using unpaired Student's *t*-test.

(B) Captured complexes in (A) were visualized by negative staining and TEM. Arrows: lipoprotein-like particles (~20 nm) attached to EVs.

To determine the relevance of ApoE-NS5A interaction for the secretion of HCV RNA, I employed a NS5A mutant (APK99AAA) reported to be unable to interact with ApoE [41]. I initially confirmed that this APK99AAA mutation impairs NS5A-ApoE binding (Figure 36A). Remarkably, Lunet cells stably harboring HCV subgenomic NS5A-APK99AAA replicon showed a significant reduction in HCV RNA secretion (Figure 36B).

A

B
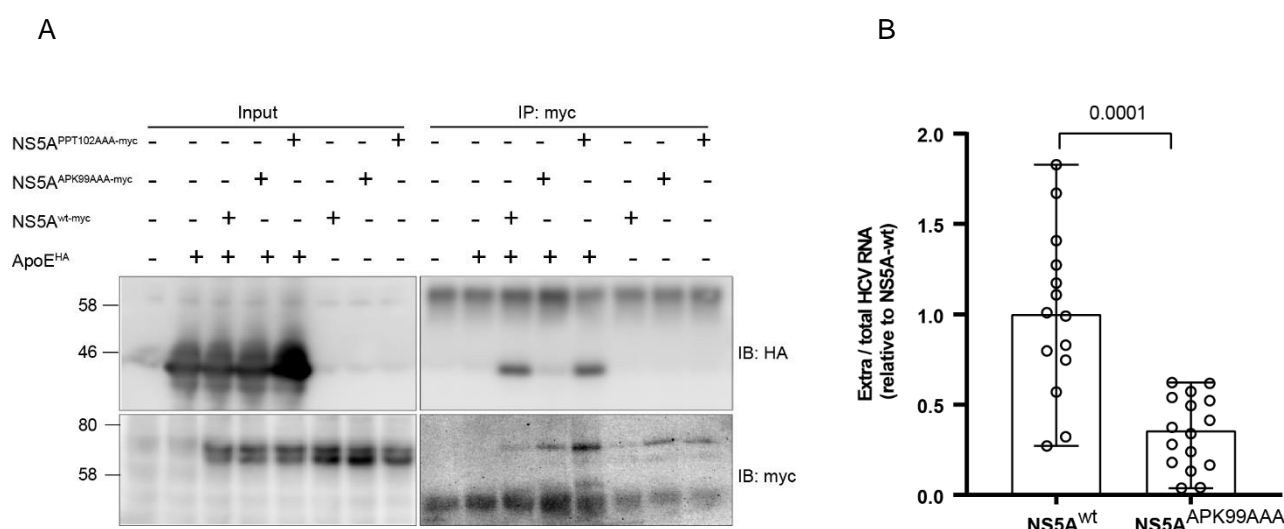
Figure 36. Reduction of HCV RNA secretion by the mitigation of ApoE-NS5A interaction by APK99AAA mutation in NS5A

A) HEK293T-miR122 were co-tranfected with HA-tagged ApoE and either an empty vector, myc-tagged NS5A[wt], NS5A[APK99AAA] or NS5A[PPT102AAA], respectively. At 30 h.p.t, cell lysates were immunoprecipitated with anti-myc antibody and bound complexes were immunoblotted with anti-HA antibody.

B) Reduced secretion of extracellular sgHCV RNA with ApoE-binding deficient NS5A. Intracellular and extracellular RNA of Lunet cells harboring sgJFH1/NS5A[wt] and sgJFH1/NS5A[APK99AAA] were extracted. HCV RNA was quantified by qPCR. Ratios of secreted HCV RNA to total were shown. Each dot represent a technical replicate that were pooled from three independent experiments. Data are median (range) and P-value was determined using unpaired Student's *t*-test.

To visualize HCV RNA, I employed single molecule Fluorescence In Situ Hybridization (smFISH) with Hulu probes (Alexa Fluor 647 conjugated) that could sensitively detect single HCV RNA

molecules without signal amplification. These probes target HCV nonstructural protein 3 RNA sites (Figure 37A). Although Hulu probes showed background staining in cell nuclei, cytoplasmic staining of HCV RNAs was specific as I detected numerous nucleus-devoid foci of HCV RNA in replicon cells but not in the control cells (Figure 37B).

A   B
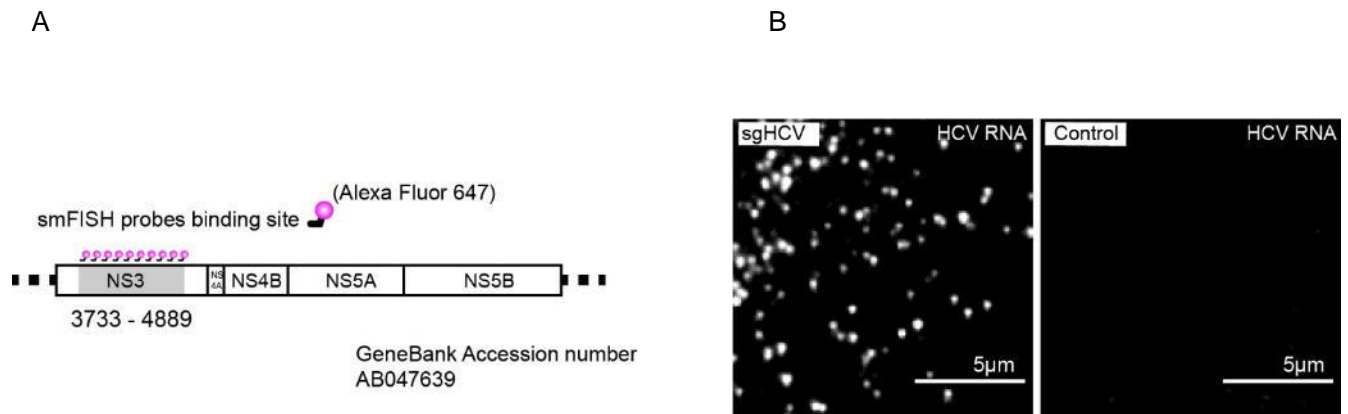
Figure 37. Detection of HCV RNA using smFISH with Hulu probes

A) Schematic of the design of smFISH probes used to detect HCV RNA.

B) Specificity of HCV RNA detection by smFISH with Hulu probes. Lunet cells harboring HCV sgJFH1 and the control cell expressing eYFP-CaaX were examined for HCV RNA by Hulu probes targeting HCV NS3 RNA. CaaX: farnesylation signal from human HRAS protein.

To test if ApoE associates with the transferred HCV RNAs in target cells, I established stable HCV subgenomic replicon cells expressing ApoE^{mT2} and CD63^{mCherry} (donor). Target recipient cells were labeled with another fluorescent protein (eYFP) which is fused with a farnesylation signal (CaaX motif from human HRAS protein) to label their membranes for easy tracking (Figure 38).
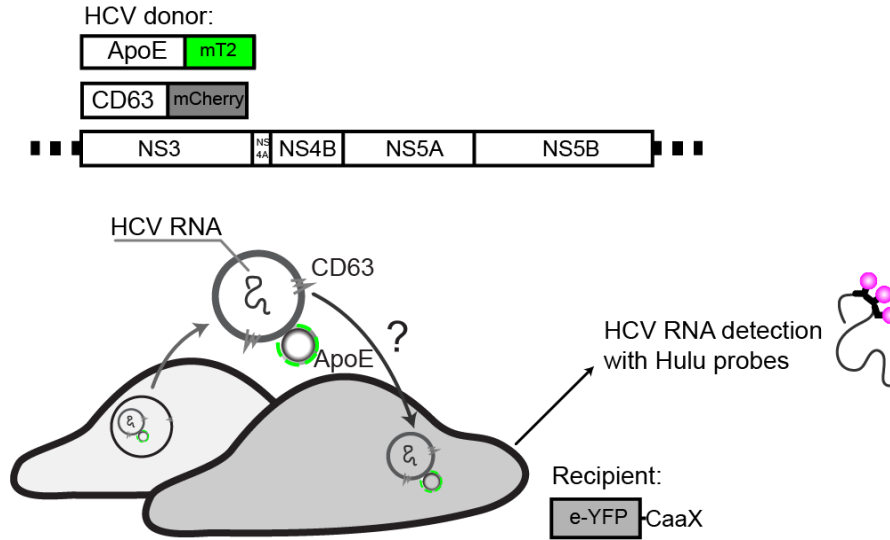
Figure 38. Schematic representation of co-culture experiment to detect ApoE-associated HCV RNA transfer via EV from cell to cell

Donor cells: HCV sgJFH1 replicon cells established based on Lunet-ApoE^{mT2}/CD63^{mCherry}.
Recipient cells: Lunet$^{eYFP-CaaX}$. CaaX: farnesylation signal from human HRAS protein.

HCV RNAs were found to partially colocalize with ApoE-CD63 dots in donor cells (Figure 39, donor, arrows). Remarkably, I could detect few distinct foci of HCV RNA in single recipient cells (mean=5.6); and roughly about 12.9% of them were ApoE-CD63 positive (Figure 39A and B, recipient, arrows). This implied that HCV RNAs could be transmitted via virion-free ApoE-associated EVs.
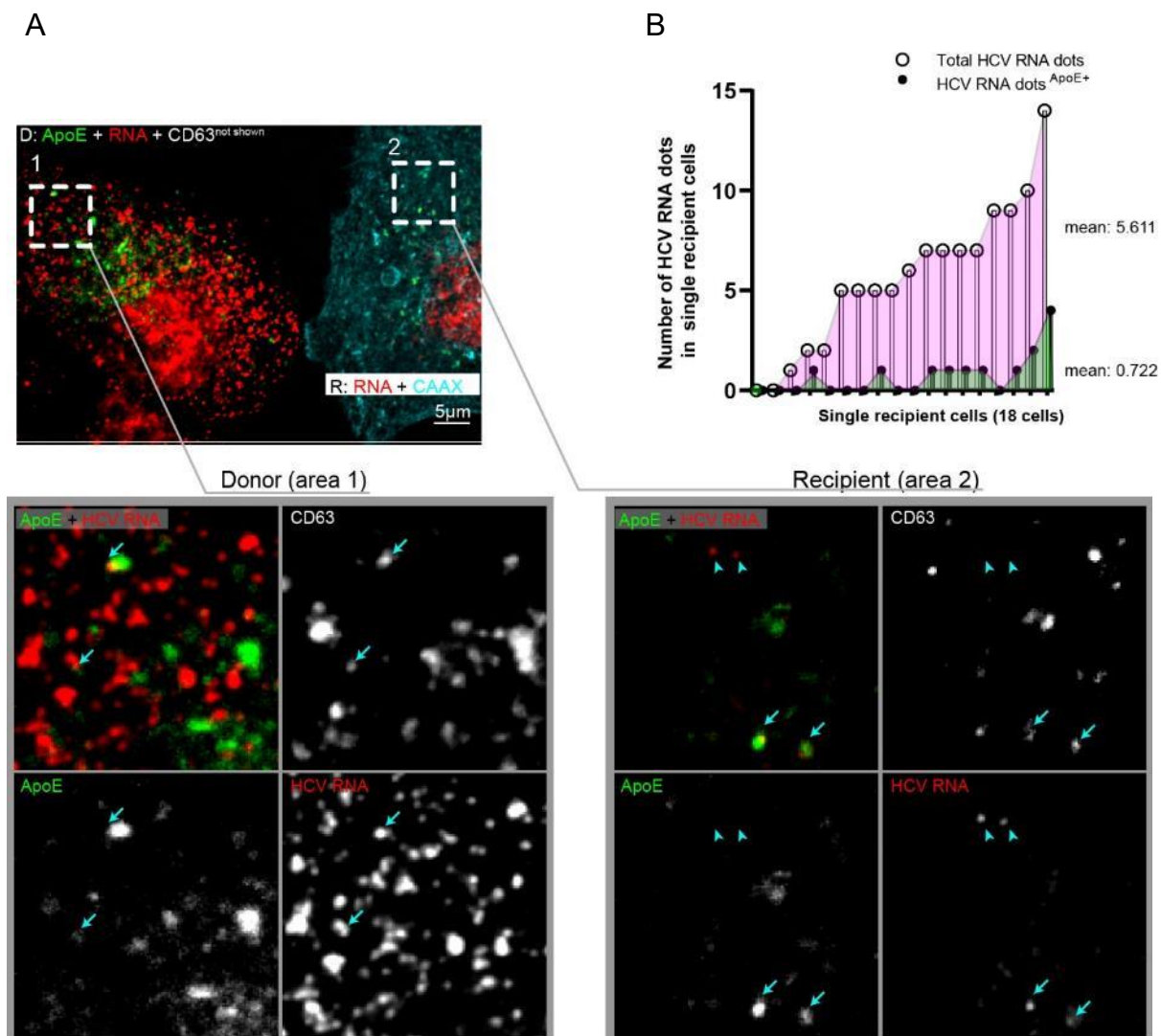
Figure 39. Detection of ApoE-associated HCV RNAs in recipient cells

(A) An example of the transfer of HCV RNA from a HCV-positive cell to a naïve cell
[Upper] HCV sgJFH1 replicon cells established based on Lunet-ApoE^{mT2}/CD63^{mCherry} (donor) were cocultured with Lunet$^{eYFP-CaaX}$ (recipient) for 24 h. Cells were then fixed and processed to visualize HCV RNAs by smFISH with Hulu probes. CaaX: farnesylation signal from human HRAS protein. Dashed area 1: donor; dashed area 2: recipient.
[Lower] Magnified views of cropped areas in the upper panel. Arrows: ApoE-positive HCV RNA dots in both donor and recipient cells; arrowheads: ApoE-negative HCV RNA dots in recipient cells.

(B) Quantification of the number of ApoE-positive and -negative HCV RNA foci in single recipient cells (n=18).

2.5. Secretion of double membrane vesicle-inducing SARS-CoV-2 proteins nsp3-4

Given the secretion of HCV-produced IVs containing NS5A and RNA in HCV-infected cells, I wondered if EVs containing viral proteins involved in DMV formation are unique to HCV or a more general property of DMV-producing viruses. I addressed this question by using severe acute respiratory syndrome coronavirus 2 (SARS-CoV2) as a model, because it also induces DMV-type replication organelles and their formation can be triggered by the sole expression of the viral polyprotein fragment nsp3-nsp4 [119] which is similar to HCV NS3-NS5B. I checked for the secretion of nsp3 after transfection of the nsp3-4 coding plasmid into permissive cell lines, i.e. HEK293T and Huh7-Lunet cells. To facilitate the readout, I added the Nluc-coding gene into the N-terminal of nsp3-nsp4 construct and measured the Nluc activity 48 h post-transfection. I observed the marked secretion of nsp3 at 48 h post-transfection in the supernatant of both transfected HEK293T and Lunet cells as measured by Nluc activity. Importantly, my preliminary data show that the blockade of exosome generation with the neutral sphingomyelinase inhibitor GW4869, reported to block exosome formation [120, 121] mitigated the secretion of nsp3 (Figure 40A). Strikingly, nsp3-4 transfected cells showed a dramatic re-distribution of CD63 and ApoE signals (Figure 40B). Taken together, these preliminary data suggest that also in the case of SARS-CoV-2, EVs containing viral proteins might be released from infected cells via the late endosomal pathway, arguing for a more general role of EVs in virus-induced signal transduction. However, these data are preliminary and due to time constraints I could not follow up in further detail.
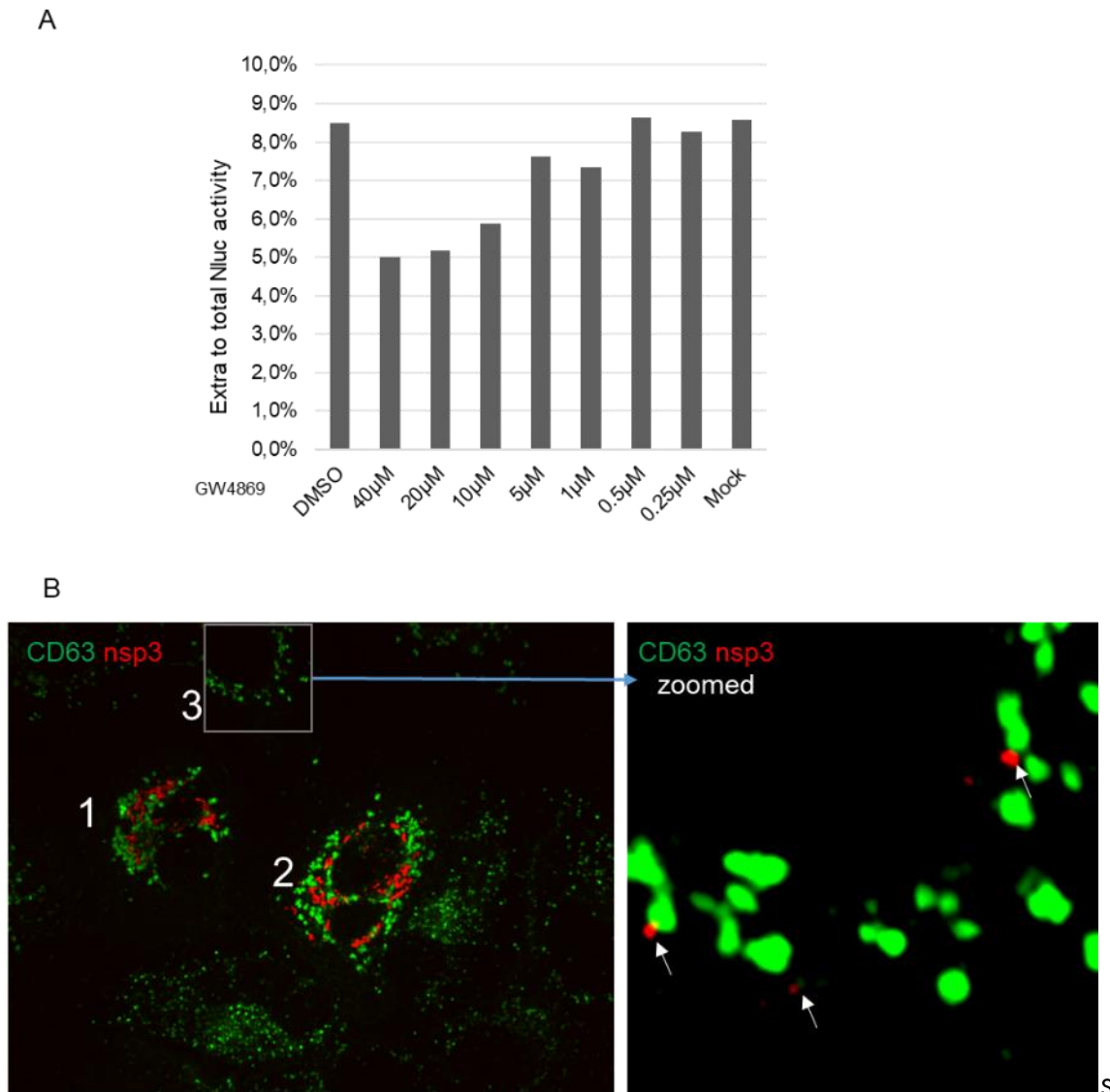
Figure 40. Secretion of SARS-CoV2 nsp3 through the endosome pathway and rearrangement of the endosomal marker in SARS-CoV2 nsp3-nsp4 transfected cells

A) Inhibition of exosome production reduced SARS-CoV2 nsp3 secretion. HEK293T cells were transfected with Nluc-tagged nsp3-4 coding plasmid. At 4 h.p.t, cells were cultured in medium containing various concentration of GW4869 as indicated. At 48 h.p.t, the amounts of intra and extracellular nsp3 were determined by the measurement of Nluc activity. The ratios of extra to total Nluc are shown on the graph (n=1).

B) Rearrangement of the endosomal marker in SARS-CoV2 nsp3-nsp4 transfected cells. Lunet/ApoE^{mT2} cells were transfected with GFP-tagged nsp3-4 coding plasmid. At 48 h.p.t, cells were fixed, permeabilized, subjected to IF labeling of CD63, and examined by confocal microscopy to examine the distribution of CD63, ApoE and nsp3. For reasons of simplicity, ApoE signal is not shown. Cell 1 and 2: nsp3-positive cells with condensed signals of CD63. Cell 3: low nsp3 expressing cell showing the close proximity of nsp3 and CD63 signals.

3. Association of ApoE-containing lipoproteins and IVs/EVs in uninfected hepatocytes

Having found that hepatic ApoE-containing lipoproteins associate with HCV-produced IVs/EVs, I wanted to know whether ApoE association with these vesicles is a general feature that takes place also in non-infected cells. In addition, I studied the question whether such ApoE-associated vesicles play a role in cell-to-cell communication. Obtained results are described in this chapter of the RESULTS section.

3.1. Intracellular late endosomal trafficking of ApoE with CD63-positive intraluminal vesicles

In the first set of experiments, I confirmed the conventional trafficking route of ApoE as reported earlier. Intracellular hepatic ApoE contains an N-terminal signal peptide and thus should be co-translationally targeted to the ER lumen to enter the secretory pathway [55, 122]. Indeed, endogenous ApoE expression in Lunet cells detected by an anti-ApoE antibody staining shows reticular ER-like staining pattern [64]. By using ApoE^{mT2} construct, I further verified the subcellular localization of ApoE in this cell line (Figure 41).
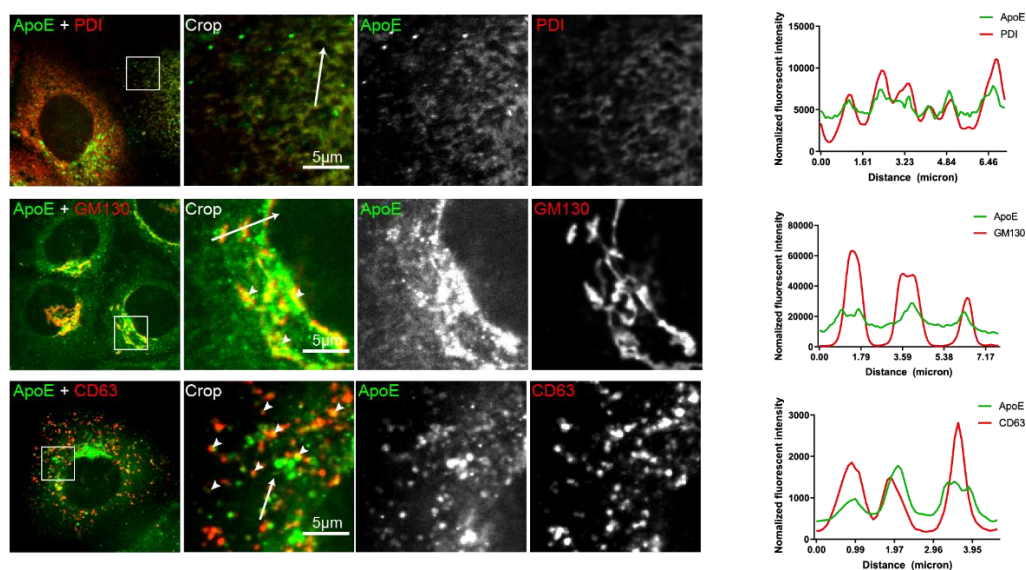
Figure 41. Colocalization of ApoE^{mT2} with markers of the ER (PDI), Golgi (GM-130) and intraluminal vesicles (CD63) in uninfected hepatocytes

Lunet-ApoE^{mT2} cells were fixed and labeled with indicated antibodies for subsequent immunofluorescent staining, and were further imaged with confocal microscopy.
[Top] anti-PDI antibody; [Middle] anti-GM130 antibody; [Bottom] anti-CD63 antibody.
Plot profiles on the right panels are from white arrows in cropped images.

Reticular ApoE^{mT2} signals were relatively dim but overlapped strongly with PDI (an ER marker) indicating the luminal ER origin of ApoE (Figure 41, top panel). Because ApoE assembles onto nascent V(LDL) particles in the Golgi lumen after these particles are transported from the ER to the Golgi apparatus [69], I anticipated to observe condensed vesicular signals of ApoE in the Golgi area. Expectedly, I further showed that vesicular ApoE^{mT2} signals were usually found to be concentrated at GM130 (Golgi marker)-positive areas implying its assembly in this compartment (Figure 41, middle panel). A study by Hossain *et al.*, 2014 suggested that hepatic ApoE exits from the trans-Golgi network and accumulates in a post-Golgi compartment before its secretion [69] but the post-Golgi trafficking of ApoE has not been characterized clearly. Importantly, I noticed numerous strong vesicular signals of ApoE^{mT2} over its dim reticular ER pattern in Golgi-devoid areas (Figure 41, bottom panel). These signals predominantly overlapped with CD63 (a marker of IVs and endosomes) indicating the accumulation of ApoE in endosomes. In addition, I showed that vesicular ApoE signals overlapped heavily with Rab7 (a marker of late endosomes) but rarely with ADRP (a marker of lipid droplets) (Figure 42).
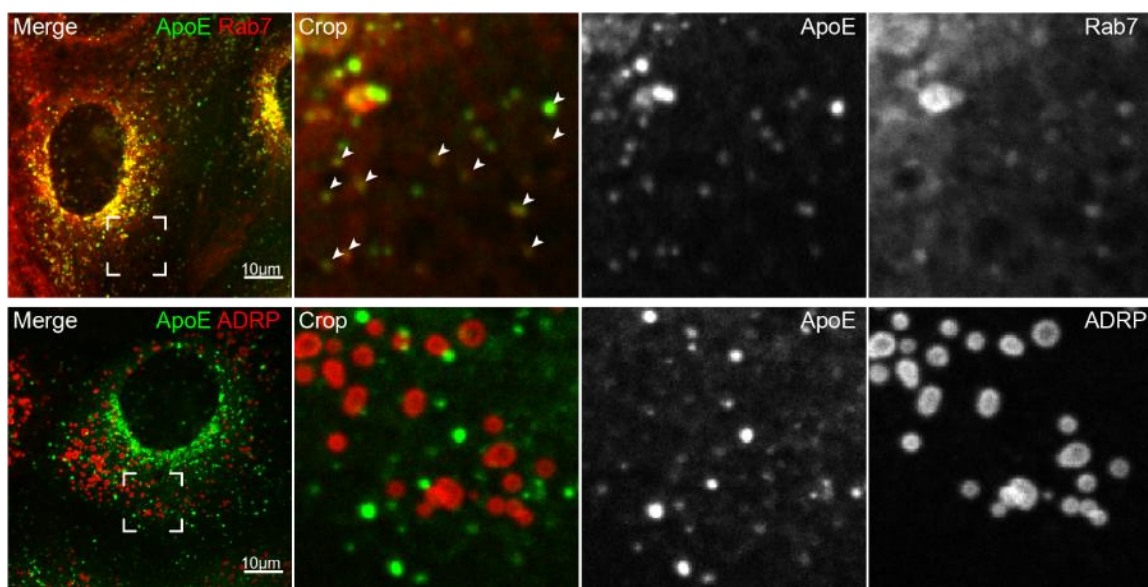
Figure 42. Colocalization of ApoE^{mT2} with Rab7 and ADRP

Lunet-ApoE^{mT2} cells were transduced with lentiviruses containing Rab7^{mCherry} [upper] or ADRP^{mCherry} [lower]. Cells were further subjected to confocal microscopy to examine the colocalization between

ApoE and late endosome (Rab7) and lipid droplet (ADRP). Each boxed area in the left panels of each subcellular marker is shown as enlarged views in the right panels. Arrowheads point to ApoE-Rab7 double-positive signals.

By CLEM, I demonstrated that ApoE-CD63 positive signals predominantly correlate to endosomes (Figure 43).
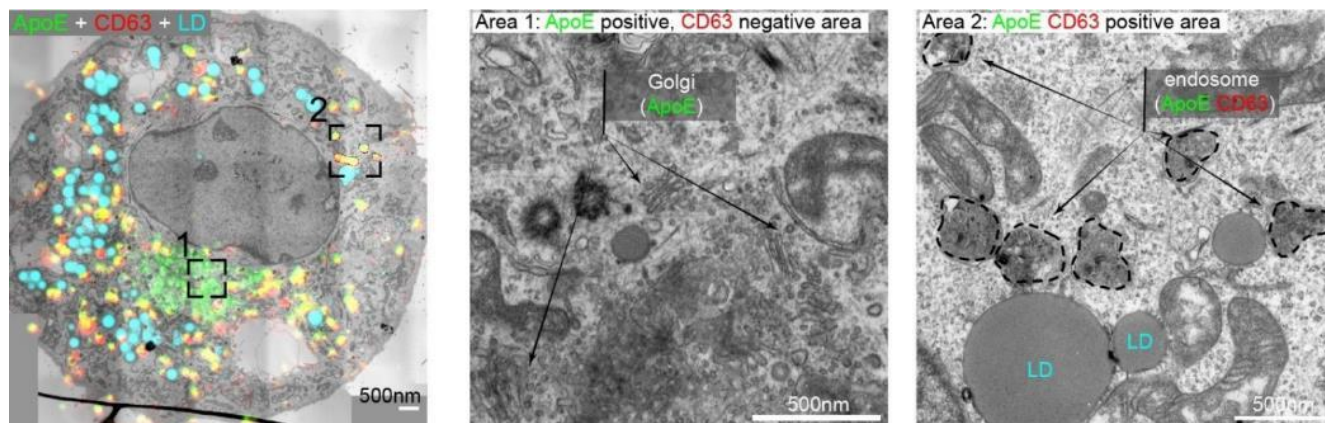
Figure 43. Endosomal localization of vesicular ApoE-CD63

[Left] Lunet-ApoE^{mT2} cells were transduced with lentiviruses containing CD63^{mcherry} and subjected to CLEM. Stained lipid droplets with lipidTox were used as fiducial markers.
[Middle]: a magnified view of the ApoE-positive, CD63-negative area in left panel showing the Golgi stacks and vesicles.
[Right]: a magnified view of the ApoE-CD63 double-positive signals in the left panel showing their endosomal localization.

Since mTurquoise2 tagging allowed the detection of ApoE in live cells, I tracked its dynamics with CD63 by time-lapse confocal microscopy (movie 4). I noticed that vesicular ApoE and CD63 signals substantially co-traffic, showing similar mean squared displacement values (Figure 44, left). The particle size and velocity of ApoE-NS5A double-positive signals were also computed, showing the heterogeneity of ApoE-CD63 motions (Figure 44, middle and right).
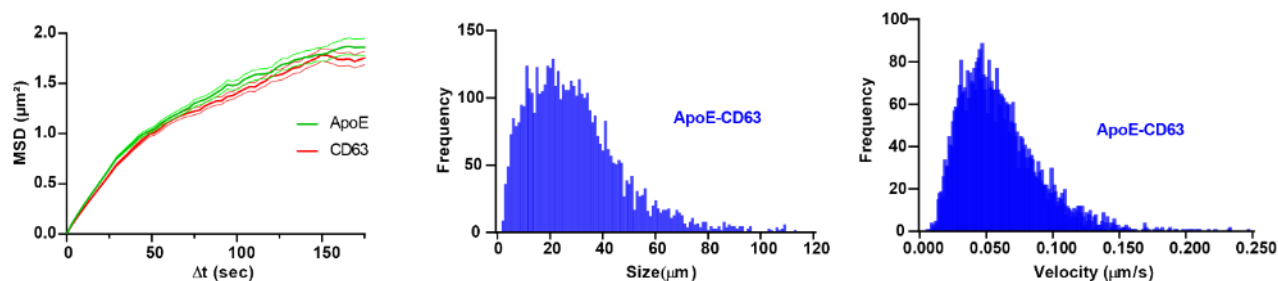
Figure 44. Motion analysis of intracellular ApoE and CD63 signals

Lunet-ApoE^{mT2} cells were transduced with lentiviruses containing CD63^{mcherry} and subjected to time-lapse confocal live-cell imaging.
[Left] Mean squared displacement (MSD) of general ApoE and CD63 trafficking. Motion parameters were obtained by regression analysis between 0 and 178.75 sec. Data are MSD (SEM - standard error of the mean); frame interval = 3.25 sec.
[Middle] Size of colocalized ApoE-CD63 signals
[Bottom] Velocity of co-trafficking ApoE-CD63 signals

(*Data analysis by Christian Ritter, BioQuant Center, Biomedical Computer Vision Group, Heidelberg University, Heidelberg, Germany*)

Importantly, ~40% of these vesicles show directed motions (Figure 45A), suggesting the microtubule-dependent trafficking of late endosomes containing ApoE-CD63 [123, 124]. An example of ApoE-CD63 trafficking with max projection overtime showing directed motion to cell periphery was shown in Figure 45B.
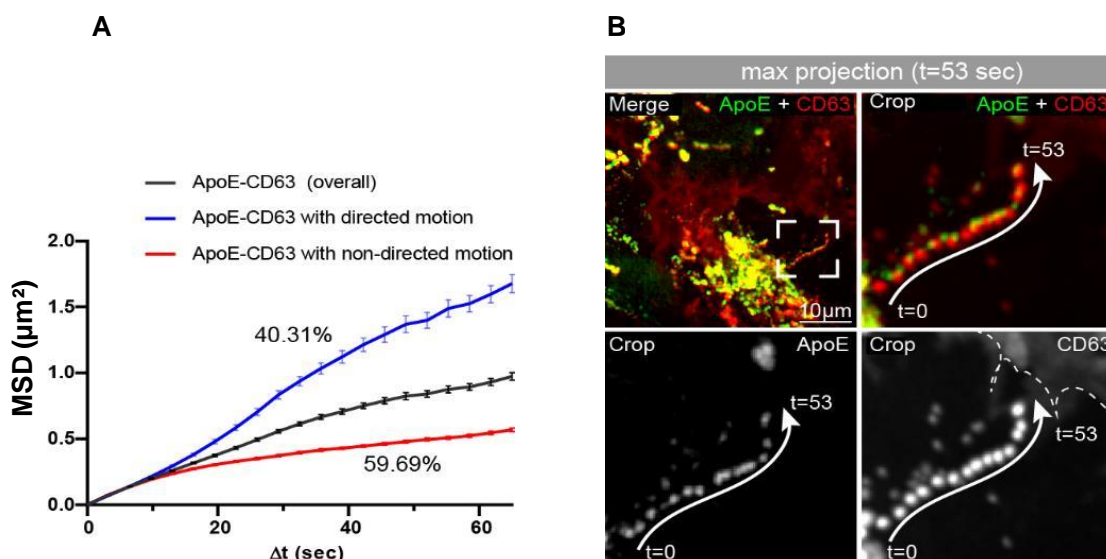
Figure 45. Directed motion of intracellular colocalized ApoE-CD63 complexes

A) Mean squared displacement (MSD) of colocalized ApoE-CD63 signals with directed and non-directed motions from Figure 44, obtained by regression analysis of 4085 colocalized particles between 0 s and 40 s. Data are MSD (SEM - standard error of the mean). *(Data analysis by Christian Ritter, BioQuant Center, Biomedical Computer Vision Group, Heidelberg University, Heidelberg, Germany.)*

B) An example of ApoE-CD63 trafficking with a directed motion. The max projection image demonstrating the co-trafficking of an ApoE-CD63 complex with a directed motion to cell peripheral region was shown. Frame interval = 2.65 sec over 53-sec duration.

3.2. Secretion of ApoE-associated CD63-positive intraluminal vesicles

Next, I aimed to visualize the secretion of ApoE-associated CD63-positive IVs, taking advantage of the acidic pH in IVs-containing endosomes that gets neutral as endosomes fuse with the plasma membrane to release vesicles contained therein. As the endosome-plasma membrane fusion sensor, I employed an improved version of pHluorin [101] that I inserted into the first extracellular loop of CD63, thus exposing pHluorin to the acidic environment of the endosomes. The signal of pHluorin-tagged CD63 is quenched in the endosomes and is exclusively excited upon leakage of endosomes to the neutral pH of extracellular environment [100]. To captured ApoE-CD63 co-secretion, I used time-lapse live-cell confocal microscopy by setting the focal plane to the plasma membrane determined by the basal fluorescence of the CD63^{pHluorin} signal (Figure 46 and Movie 5). As expected, CD63^{pHluorin} expressed in Lunet cells generally showed exclusively and evenly basal fluorescent signal in the plasma membrane that did not colocalize with vesicular ApoE signals under conditions of live-cell imaging. Occasionally, the pHluorin signal became marginally visible over the fluorescent background, marking the initiation of the fusion event (Figure 46, time point t_1), followed by a steep and rapid increase of the ApoE-associated pHluorin signal (Figure 46, time point t_2), likely corresponding to the ongoing secretion of ApoE-associated CD63-positive IVs when ApoE-CD63 containing endosomes fused with the plasma membrane. ApoE-associated CD63 signals reduced at a later time point (t_3) and diminished ~5 min after the secretion events.
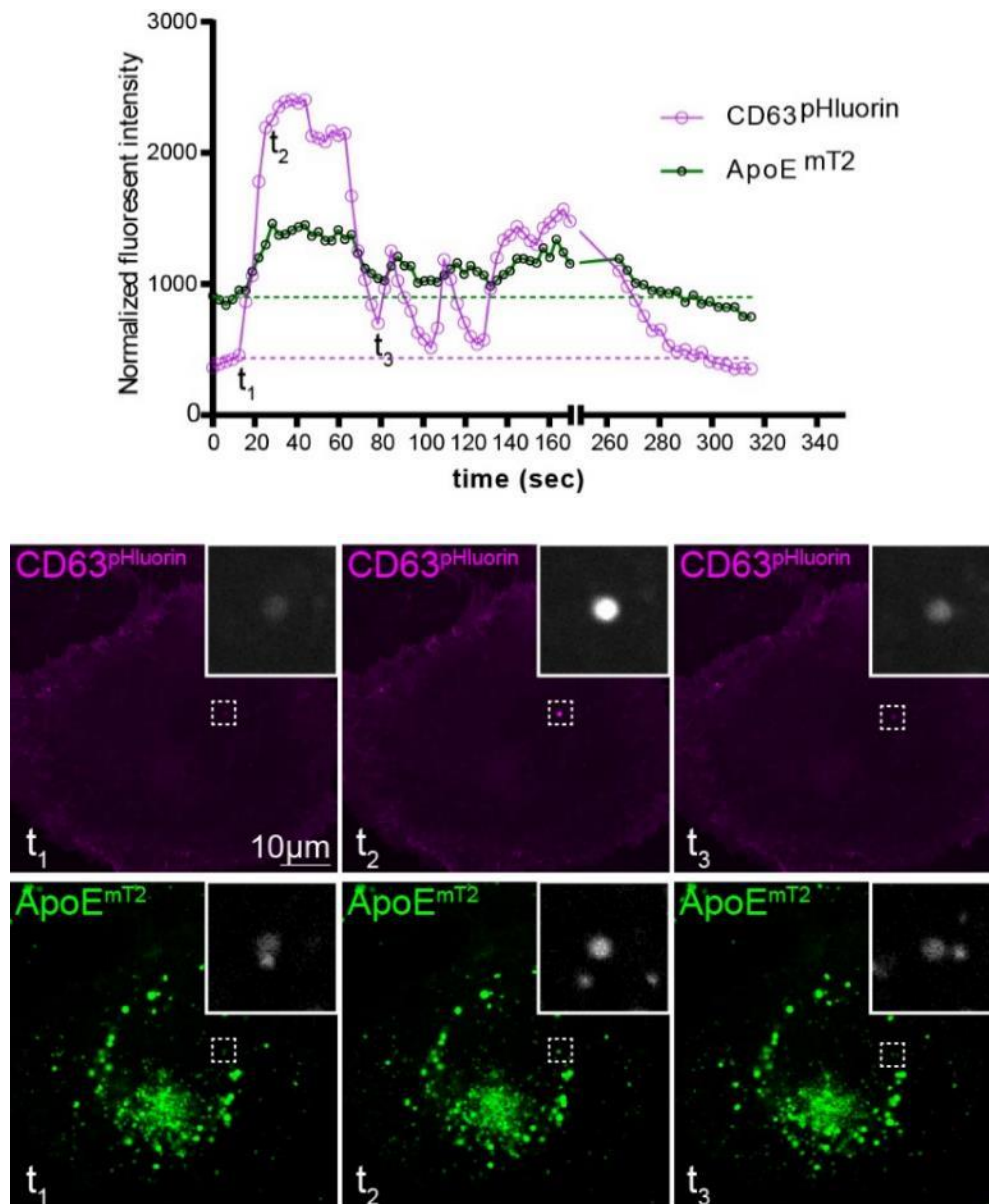
Figure 46. Secretion of ApoE-positive IVs visualized by pHluorin-tagged CD63

Lunet-ApoE^{mT2}/CD63^{pHluorin} were cultured in 25mM Hepes-containing imaging medium (pH 7.4) and were subjected to time-lapse confocal imaging with a focus on the plasma membrane (PM) based on CD63-basal fluorescent signals.

[Upper] Max fluorescent intensity of CD63^{pHluorin} and associated ApoE signal over time in the selected area showing secretion (refers to movie 5).

t_1: pre-secretion time point; t_2: early secretion time with peaked CD63-ApoE signals; t_3: late secretion time point

[Lower] ApoE-CD63^{pHluorin} release event at indicated time frames. Insets: magnified views of the selected area showing secretion.

I further checked if I could detect any association of EVs with purified secreted lipoproteins. To this end, I firstly purified secreted ApoE-associated structures and checked for the presence of EVs by CD63-immunogold labeling. Immuno-captured ApoE in the conditioned medium of Lunet cells predominantly contained small vesicles with the size of LDL or big HDLs (mean diameter of ~25nm) (Figure 47A, arrows). Noticeably, a minor number of co-captured bigger vesicles (>=50nm) were also detected, showing the association with putative lipoprotein particles (Figure 47A, stars). These co-captured vesicles were CD63-positive indicating the interaction between lipoproteins and CD63-positive EVs that withstood the purification process (Figure 47B).
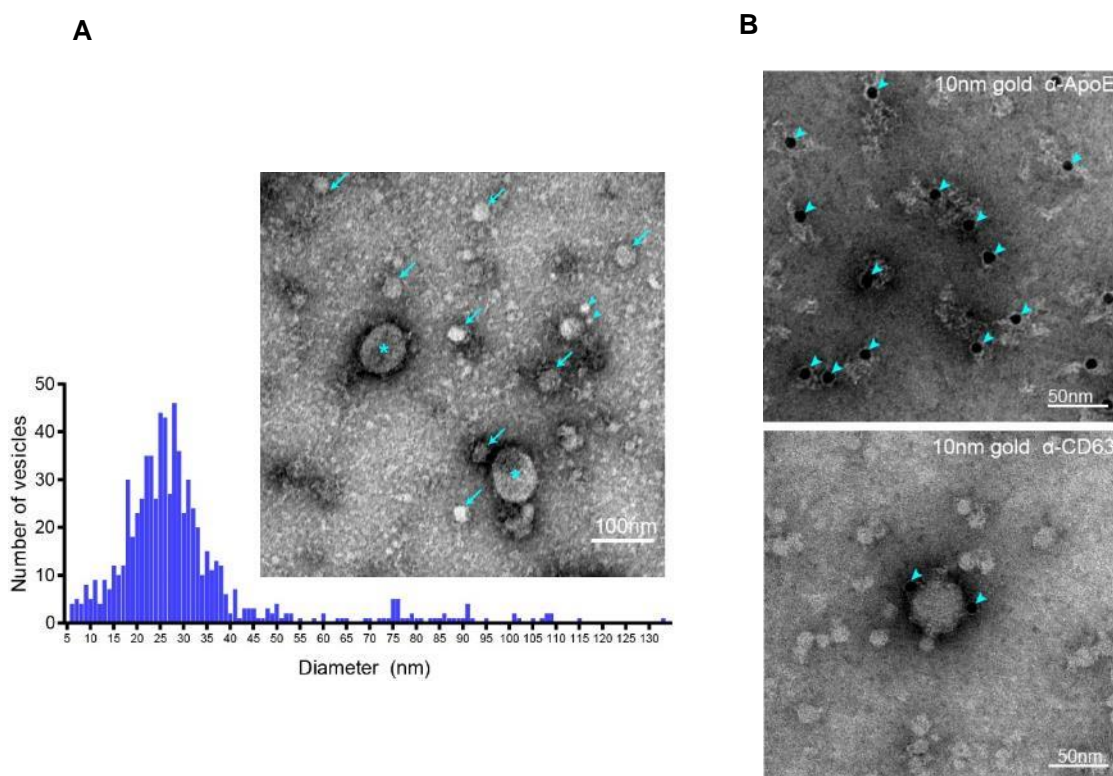
Figure 47. Association of EVs with purified secreted lipoproteins

(A) Purification of secreted native ApoE structures
[Upper] Lunet cells were cultured in EV-depleted medium. Secreted ApoE-containing vesicles in the cell-conditioned medium were immunocaptured with an anti-ApoE antibody and were subjected to negative-staining and analyzed by TEM. Arrowheads: ~5-10 nm vesicles; arrows: ~20-30 nm vesicles; stars: ~50-60 nm vesicles.
[Lower] Vesicular structures in the electron micrographs were segmented using Ilastik and the diameters of vesicles (nm) were measured and shown in the histogram.
(B) Purified ApoE vesicles from (A) were immunogold-labeled with anti-ApoE (upper) and anti-CD63 antibodies (lower). Arrowheads: gold particles.

3.3. Intercellular transmission of ApoE-associated extracellular vesicles

So far, my data indicate the intracellular cotrafficking and co-secretion of ApoE-containing lipoproteins and CD63-positive IVs. However, to the best of my knowledge, it is not known if there is any genuine co-transmission of hepatic ApoE and EVs under the physiological condition without HCV infection. To answer this question, I examined the concomitant uptake of fluorescently labeled ApoE^{mT2} and CD63^{mCherry} by recipient cells from co-cultured donor cells (Figure 48A). As a result, I detected clearly the signals of donor-derived ApoE-CD63 in recipient cells, indicating the transfer and uptake of lipoprotein-EV complexes (Figure 48B, arrows; movie 6). The number of ApoE-CD63 signals quantified in single recipient cells, especially at 48h post-seeding, showed remarkable transfer and uptake of these complexes among cell population (Figure 48C). Taken together, I report the first direct evidence of intercellular hepatic lipoprotein-EV transmission.
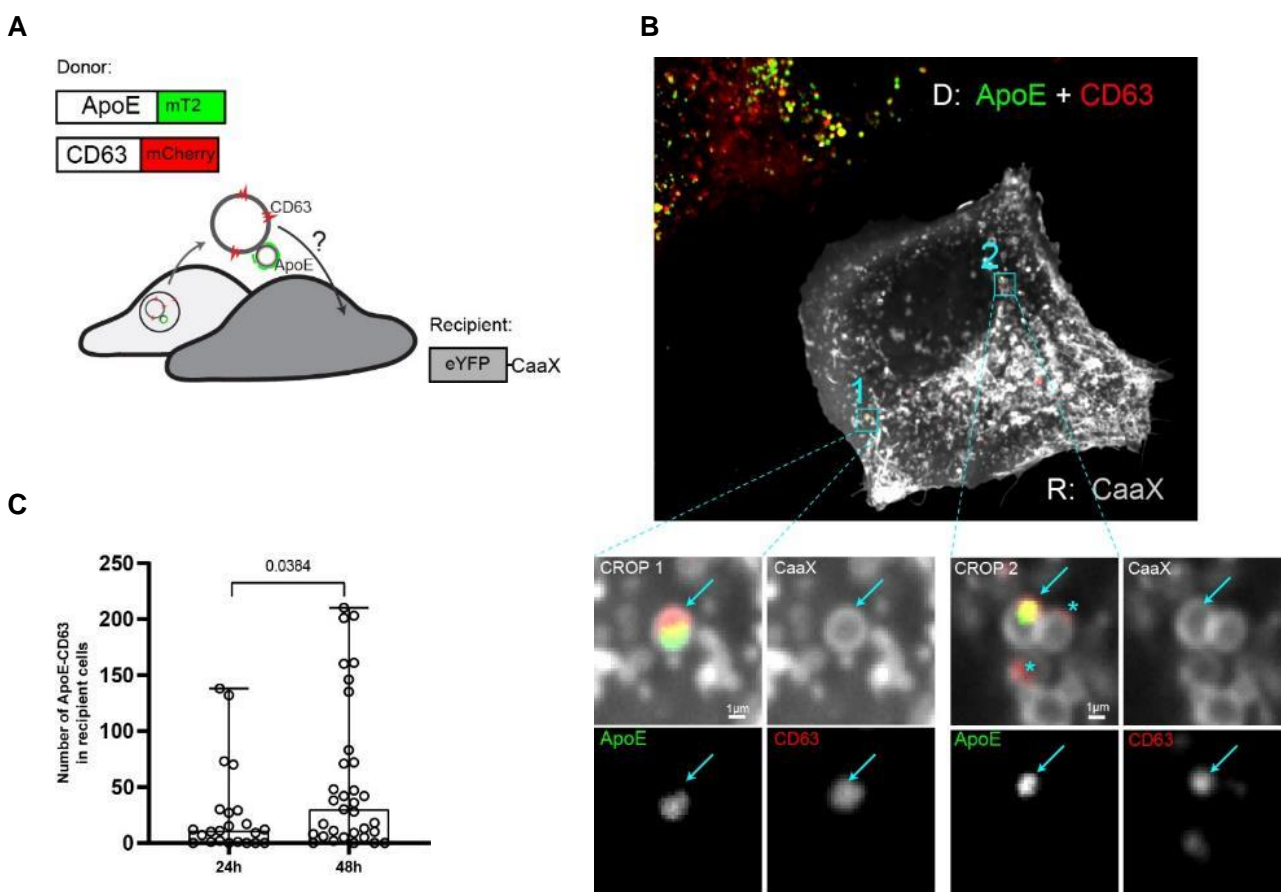
Figure 48. Detection of the co-uptake of lipoprotein-EV complexes in uninfected hepatocytes

(A) Schematic representation of the labelling approach for the detection of the co-uptake of lipoprotein-EV complexes. Donor cells: Lunet-ApoE^{mT2}/CD63^{mCherry}. Recipient cells: Lunet$^{eYFP-CaaX}$. CaaX: farnesylation signal from human HRAS protein.

(B) Donor and recipient cells from (A) were cocultured for 16 h and were further subjected to live-cell confocal imaging (refers to supplementary movie 5). D: donor; R: recipient. Arrows: transferred ApoE-CD63 signals; stars: transferred CD63-only signals.

(C) Donor and recipient cells from (A) were cocultured and fixed at 24 h and 48 h post-seeding. The number of ApoE-CD63 positive signals in single recipient cells were quantified. Each dot represents single cells. P-value was determined using unpaired Student's t-test.

IV. DISCUSSION

1.   Attempts to identify HCV assembly sites

Based on a recent study by Lee and colleagues suggesting that HCV assembly might take place at DMV-connected ER membranes in close proximity to lipid droplets where NS5A and E2 colocalize [21] and a recent estimate that around 300 copies of ApoE are incorporated into a single HCV particle [125], I assumed that the labeling of HCV particles should be feasible. To increase confidence, I included ApoE as a critical cellular factor for HCV assembly on top of these two essential viral factors in order to identify HCV assembly sites and intracellular HCV particles. I assumed that ApoE signals join with or come close to NS5A-E2 puncta at the assembly sites because it has been suggested that HCV particles acquire ApoE-containing lipid shields intracellularly [64, 95, 126, 127]. Indeed, the triple-colocalizing signals did exist but I was not able to find any convincing evidence of HCV budding events or HCV particles in these subcellular areas.

One of the major disadvantage of using ApoE as HCV particle marker that I did not expect was its very high abundance in the endosomes of hepatocytes. Since ApoE enters the ER lumen cotranslationally, it is commonly assumed that ApoE is well abundant in this compartment but not in the endosomes. Actually, indirect immunostaining of ApoE in fixed cells using ApoE-specific antibody generally revealed diffuse ER-like pattern of this protein. However, live-cell imaging with both FP-tagged and SNAP-tagged ApoE showed the massive accumulation of this protein in the late endosomes which possibly masked the weaker ER-luminal ApoE and ApoE signals on HCV particles. My data showed that triple-colocalizing dots of ApoE-NS5A-E2 existed periodically (~17-32 minutes) and might reflect the interplay between ApoE-containing endosomes and the NS5A-E2 localizing ER established by HCV. Such an ER-endosome contact mediated by HCV is an interesting observation that requires more comprehensive investigation.

In addition, I also attempted to search for HCV particles unbiasedly by screening whole-cell volumes with serial thin sections by TEM or thick sections with electron tomography of plastic-embedded HCV-replicating cells. Indeed, in one particular sample preparation I observed a dilated ER compartment connected to the rough ER via a narrow-neck structure, similar to a structure reported earlier with a surrogate HCV assembly model (PMC136094P). In addition, the neck-like structure was linked to DMVs (putative sites of viral RNA replication). Notably, two ~70nm spherical particles were found in this ER-derived compartment (Figure 49). Since the dilated ER lumen was also suggested be the HCV budding site [128] and viral RNA-replication happened in vicinity of the particle assembly process [21], I assumed the identified subcellular

structure above was potentially HCV assembly site. However, I could not correlate precisely these electron-dense spheres to the corresponding E2 and ApoE IF signals.
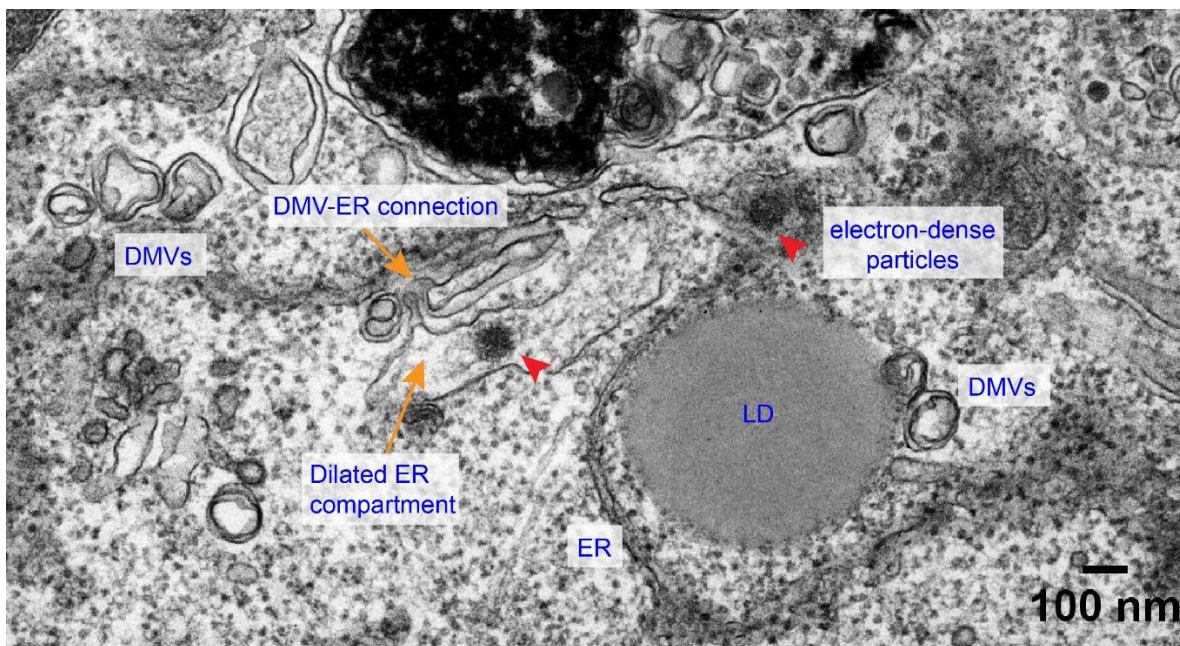
Figure 49. Unbiased screening of HCV particles in HCV-replicating cells

Lunet/ApoE^{mT2} cells harboring HCV Core-NS2/E2^{eYFP} were electroporated with *in vitro*-transcribed sgJFH1/NS5A^{mCherry} RNA. Cells were subjected to confocal imaging at 36 h.p.e to acquire ApoE, NS5A, and E2 signals. Cells were subjected to the CLEM protocol. Plastic-embedded cells were cut into serial 70nm-sections and unbiasedly screened for HCV particles by TEM. This region of interest showing two electron-dense spherical structures was correlated to the IF micrograph to find the IF signature of the structures. Arrowheads point to electron-dense particles in the dilated EM compartment which is connected to the DMVs and is close to a lipid droplet.

Apart from these approaches, I pursued various alternative strategies to visualize HCV assembly sites. For example, I truncated the HCV E2 glycoprotein in order to arrest assembling HCV particles [129]. Along the same lines, I used a HCV NS3 mutant (E530A/G) having a defect in virus particle morphogenesis. In both cases, I expected to observe arrested assembling HCV particles at the virus budding sites that I wanted to visualize by CLEM. However, in spite of using various imaging protocols obtained results were inconclusive (for a summary see Chapter 2 of the APPENDIX section).

There are many reasons for the failure of my attempts, including the rarity of assembly events and the amorphous structure of HCV particles. In addition, the sizes of HCV particles are below the diffraction limit of confocal microscopy and the low precision of IF-EM correlation in the axial dimension complicates the problem. Finally, weak signals of ApoE and E2 decorated on virus particles might be further dampened after EM fixation, giving rise to low signal-to-noise ratio.

2. Intercellular co-transmission of ApoE-containing lipoproteins and extracellular vesicles in HCV-infected cells

Although I could not faithfully discover HCV assembly sites in HCV-replicating cells, the imaging systems I had created, including FP-tagged and SNAP-tagged ApoE and the engineered HCV genomes with labeled NS5A and E2 allowed me to discover another important aspect of HCV biology, particularly HCV-produced NS5A-and viral RNA-containing EVs, which were found to associate with ApoE-containing lipoproteins. Indeed, ApoE imaging with fully functional tags allowed me to track ApoE-lipoprotein egress in HCV-infected and naïve hepatocytes. Remarkably, I detected strong accumulation of ApoE in late endosomes, indicating that they are potential storage places of lipoproteins in hepatocytes, which so far has been underestimated by ApoE staining in fixed-cell conditions.

EVs are a "language" exploited by both host cells and viruses to conduct intercellular communication. In addition to the formation of the infectious virus particles, numerous viruses including HCV modify the host endosomal machinery to make their own vesicles that could also transmit their genetic materials [71]. In my studies, I demonstrate that HCV infection produced intraluminal ApoE-associated NS5A-positive vesicles inside the late endosomes at a post-assembly time point of HCV infection. However, how HCV-produced NS5A-and RNA-containing IVs gets into late endosomes remains a challenging puzzle to be solved.

Previous reports have shown possible interaction between ApoE and NS5A which is critical for HCV assembly [41, 42]. Paradoxically, ApoE and NS5A were thought to localize to the luminal and the cytoplasmic leaflet of the ER, respectively. Given the contradictory topologies of these two proteins in the ER- localizing sites, the interaction between them was not explained. My study suggests that late endosomes are the potential interaction sites of ApoE and NS5A; and this

interaction not only plays a role in HCV assembly, as demonstrated in earlier reports, but also is relevant to the non-virion EV-mediated release of HCV RNA. The release of HCV RNA can benefit the virus by avoiding the recognition by innate RNA sensors such as TLR3 [88] and may establish a new infection when the RNA-bearing EVs are taken up by the bystander cells [84, 86]. Alternatively, these EVs can transmit HCV-derived factors to uninfected cells and promote pathogenesis. For example, miR-19a containing EVs released from HCV-infected hepatocytes activate hepatic stellate cells and promote liver fibrosis [85].

Remarkably, my data also argue for the presence of NS5A on the surface of HCV-produced IVs/EVs making it well accessible for the binding of NS5A-specific antibody. It is likely that NS5A might be a part of a "putative pore" of HCV-produced IVs/EVs which is reminiscent to what has been demonstrated for murine hepatitis coronavirus (MHV) and SARS-CoV-2 [121] with NS5A localizing to the external structure of such a pore. To corroborate this observation, I have been studying the ultrastructure of HCV DMVs by cryo-FIB-SEM. My preliminary data suggest the presence of "pore-like" structures in HCV DMVs. Importantly, there are protruding electron-dense structures connected to the outer surface of such a "pore" (Chapter 3 of the APPENDIX section) that could potentially be NS5A. However, much more work is required to corroborate this assumption.

3.   Extracellular vesicles and virus infection in general

Apart from HCV, EVs have emerged as a novel and important mean of intercellular communication of various other RNA viruses. The molecular signatures and functions of these EVs vary depending on the particular virus system. One major contributing factor of the complex functions of EVs is the overlap between virus particle biogenesis and host EV-producing pathways, resulting in the formation of a mixed variety of EVs with different cellular and viral imprinted components [70, 71, 80]. The components and functions of EVs produced by several important pathogenic RNA viruses, including SARS-CoV2, Zika, and Dengue virus are listed in Table 12.

Table 12. Components and functions of RNA virus-produced EVs

Viruses	Discovered cellular/viral components in EVs	Implication for the virus/host	References
SARS-CoV2	SARS-CoV-2 Spike, CD9, CD41a	modulate the adaptive immune response	[130]
	SARS-CoV-2 RNA, Numerous cellular proteins including apolipoproteins	contributes to viral transmission contribute to inflammation, coagulation, and immunomodulation	[131]
	ACE2	neutralizes SARS-CoV-2 infection	[132, 133]
Zika virus	ZIKV RNA, ZIKV E protein	mediate viral transmission induce cell damage and inflammation	[134-136]
Dengue virus	IFITM3	contributes to antiviral effect from infected to non-infected cells	[137]
	CD9, CD81, and CD83	possibly protect virus by antibodies targeting the viral envelope	[138]
	DENV RNA, mosquito glycoprotein Tsp29Fb (CD63 ortholog)	mediate dengue virus transmission	[139]

In addition, EVs have been reported to be involved in transmission and pathogenesis of numerous viruses, including human immunodeficiency virus (HIV), Epstein-Barr virus (EBV), Herpes simplex virus (HSV), Human papillomavirus (HPV), Hepatitis B virus (HBV), and Influenza [71, 140]... Moreover, fungi, protozoa and bacteria have been documented to employ certain types of EVs facilitating their dissemination and evading the host immunity [79]. I would anticipate that in the upcoming years, we will witness an explosion of research into extracellular vesicles and viruses as well as other pathogens.

4. Intercellular co-transmission of ApoE-containing lipoproteins and extracellular vesicles under physiological conditions

Under conditions without virus-induced perturbation of the host, EVs are also considered as important means for the signal transduction from cell to cell. The net effect of the donor-derived EVs in recipient cells differs greatly according to the encapsulated signals in EVs at various levels i.e. EV-cell surface interaction or complete transfer of nucleic acids, proteins, cytokines, lipids, or metabolites. EVs have been reported as modulators of the complex communication between malignant and normal cells in every step of tumor development including initiation and evolution [141, 142]. In addition, this effect is not restricted to a local environment but well applicable to metastatic niches and organs, arguing for EVs as potential biomarkers for the diagnosis of cancer

[143]. Interestingly, in the central nervous system (CNS), EVs have been found to act as signal carriers. Exosomes are secreted by cells of the CNS including neurons, microglia, and oligodendroglia, as well as by cultured astrocytes and potentially involved in cell-cell communication in the CNS i.e. the exosomes released from the astrocytes selectively target neurons [144].

There are numerous significant similarities between EVs and lipoproteins, raising the question if there is a genuine physical interaction and functional relationship between these two vesicle species (refer to the Chapter 4.6 of the INTRODUCTION part). To the best of my knowledge, the interaction between ApoE-containing lipoproteins and CD63-positive IVs/EVs is exclusively reported in the pigment cells but not in other contexts [93]. Besides, there is evidence indicating that APOE4 genotype lowers exosome production in the brain where APOE4 is well recognized as the greatest risk factor for Alzheimer's disease [145]. In this present work, I demonstrated that, in uninfected hepatocytes, ApoE and CD63 (IV/EV marker) share the intracellular late endosomal trafficking route, are co-secreted, and partially co-enter target cells, suggesting a stable interaction between lipoproteins and CD63-positive IVs/EVs. This would explain why in various reports people found "contamination" of lipoproteins in their purified EVs, which turned out difficult to be separated [89, 90]. Perhaps, scavenger receptor class B type 1 (SR-BI) and heparan sulfate (HS) side chains decorating the IV/EV surface might mediate lipoprotein-IV/EV interaction or modulate lipid transfer from lipoproteins to IVs/EVs [92]. Since hepatic ApoE-containing lipoproteins are secreted into the bloodstream and circulate throughout the body, it is likely that they potentially modulate systemic changes in multiorganelle signaling through the interaction with their interacting EVs. This important topic in cell biology will most likely gain increasing attention in the future.

Collectively, this study not only clarifies the contribution of ApoE to the HCV replication cycle via the interaction with NS5A but also suggests its universal role in EV-mediated cell-to-cell communication with the first direct evidence of genuine intercellular co-transmission of ApoE-EVs. The key findings of this research project are depicted in Figure 50.
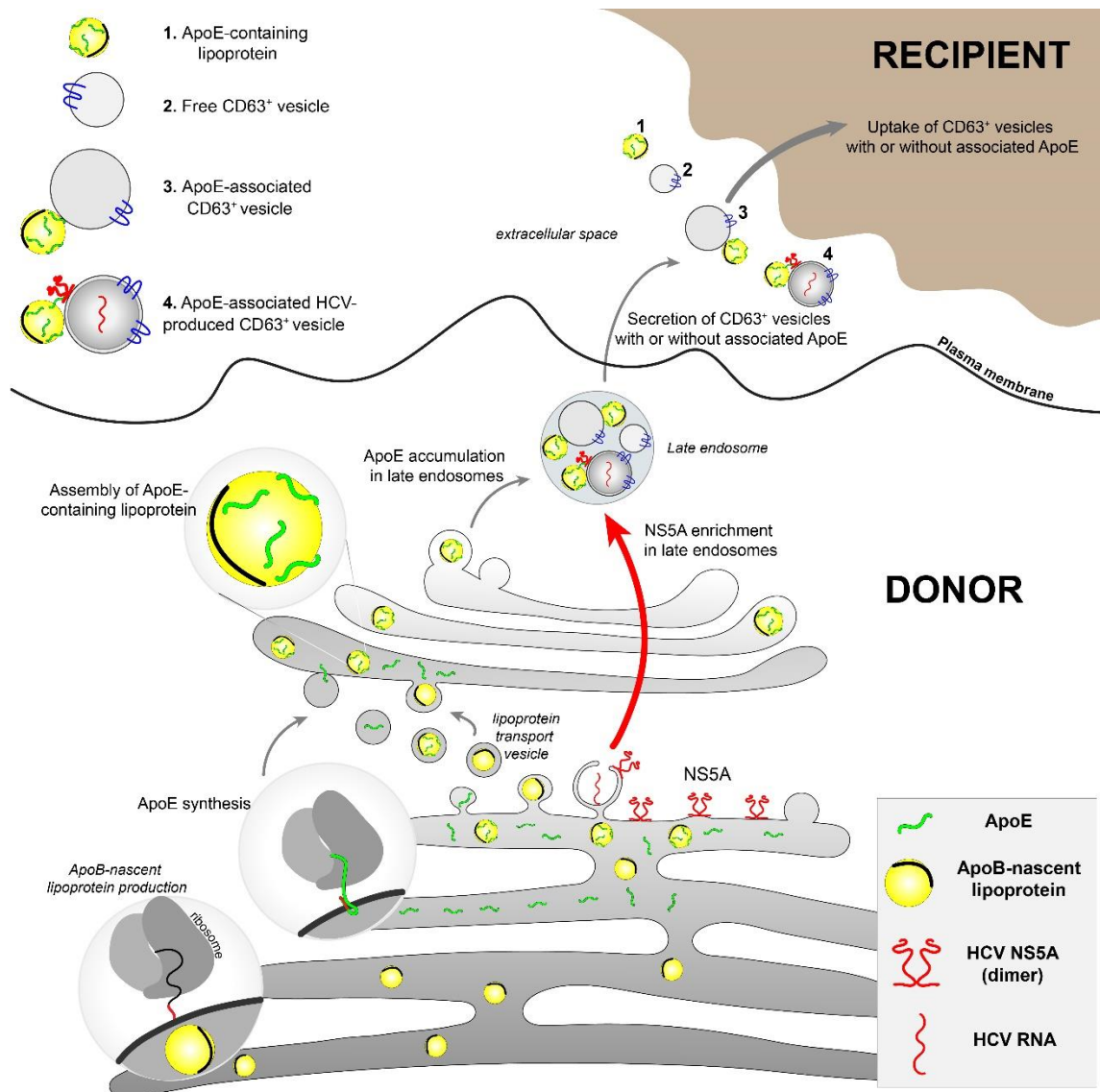
Figure 50. Intercellular co-transmission of hepatic ApoE-extracellular vesicle in naïve and HCV-infected cells

Under the physiological conditions, ApoE is co-translationally targeted to the ER lumen to enter the secretory pathway. Next, ApoE is further transported to the Golgi apparatus where the assembly of ApoE-containing lipoproteins occurs. ApoE-containing lipoproteins subsequently enter the late multivesicular endosomes where they meet and bind CD63-positive IVs. Thereafter, these endosomes fuse with the plasma membrane to release the inner content into the extracellular space. ApoE-containing lipoproteins could either enter the recipient cells alone or in association with EVs (case 1, 2 and 3).

In the HCV-infection context, HCV produces NS5A- and RNA-containing IVs inside the multivesicular endosomes where ApoE accumulates. The interaction between ApoE-NS5A in this compartment is essential for the efficient release of HCV RNA via EVs. The released ApoE-associated HCV-produced EVs enter the targets (case 4) which could probably transmit HCV RNA and establish new infection or trigger cellular responses. Figure taken from Pham *et al.*, submitted for publication.

5.   Association of ApoE-containing lipoproteins and Hepatitis B virus

Given that ApoE-containing lipoproteins associate with HCV particles and form lipoviroparticles as demonstrated previously [2], I wondered if there is any interplay between ApoE-containing lipoproteins with other host- or pathogen-derived vesicle species containing membrane phospholipids. Therefore, I examined infectious HBV virions (Dane particles) and sub-viral particles (SVPs) to determine possible interaction between ApoE-containing lipoproteins and virions or SVPs. I chose this virus system because endosomes were reported to be required for the budding and release of enveloped HBV virions and SVPs, similar to HCV [146-148]. Moreover, ApoE is required for the assembly and entry of this virus, arguing for the association of ApoE and HBV particles [147, 149, 150].

The purified infectious HBV particles and SVPs preparations were received from Firat Nebioglu, Department of Infectious Diseases, Molecular Virology, University of Heidelberg, Heidelberg, Germany. Note that HBV particles were often found to associate with small vesicles (Figure 51). The result of ApoE-immunogold labeling experiment suggested that ApoE is not a part of HBV structures *per se* but rather belongs to an associated lipoprotein (Figure 52) which is in good agreement with a study by Gomez-Escobar et al., 2022 [151]. Collectively, these results argue for a more universal function of ApoE-containing lipoproteins in association with pathogen-derived vesicles formed within the endosomal system of the cell.
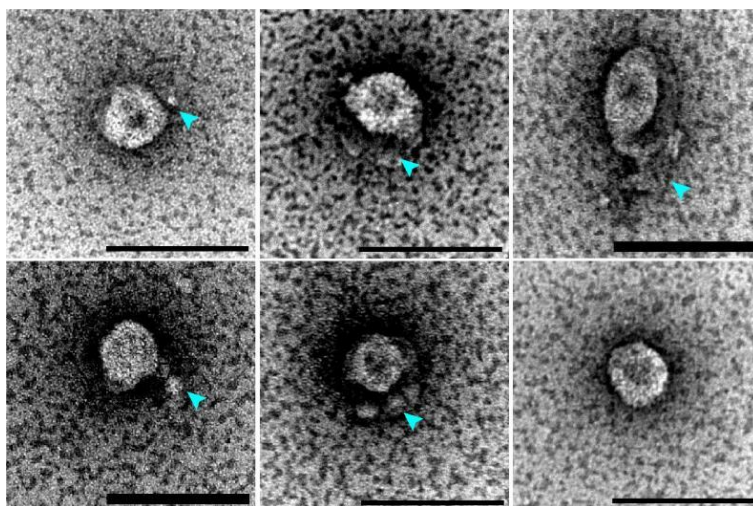
Figure 51. Negative staining of purified HBV Dane particles

Purified HBV Dane particles were negatively stained using 3% uranyl acetate and visualized by TEM. Arrowheads point to associated vesicles with HBV Dane particles. Scale bars: 100nm.

HBV Dane particle

HBV subviral particle

Anti-HBsAg

Anti-ApoE
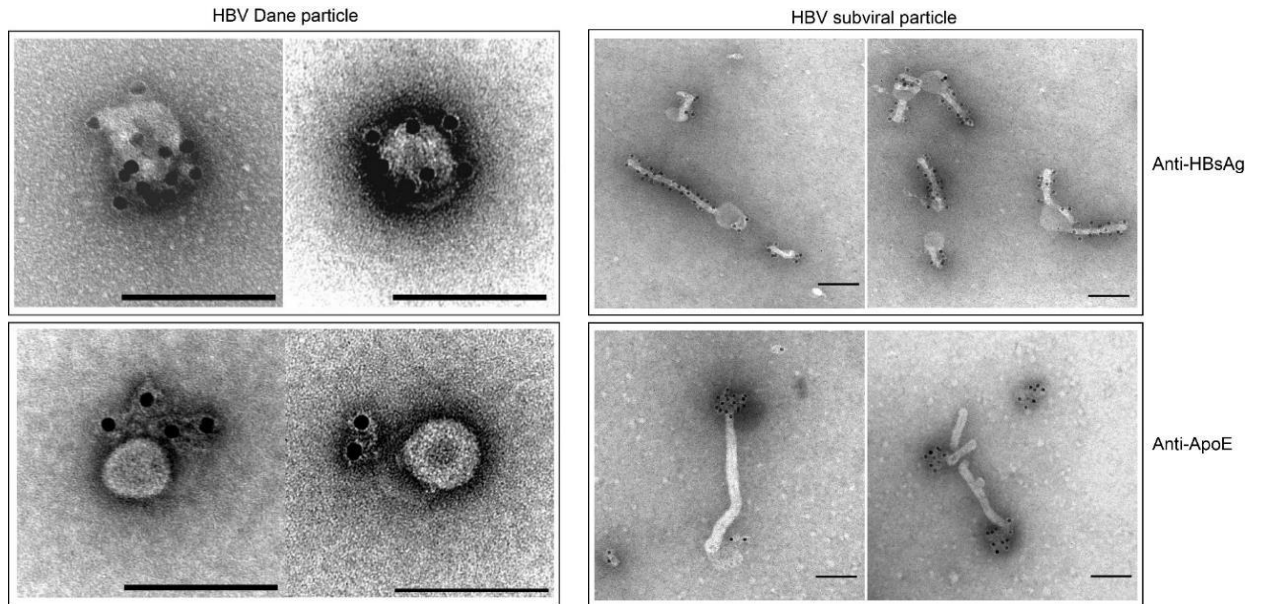
**Figure 52. Immunogold labeling of HBV Dane and subviral particles
with HBsAg- and ApoE-specific antibodies**

Purified HBV Dane particles (left) and SVPs (right) were either incubated with ApoE- (upper) or HBsAg-specific antibodies (lower) and subjected to immuno-gold labeling procedure using gold-conjugated protein A. Afterwards, samples were negatively stained using 2% uranyl acetate and visualized by TEM. Scale bars: 100nm.

V. BIBLIOGRAPHY

1.   WHO, 2022.
2.   Bartenschlager, R., et al., *Assembly of infectious hepatitis C virus particles.* Trends Microbiol, 2011. **19**(2): p. 95-103.
3.   Hepatitis C Online - DEV, U.o.W.I.D.E.A.I.p., *HCV life cycle*. 2022. p. https://www.hepatitisc.uw.edu/biology/lifecycle.
4.   Catanese, M.T., et al., *Ultrastructural analysis of hepatitis C virus particles.* Proc Natl Acad Sci U S A, 2013. **110**(23): p. 9505-10.
5.   Simmonds, P., *The origin of hepatitis C virus.* Curr Top Microbiol Immunol, 2013. **369**: p. 1-15.
6.   Lohmann, V., et al., *Replication of subgenomic hepatitis C virus RNAs in a hepatoma cell line.* Science, 1999. **285**(5424): p. 110-3.
7.   Bartenschlager, R., V. Lohmann, and F. Penin, *The molecular and structural basis of advanced antiviral therapy for hepatitis C virus infection.* Nat Rev Microbiol, 2013. **11**(7): p. 482-96.
8.   Agnello, V., et al., *Hepatitis C virus and other flaviviridae viruses enter cells via low density lipoprotein receptor.* Proc Natl Acad Sci U S A, 1999. **96**(22): p. 12766-71.
9.   Pileri, P., et al., *Binding of hepatitis C virus to CD81.* Science, 1998. **282**(5390): p. 938-41.
10.   Dubuisson, J. and F.L. Cosset, *Virology and cell biology of the hepatitis C virus life cycle: an update.* J Hepatol, 2014. **61**(1 Suppl): p. S3-s13.
11.   Lindenbach, B.D. and C.M. Rice, *The ins and outs of hepatitis C virus entry and assembly.* Nat Rev Microbiol, 2013. **11**(10): p. 688-700.
12.   Blanchard, E., et al., *Hepatitis C virus entry depends on clathrin-mediated endocytosis.* J Virol, 2006. **80**(14): p. 6964-72.
13.   Evans, M.J., et al., *Claudin-1 is a hepatitis C virus co-receptor required for a late step in entry.* Nature, 2007. **446**(7137): p. 801-5.
14.   Koutsoudakis, G., et al., *Characterization of the early steps of hepatitis C virus infection by using luciferase reporter viruses.* J Virol, 2006. **80**(11): p. 5308-20.
15.   Tscherne, D.M., et al., *Time- and temperature-dependent activation of hepatitis C virus for low-pH-triggered entry.* J Virol, 2006. **80**(4): p. 1734-41.
16.   Niepmann, M. and G.K. Gerresheim, *Hepatitis C Virus Translation Regulation.* Int J Mol Sci, 2020. **21**(7).
17.   Neddermann, P., et al., *The nonstructural proteins of the hepatitis C virus: structure and functions.* Biol Chem, 1997. **378**(6): p. 469-76.
18.   Lohmann, V., J.O. Koch, and R. Bartenschlager, *Processing pathways of the hepatitis C virus proteins.* J Hepatol, 1996. **24**(2 Suppl): p. 11-9.
19.   Carrère-Kremer, S., et al., *Regulation of hepatitis C virus polyprotein processing by signal peptidase involves structural determinants at the p7 sequence junctions.* J Biol Chem, 2004. **279**(40): p. 41384-92.
20.   Lohmann, V., *Hepatitis C virus RNA replication.* Curr Top Microbiol Immunol, 2013. **369**: p. 167-98.
21.   Lee, J.Y., et al., *Spatiotemporal Coupling of the Hepatitis C Virus Replication Cycle by Creating a Lipid Droplet- Proximal Membranous Replication Compartment.* Cell Rep, 2019. **27**(12): p. 3602-3617.e5.
22.   Bartenschlager, R., M. Frese, and T. Pietschmann, *Novel insights into hepatitis C virus replication and persistence.* Adv Virus Res, 2004. **63**: p. 71-180.

23. Romero-Brey, I., et al., *Three-dimensional architecture and biogenesis of membrane structures associated with hepatitis C virus replication.* PLoS Pathog, 2012. **8**(12): p. e1003056.

24. Appleby, T.C., et al., *Viral replication. Structural basis for RNA replication by the hepatitis C virus polymerase.* Science, 2015. **347**(6223): p. 771-5.

25. Paul, D., V. Madan, and R. Bartenschlager, *Hepatitis C virus RNA replication and assembly: living on the fat of the land.* Cell Host Microbe, 2014. **16**(5): p. 569-79.

26. Zayas, M., et al., *Coordination of Hepatitis C Virus Assembly by Distinct Regulatory Regions in Nonstructural Protein 5A.* PLoS Pathog, 2016. **12**(1): p. e1005376.

27. Gentzsch, J., et al., *hepatitis c Virus p7 is critical for capsid assembly and envelopment.* PLoS Pathog, 2013. **9**(5): p. e1003355.

28. Corless, L., et al., *Vps4 and the ESCRT-III complex are required for the release of infectious hepatitis C virus particles.* J Gen Virol, 2010. **91**(Pt 2): p. 362-72.

29. Gastaminza, P., et al., *Cellular determinants of hepatitis C virus assembly, maturation, degradation, and secretion.* J Virol, 2008. **82**(5): p. 2120-9.

30. Coller, K.E., et al., *Molecular determinants and dynamics of hepatitis C virus secretion.* PLoS Pathog, 2012. **8**(1): p. e1002466.

31. Brass, V., et al., *An Amino-terminal Amphipathic α-Helix Mediates Membrane Association of the Hepatitis C Virus Nonstructural Protein 5A*.* Journal of Biological Chemistry, 2002. **277**(10): p. 8130-8139.

32. Penin, F., et al., *Structure and function of the membrane anchor domain of hepatitis C virus nonstructural protein 5A.* J Biol Chem, 2004. **279**(39): p. 40835-43.

33. Badillo, A., et al., *Overall Structural Model of NS5A Protein from Hepatitis C Virus and Modulation by Mutations Confering Resistance of Virus Replication to Cyclosporin A.* Biochemistry, 2017. **56**(24): p. 3029-3048.

34. Tellinghuisen, T.L., J. Marcotrigiano, and C.M. Rice, *Structure of the zinc-binding domain of an essential component of the hepatitis C virus replicase.* Nature, 2005. **435**(7040): p. 374-9.

35. Tellinghuisen, T.L., et al., *The NS5A Protein of Hepatitis C Virus Is a Zinc Metalloprotein*.* Journal of Biological Chemistry, 2004. **279**(47): p. 48576-48587.

36. Quintavalle, M., et al., *The alpha isoform of protein kinase CKI is responsible for hepatitis C virus NS5A hyperphosphorylation.* Journal of virology, 2006. **80**(22): p. 11305-11312.

37. Tellinghuisen, T.L., K.L. Foss, and J. Treadaway, *Regulation of Hepatitis C Virion Production via Phosphorylation of the NS5A Protein.* PLOS Pathogens, 2008. **4**(3): p. e1000032.

38. Kim, J., D. Lee, and J. Choe, *Hepatitis C Virus NS5A Protein Is Phosphorylated by Casein Kinase II.* Biochemical and Biophysical Research Communications, 1999. **257**(3): p. 777-781.

39. Chen, Y.C., et al., *Polo-like kinase 1 is involved in hepatitis C virus replication by hyperphosphorylating NS5A.* J Virol, 2010. **84**(16): p. 7983-93.

40. Evans, M.J., C.M. Rice, and S.P. Goff, *Phosphorylation of hepatitis C virus nonstructural protein 5A modulates its protein interactions and viral RNA replication.* Proc Natl Acad Sci U S A, 2004. **101**(35): p. 13038-43.

41. Benga, W.J., et al., *Apolipoprotein E interacts with hepatitis C virus nonstructural protein 5A and determines assembly of infectious particles.* Hepatology, 2010. **51**(1): p. 43-53.

42. Cun, W., J. Jiang, and G. Luo, *The C-terminal alpha-helix domain of apolipoprotein E is required for interaction with nonstructural protein 5A and assembly of hepatitis C virus.* J Virol, 2010. **84**(21): p. 11532-41.

43. Romero-Brey, I., et al., *NS5A Domain 1 and Polyprotein Cleavage Kinetics Are Critical for Induction of Double-Membrane Vesicles Associated with Hepatitis C Virus Replication.* mBio, 2015. **6**(4): p. e00759.

44. Reiss, S., et al., *Recruitment and activation of a lipid kinase by hepatitis C virus NS5A is essential for integrity of the membranous replication compartment.* Cell host & microbe, 2011. **9**(1): p. 32-45.

45. Ascher, D.B., et al., *Potent hepatitis C inhibitors bind directly to NS5A and reduce its affinity for RNA.* Sci Rep, 2014. **4**: p. 4765.

46. Verdegem, D., et al., *Domain 3 of NS5A protein from the hepatitis C virus has intrinsic alpha-helical propensity and is a substrate of cyclophilin A.* J Biol Chem, 2011. **286**(23): p. 20441-54.

47. Appel, N., et al., *Essential role of domain III of nonstructural protein 5A for hepatitis C virus infectious particle assembly.* PLoS Pathog, 2008. **4**(3): p. e1000035.

48. Reyes, G.R., *The nonstructural NS5A protein of hepatitis C virus: an expanding, multifunctional role in enhancing hepatitis C virus pathogenesis.* J Biomed Sci, 2002. **9**(3): p. 187-97.

49. He, Y., K.A. Staschke, and S.L. Tan, *HCV NS5A: A Multifunctional Regulator of Cellular Pathways and Virus Replication*, in *Hepatitis C Viruses: Genomes and Molecular Biology*, S.L. Tan, Editor. 2006, Horizon Bioscience Copyright © 2006, Horizon Bioscience.: Norfolk (UK).

50. Macdonald, A. and M. Harris, *Hepatitis C virus NS5A: tales of a promiscuous protein.* J Gen Virol, 2004. **85**(Pt 9): p. 2485-2502.

51. Mahley, R.W., et al., *Plasma lipoproteins: apolipoprotein structure and function.* J Lipid Res, 1984. **25**(12): p. 1277-94.

52. Pettersson, C., *Studies on the atherogenicity of apoB-containing lipoproteins in type 2 diabetes.* 2022.

53. Zannis, V.I., P.W. Just, and J.L. Breslow, *Human apolipoprotein E isoprotein subclasses are genetically determined.* Am J Hum Genet, 1981. **33**(1): p. 11-24.

54. Zannis, V.I., et al., *Proposed nomenclature of apoE isoproteins, apoE genotypes, and phenotypes.* J Lipid Res, 1982. **23**(6): p. 911-4.

55. Zannis, V.I., et al., *Synthesis, intracellular processing, and signal peptide of human apolipoprotein E.* Journal of Biological Chemistry, 1984. **259**(9): p. 5495-5499.

56. Yamazaki, Y., et al., *Apolipoprotein E and Alzheimer disease: pathobiology and targeting strategies.* Nat Rev Neurol, 2019. **15**(9): p. 501-518.

57. Huang, Y. and R.W. Mahley, *Apolipoprotein E: structure and function in lipid metabolism, neurobiology, and Alzheimer's diseases.* Neurobiol Dis, 2014. **72 Pt A**: p. 3-12.

58. Mahley, R.W. and B. Angelin, *Type III hyperlipoproteinemia: recent insights into the genetic defect of familial dysbetalipoproteinemia.* Adv Intern Med, 1984. **29**: p. 385-411.

59. Henneman, P., et al., *The expression of type III hyperlipoproteinemia: involvement of lipolysis genes.* Eur J Hum Genet, 2009. **17**(5): p. 620-8.

60. Dove, D.E., M.F. Linton, and S. Fazio, *ApoE-mediated cholesterol efflux from macrophages: separation of autocrine and paracrine effects.* Am J Physiol Cell Physiol, 2005. **288**(3): p. C586-92.

61. Annema, W., et al., *ApoE promotes hepatic selective uptake but not RCT due to increased ABCA1-mediated cholesterol efflux to plasma.* Journal of Lipid Research, 2012. **53**(5): p. 929-940.

62. Huang, Z.H., et al., *Sterol efflux mediated by endogenous macrophage ApoE expression is independent of ABCA1.* Arterioscler Thromb Vasc Biol, 2001. **21**(12): p. 2019-25.

63. Lumsden, A.L., et al., *Apolipoprotein E (APOE) genotype-associated disease risks: a phenome-wide, registry-based, case-control study utilising the UK Biobank.* EBioMedicine, 2020. **59**: p. 102954.

64. Lee, J.-Y., et al., *Apolipoprotein E likely contributes to a maturation step of infectious hepatitis C virus particles and interacts with viral envelope glycoproteins.* Journal of virology, 2014. **88**(21): p. 12422-12437.

65. Long, G., et al., *Mouse hepatic cells support assembly of infectious hepatitis C virus particles.* Gastroenterology, 2011. **141**(3): p. 1057-66.

66. Crouchet, E., et al., *Extracellular lipid-free apolipoprotein E inhibits HCV replication and induces ABCG1-dependent cholesterol efflux.* Gut, 2017. **66**(5): p. 896-907.

67. Liu, S., et al., *Human apolipoprotein E peptides inhibit hepatitis C virus entry by blocking virus binding.* Hepatology, 2012. **56**(2): p. 484-91.

68. Evans, M.J., C.M. Rice, and S.P. Goff, *Phosphorylation of hepatitis C virus nonstructural protein 5A modulates its protein interactions and viral RNA replication.* 2004. **101**(35): p. 13038-13043.

69. Hossain, T., et al., *Mature VLDL triggers the biogenesis of a distinct vesicle from the trans-Golgi network for its export to the plasma membrane.* Biochem J, 2014. **459**(1): p. 47-58.

70. Nolte-'t Hoen, E., et al., *Extracellular vesicles and viruses: Are they close relatives?* Proc Natl Acad Sci U S A, 2016. **113**(33): p. 9155-61.

71. Martins, S.d.T. and L.R. Alves, *Extracellular Vesicles in Viral Infections: Two Sides of the Same Coin?* 2020. **10**(737).

72. O'Brien, K., et al., *RNA delivery by extracellular vesicles in mammalian cells and its applications.* Nature Reviews Molecular Cell Biology, 2020. **21**(10): p. 585-606.

73. Schorey, J.S., et al., *Exosomes and other extracellular vesicles in host-pathogen interactions.* EMBO Rep, 2015. **16**(1): p. 24-43.

74. Nederveen, J.P., et al., *Extracellular Vesicles and Exosomes: Insights From Exercise Science.* Front Physiol, 2020. **11**: p. 604274.

75. van Niel, G., G. D'Angelo, and G. Raposo, *Shedding light on the cell biology of extracellular vesicles.* Nature Reviews Molecular Cell Biology, 2018. **19**(4): p. 213-228.

76. Kalluri, R. and V.S. LeBleu, *The biology, function, and biomedical applications of exosomes.* Science, 2020. **367**(6478).

77. Clancy, J.W., M. Schmidtmann, and C. D'Souza-Schorey, *The ins and outs of microvesicles.* FASEB BioAdvances, 2021. **3**(6): p. 399-406.

78. Gurung, S., et al., *The exosome journey: from biogenesis to uptake and intracellular signalling.* Cell Communication and Signaling, 2021. **19**(1): p. 47.

79. Delabranche, X., et al., *Microparticles and infectious diseases.* Médecine et Maladies Infectieuses, 2012. **42**(8): p. 335-343.

80. Wang, J., et al., *Host derived exosomes-pathogens interactions: Potential functions of exosomes in pathogen infection.* Biomedicine & Pharmacotherapy, 2018. **108**: p. 1451-1459.

81. Chen, L., et al., *Exosomes derived from HIV-1-infected cells promote growth and progression of cancer via HIV TAR RNA.* Nature Communications, 2018. **9**(1): p. 4585.

82. Barberis, E., et al., *Circulating Exosomes Are Strongly Involved in SARS-CoV-2 Infection.* Frontiers in Molecular Biosciences, 2021. **8**.

83. Douam, F., D. Lavillette, and F.L. Cosset, *The mechanism of HCV entry into host cells.* Prog Mol Biol Transl Sci, 2015. **129**: p. 63-107.

84. Dreux, M., et al., *Short-range exosomal transfer of viral RNA from infected cells to plasmacytoid dendritic cells triggers innate immunity.* Cell Host Microbe, 2012. **12**(4): p. 558-70.

85. Devhare, P.B., et al., *Exosome-Mediated Intercellular Communication between Hepatitis C Virus-Infected Hepatocytes and Hepatic Stellate Cells.* J Virol, 2017. **91**(6).

86. Bukong, T.N., et al., *Exosomes from hepatitis C infected patients transmit HCV infection and contain replication competent viral RNA in complex with Ago2-miR122-HSP90.* PLoS Pathog, 2014. **10**(10): p. e1004424.

87. Eyre, N.S., et al., *Sensitive luminescent reporter viruses reveal appreciable release of hepatitis C virus NS5A protein into the extracellular environment.* Virology, 2017. **507**: p. 20-31.

88. Grünvogel, O., et al., *Secretion of Hepatitis C Virus Replication Intermediates Reduces Activation of Toll-Like Receptor 3 in Hepatocytes.* Gastroenterology, 2018. **154**(8): p. 2237-2251.e16.

89.   Onódi, Z., et al., *Isolation of High-Purity Extracellular Vesicles by the Combination of Iodixanol Density Gradient Ultracentrifugation and Bind-Elute Chromatography From Blood Plasma.* 2018. **9**(1479).

90.   Brennan, K., et al., *A comparison of methods for the isolation and separation of extracellular vesicles from protein and lipid particles in human serum.* Scientific Reports, 2020. **10**(1): p. 1039.

91.   Sódar, B.W., et al., *Low-density lipoprotein mimics blood plasma-derived exosomes and microvesicles during isolation and detection.* Scientific Reports, 2016. **6**(1): p. 24316.

92.   Angeloni, N.L., et al., *Pathways for Modulating Exosome Lipids Identified By High-Density Lipoprotein-Like Nanoparticle Binding to Scavenger Receptor Type B-1.* Scientific Reports, 2016. **6**(1): p. 22915.

93.   van Niel, G., et al., *Apolipoprotein E Regulates Amyloid Formation within Endosomes of Pigment Cells.* Cell Reports, 2015. **13**(1): p. 43-51.

94.   Graham, F.L., et al., *Characteristics of a human cell line transformed by DNA from human adenovirus type 5.* J Gen Virol, 1977. **36**(1): p. 59-74.

95.   Hueging, K., et al., *Apolipoprotein E codetermines tissue tropism of hepatitis C virus and is crucial for viral cell-to-cell transmission by contributing to a postenvelopment step of assembly.* J Virol, 2014. **88**(3): p. 1433-46.

96.   Blight, K.J., J.A. McKeating, and C.M. Rice, *Highly permissive cell lines for subgenomic and genomic hepatitis C virus RNA replication.* J Virol, 2002. **76**(24): p. 13001-14.

97.   Pietschmann, T., et al., *Construction and characterization of infectious intragenotypic and intergenotypic hepatitis C virus chimeras.* 2006. **103**(19): p. 7408-7413.

98.   Ruggieri, A., et al., *Dynamic oscillation of translation and stress granule formation mark the cellular response to virus infection.* Cell Host Microbe, 2012. **12**(1): p. 71-85.

99.   Friebe, P., et al., *Kissing-loop interaction in the 3' end of the hepatitis C virus genome essential for RNA replication.* Journal of virology, 2005. **79**(1): p. 380-392.

100.   Verweij, F.J., et al., *Quantifying exosome secretion from single cells reveals a modulatory role for GPCR signaling.* J Cell Biol, 2018. **217**(3): p. 1129-1142.

101.   Sung, B.H., et al., *A live cell reporter of exosome secretion and uptake reveals pathfinding behavior of migrating cells.* Nature communications, 2020. **11**(1): p. 2092-2092.

102.   Somiya, M. and S. Kuroda, *Reporter gene assay for membrane fusion of extracellular vesicles.* J Extracell Vesicles, 2021. **10**(13): p. e12171.

103.   Miyanari, Y., et al., *The lipid droplet is an important organelle for hepatitis C virus production.* Nat Cell Biol, 2007. **9**(9): p. 1089-97.

104.   Paul, D., et al., *NS4B self-interaction through conserved C-terminal elements is required for the establishment of functional hepatitis C virus replication complexes.* Journal of virology, 2011. **85**(14): p. 6963-6976.

105.   van den Hoff, M.J., A.F. Moorman, and W.H. Lamers, *Electroporation in 'intracellular' buffer increases cell survival.* Nucleic Acids Res, 1992. **20**(11): p. 2902.

106.   Neufeldt, C.J., et al., *ER-shaping atlastin proteins act as central hubs to promote flavivirus replication and virion assembly.* Nature Microbiology, 2019. **4**(12): p. 2416-2429.

107.   Mastronarde, D.N., *Automated electron microscope tomography using robust prediction of specimen movements.* J Struct Biol, 2005. **152**(1): p. 36-51.

108.   Paul, D., et al., *Morphological and biochemical characterization of the membranous hepatitis C virus replication compartment.* Journal of virology, 2013. **87**(19): p. 10612-10627.

109.   Ritter, C., et al., *Data fusion and smoothing for probabilistic tracking of viral structures in fluorescence microscopy images.* Medical Image Analysis, 2021. **73**: p. 102168.

110.   Godinez, W.J. and K. Rohr, *Tracking multiple particles in fluorescence time-lapse microscopy images via probabilistic data association.* IEEE Trans Med Imaging, 2015. **34**(2): p. 415-32.

111.   Sage, D., et al., *Automatic tracking of individual fluorescence particles: application to the study of chromosome dynamics.* IEEE Transactions on Image Processing, 2005. **14**(9): p. 1372-1383.

112.   Saxton, M.J., *Single-particle tracking: the distribution of diffusion coefficients.* Biophys J, 1997. **72**(4): p. 1744-53.

113.   Imle, A., et al., *Experimental and computational analyses reveal that environmental restrictions shape HIV-1 spread in 3D cultures.* Nat Commun, 2019. **10**(1): p. 2144.

114.   Takacs, C.N., et al., *Green fluorescent protein-tagged apolipoprotein E: A useful marker for the study of hepatic lipoprotein egress.* Traffic, 2017. **18**(3): p. 192-204.

115.   Goedhart, J., et al., *Structure-guided evolution of cyan fluorescent proteins towards a quantum yield of 93%.* Nature Communications, 2012. **3**(1): p. 751.

116.   Fukuhara, T., et al., *Amphipathic α-helices in apolipoproteins are crucial to the formation of infectious hepatitis C virus particles.* PLoS pathogens, 2014. **10**(12): p. e1004534-e1004534.

117.   Lussignol, M., et al., *Proteomics of HCV virions reveals an essential role for the nucleoporin Nup98 in virus morphogenesis.* Proceedings of the National Academy of Sciences, 2016. **113**(9): p. 2484-2489.

118.   Wozniak Ann, L., et al., *Hepatitis C virus promotes virion secretion through cleavage of the Rab7 adaptor protein RILP.* Proceedings of the National Academy of Sciences, 2016. **113**(44): p. 12484-12489.

119.   Ji, M., et al., *VMP1 and TMEM41B are essential for DMV formation during β-coronavirus infection.* Journal of Cell Biology, 2022. **221**(6).

120.   Catalano, M. and L. O'Driscoll, *Inhibiting extracellular vesicles formation and release: a review of EV inhibitors.* J Extracell Vesicles, 2020. **9**(1): p. 1703244.

121.   Shamseddine, A.A., M.V. Airola, and Y.A. Hannun, *Roles and regulation of neutral sphingomyelinase-2 in cellular and pathological processes.* Adv Biol Regul, 2015. **57**: p. 24-41.

122.   Nyathi, Y., B.M. Wilkinson, and M.R. Pool, *Co-translational targeting and translocation of proteins to the endoplasmic reticulum.* Biochimica et Biophysica Acta (BBA) - Molecular Cell Research, 2013. **1833**(11): p. 2392-2402.

123.   Cabukusta, B. and J. Neefjes, *Mechanisms of lysosomal positioning and movement.* Traffic, 2018. **19**(10): p. 761-769.

124.   Dennis, J.R., J. Howard, and V. Vogel, *Molecular shuttles: directed motion of microtubules along nanoscale kinesin tracks.* Nanotechnology, 1999. **10**: p. 232-236.

125.   Merz, A., et al., *Biochemical and morphological properties of hepatitis C virus particles and determination of their lipidome.* J Biol Chem, 2011. **286**(4): p. 3018-32.

126.   Cosset, F.L., et al., *HCV Interplay with Lipoproteins: Inside or Outside the Cells?* Viruses, 2020. **12**(4).

127.   Fukuhara, T., et al., *Amphipathic α-helices in apolipoproteins are crucial to the formation of infectious hepatitis C virus particles.* PLoS Pathog, 2014. **10**(12): p. e1004534.

128.   Blanchard, E., et al., *Hepatitis C virus-like particle morphogenesis.* J Virol, 2002. **76**(8): p. 4073-9.

129.   Vieyres, G., J. Dubuisson, and T. Pietschmann, *Incorporation of Hepatitis C Virus E1 and E2 Glycoproteins: The Keystones on a Peculiar Virion.* Viruses, 2014. **6**: p. 1149-87.

130.   Pesce, E., et al., *Exosomes Recovered From the Plasma of COVID-19 Patients Expose SARS-CoV-2 Spike-Derived Fragments and Contribute to the Adaptive Immune Response.* Front Immunol, 2021. **12**: p. 785941.

131.   Barberis, E., et al., *Circulating Exosomes Are Strongly Involved in SARS-CoV-2 Infection.* 2021. **8**(29).

132.   El-Shennawy, L., et al., *Circulating ACE2-expressing extracellular vesicles block broad strains of SARS-CoV-2.* Nature Communications, 2022. **13**(1): p. 405.

133.   Troyer, Z., et al., *Extracellular vesicles carry SARS-CoV-2 spike protein and serve as decoys for neutralizing antibodies.* J Extracell Vesicles, 2021. **10**(8): p. e12112.

134.   Martínez-Rojas, P.P., et al., *Participation of Extracellular Vesicles from Zika-Virus-Infected Mosquito Cells in the Modification of Naïve Cells' Behavior by Mediating Cell-to-Cell Transmission of Viral Elements.* Cells, 2020. **9**(1).

135.   Zhou, W., et al., *Exosomes mediate Zika virus transmission through SMPD3 neutral Sphingomyelinase in cortical neurons.* Emerg Microbes Infect, 2019. **8**(1): p. 307-326.

136.   York, S.B., et al., *Zika Virus Hijacks Extracellular Vesicle Tetraspanin Pathways for Cell-to-Cell Transmission.* mSphere, 2021. **6**(3): p. e0019221.

137.   Zhu, X., et al., *IFITM3-containing exosome as a novel mediator for anti-viral response in dengue virus infection.* Cell Microbiol, 2015. **17**(1): p. 105-18.

138.   Martins, S.T., et al., *Characterization of Dendritic Cell-Derived Extracellular Vesicles During Dengue Virus Infection.* Front Microbiol, 2018. **9**: p. 1792.

139.   Vora, A., et al., *Arthropod EVs mediate dengue virus transmission through interaction with a tetraspanin domain containing glycoprotein Tsp29Fb.* Proc Natl Acad Sci U S A, 2018. **115**(28): p. E6604-e6613.

140.   Kumar, A., et al., *Extracellular Vesicles in Viral Replication and Pathogenesis and Their Potential Role in Therapeutic Intervention.* Viruses, 2020. **12**(8).

141.   Whiteside, T.L., *Tumor-Derived Exosomes and Their Role in Cancer Progression.* Adv Clin Chem, 2016. **74**: p. 103-41.

142.   Syn, N., et al., *Exosome-Mediated Metastasis: From Epithelial-Mesenchymal Transition to Escape from Immunosurveillance.* Trends Pharmacol Sci, 2016. **37**(7): p. 606-617.

143.   Hoshino, A., et al., *Tumour exosome integrins determine organotropic metastasis.* Nature, 2015. **527**(7578): p. 329-35.

144.   Venturini, A., et al., *Exosomes From Astrocyte Processes: Signaling to Neurons.* Front Pharmacol, 2019. **10**: p. 1452.

145.   Peng, K.Y., et al., *Apolipoprotein E4 genotype compromises brain exosome production.* Brain, 2019. **142**(1): p. 163-175.

146.   Watanabe, T., et al., *Involvement of host cellular multivesicular body functions in hepatitis B virus budding.* Proc Natl Acad Sci U S A, 2007. **104**(24): p. 10205-10.

147.   Jiang, B. and E. Hildt, *Intracellular Trafficking of HBV Particles.* Cells, 2020. **9**(9).

148.   Blondot, M.L., V. Bruss, and M. Kann, *Intracellular transport and egress of hepatitis B virus.* J Hepatol, 2016. **64**(1 Suppl): p. S49-s59.

149.   Tréguier, Y., A. Bull, and P. Roingeard, *Apolipoprotein E, a Crucial Cellular Protein in the Lifecycle of Hepatitis Viruses.* International Journal of Molecular Sciences, 2022. **23**: p. 3676.

150.   Qiao, L. and G.G. Luo, *Human apolipoprotein E promotes hepatitis B virus infection and production.* PLoS Pathog, 2019. **15**(8): p. e1007874.

151.   Gomez-Escobar, E., et al., *Incorporation of apolipoprotein E into HBV–HCV subviral envelope particles to improve the hepatitis vaccine strategy.* Scientific Reports, 2021. **11**(1): p. 21856.

VI. PUBLICATION

- K. Tabata, V. Prasad, D. Paul, J. Y. Lee, **M. T. Pham**, W. I. Twu, C. J. Neufeldt, M. Cortese, B. Cerikan, Y. Stahl, S. Joecks, C. S. Tran, C. Lüchtenborg, P. V'Kovski, K. Hörmann, A. C. Müller, C. Zitzmann, U. Haselmann, J. Beneke, L. Kaderali, H. Erfle, V. Thiel, V. Lohmann, G. Superti-Furga, B. Brügger and R. Bartenschlager (2021). "Convergent use of phosphatidic acid for hepatitis C virus and SARS-CoV-2 replication organelle formation." **Nat Commun** 12(1): 7276.

- O. Isken, **M. T. Pham**, H. Schwanke, F. Schlotthauer, R. Bartenschlager, and N. Tautz (2022). "Characterization of a multipurpose NS3 Surface patch coordinating HCV Replicase Assembly and Virion Morphogenesis." Manuscript in revision with **PloS pathogens**.

- **M. T. Pham**, J. Y. Lee, C. Ritter, R. Thielemann, U. Haselmann, C. Funaya, V. Laketa, K. Roth and R. Bartenschlager (2022). "Intercellular transmission of viral RNA by Apolipoprotein E-associated extracellular vesicles." Manuscript submitted to **Cell Reports** on June 17, 2022.

- C. Ritter, J. Y. Lee, **M. T. Pham**, M. K. Pabba, M. C. Cardoso, R. Bartenschlager, K. Rohr (2022). "Multi-Detector fusion and Bayesian smoothing for tracking viral and chromatin structure." Manuscript submitted to **Medical Image Analysis** on July 08, 2022.

- C. Ritter, R. Thielemann, J. Y. Lee, **M. T. Pham**, R. Bartenschlager, K. Rohr (2022). "ColocQuant and ColocJ: Multi-Channel colocalization analysis of viral proteins in fluorescence microscopy images." Manuscript will be submitted to **Scientific Reports** in August, 2022.

VII. APPENDIX

1. Characterization of ApoE mutants and HCV production

In addition to the characterization of ApoE^{mT2}, I also examined various ApoE mutants to study different aspects of the functional contribution of this protein to HCV production.
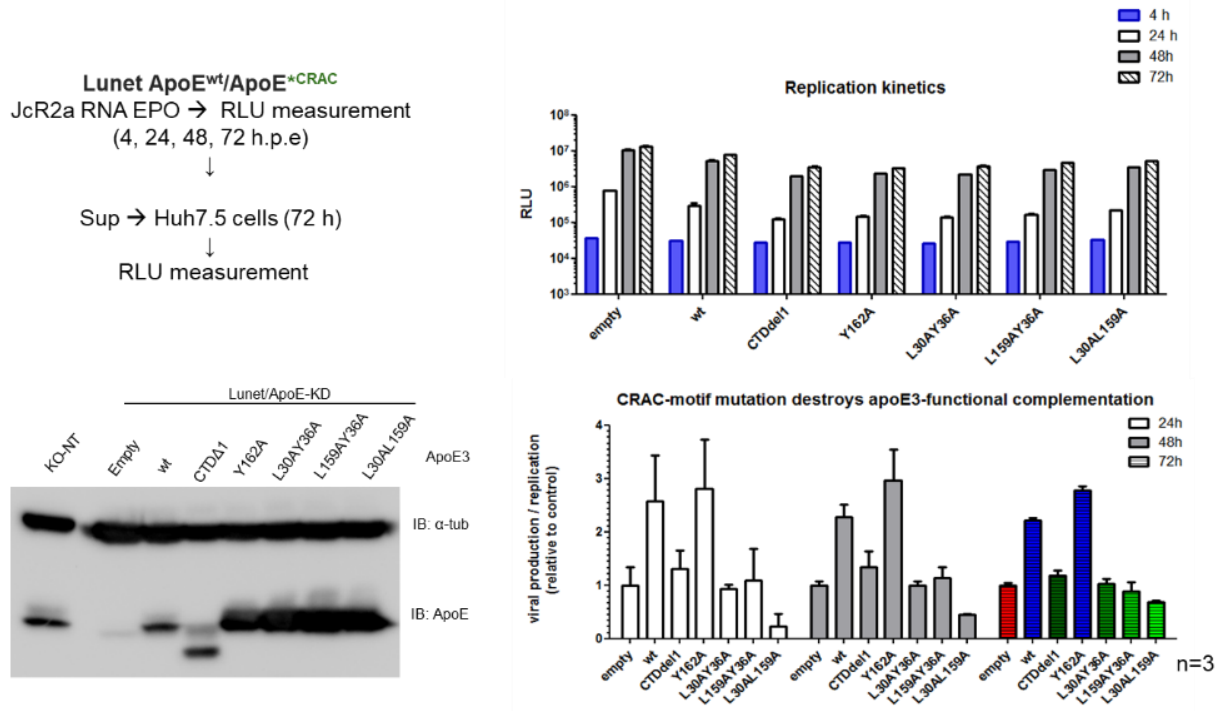
App. Tab/Fig 1. ApoE-CRAC mutants do not support the production of infectious HCV

[Left, upper] Experimental procedure: Lunet/ApoE-KD cells were transduced with lentiviruses containing either an empty vector (empty), ApoE^{wt} (wt), ApoE-C-terminal deletion (CTDΔ1), or ApoE CRAC mutants (ApoE^{CRAC*}) including Y162A, L30A-Y36A, L159A-Y36A, L30A-L159A, respectively and electroporated with *in vitro*-transcribed HCV JcR2a RNA. HCV-containing supernatants harvested at indicated time points were inoculated into naïve Huh7.5 cells.

[Left, lower] ApoE expression in ApoE-reconstituted cells. KO-NT: Lunet/non-targeting-knockout cell line was used as a reference for ApoE expression. ApoE was detected by ApoE-specific antibody. α-tubulin was used as an internal loading control.

[Right, upper] The replication of HCV at indicated time points were measured by RLU activity.

[Right, lower] Production of infectious HCV was measured by RLU activity at 72 h after inoculation. HCV infectivity normalized to HCV RNA replication is shown. Data are means (SD) from a representative experiment (n=3).

Note that ApoE CRAC mutants including L30A-Y36A, L159A-Y36A, L30A-L159A did not favor the production of infectious HCV. (CRAC: cholesterol recognition/interaction amino acid consensus sequence).
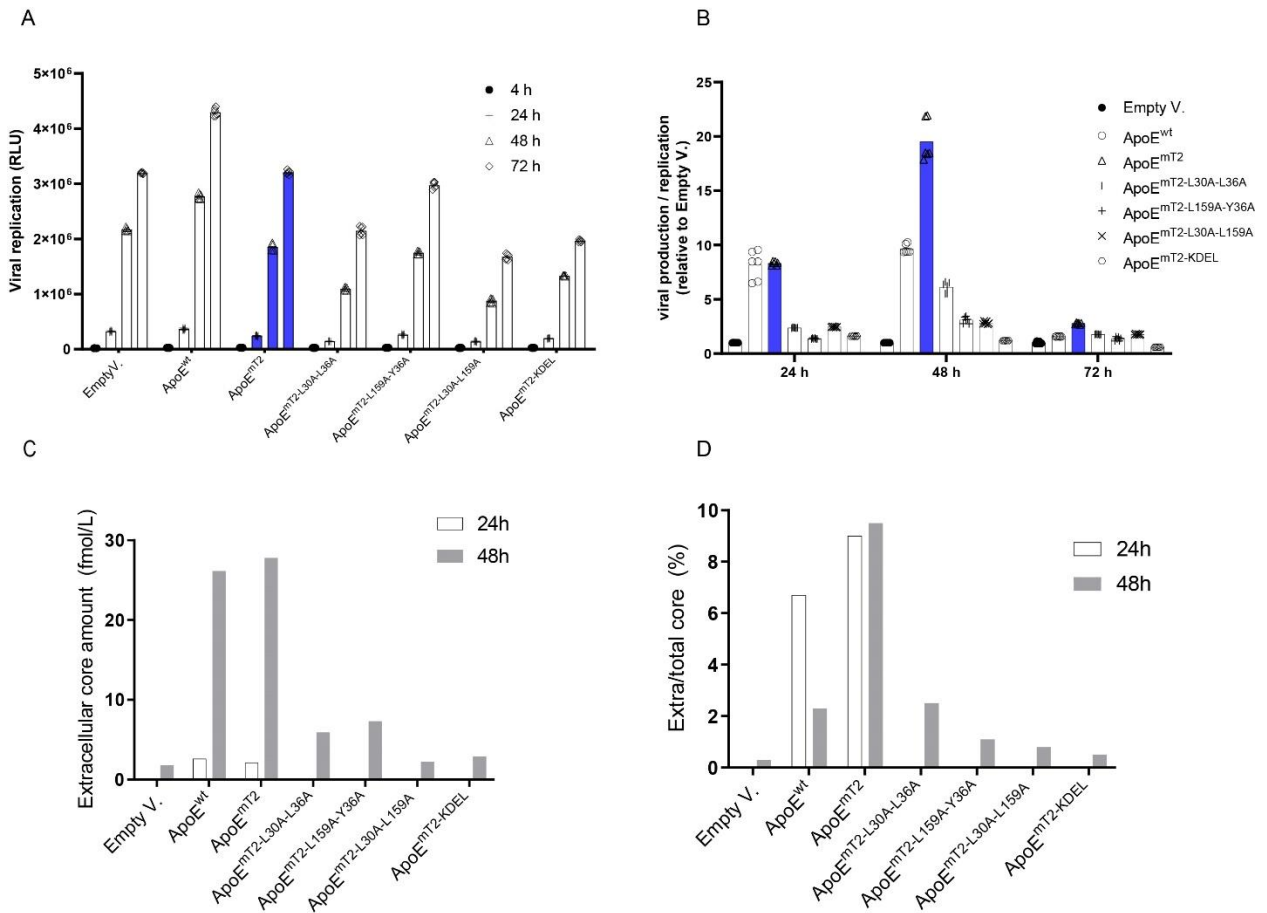
App. Tab/Fig 2. Functional validation of mT2-tagged ApoE^{wt} and mutants in HCV transmission

A) HEK293T-miR122 cells were transduced with either an empty vector (Empty V.), ApoE^{wt}, mT2-tagged ApoE^{wt} or mT2-tagged ApoE mutants as indicated, respectively and electroporated with *in vitro*-transcribed HCV JcR2a RNA. The replication of HCV at indicated time points were measured by RLU activity.

B) HCV-containing supernatants harvested at indicated time points were inoculated into naïve Huh7.5 cells. HCV infectivity was measured by RLU activity at 72 h after inoculation. HCV infectivity normalized to HCV RNA replication is shown.

C) The amounts of intracellular core protein (fmol/L) from A at indicated time points were measured by Core CMIA.

D) The amounts of extracellular core protein detected in culture supernatant from A at indicated time points were measured by Core CMIA. Ratios of extracellular core to total core are shown.
Data in panel A and B are means (SD) for a representative experiment (n=2).
Data in panel C and D are means for a representative experiment (n=2).

First replicate

	Sample name	Infectivity			Ratio to Total infectivity		Core amount			Ratio to Total infectivity	
		Extra/2ml	Intra/0,5ml	Total infectivity	Extra	Intra	extra core (fmol/12ml)	intra core (fmol/6ml)	Total core	Extra	Intra
1	ApoE-KD/ Empty V.	47.063	8.728	55.791	84,4%	15,64%	739	4.388	5.127	14%	86%
2	ApoE-KD/ ApoE-wt	382.268	8.728	390.996	97,8%	2,23%	841	2.026	2.868	29%	71%
3	ApoE-KD/ ApoE-CTDdel	85.518	1.482	87.001	98,3%	1,70%	567	2.059	2.626	22%	78%
4	ApoE-KD/ Y162A	156.060	4.803	160.864	97,0%	2,99%	1.421	1.870	3.291	43%	57%
5	**ApoE-KD/ L30A-Y36A**	85.518	6.475	91.993	93,0%	**7,04%**	381	2.189	2.569	15%	**85%**
6	**ApoE-KD/ Y36A-L159A**	25.900	4.803	30.703	84,4%	**15,64%**	206	2.474	2.681	8%	**92%**
7	**ApoE-KD/ L30A-L159A**	26.390	3.563	29.954	88,1%	**11,90%**	111	2.033	2.143	5%	**95%**
8	Naive-cell	284.790	8.728	293.518	97,0%	2,97%	2.106	4.186	6.293	33%	67%

Second replicate

	Sample name	Infectivity			Ratio to Total infectivity		Core amount			Ratio to Total infectivity	
		Extra/2ml	Intra/0,5ml	Total infectivity	Extra	Intra	extra core (fmol/12ml)	intra core (fmol/6ml)	Total core	Extra	Intra
1	ApoE-KD/ Empty V.	156.060	2.643	158.704	98,3%	1,67%	1.070	2.814	3.884	28%	72%
2	ApoE-KD/ ApoE-wt	697.591	3.563	701.154	99,5%	0,51%	1.631	1.877	3.508	47%	53%
3	ApoE-KD/ ApoE-CTDdel	156.060	3.563	159.624	97,8%	2,23%	594	1.516	2.109	28%	72%
4	ApoE-KD/ Y162A	517.498	3.563	521.061	99,3%	0,68%	1.317	1.076	2.393	55%	45%
5	**ApoE-KD/ L30A-Y36A**	85.883	3.563	89.447	96,0%	**3,98%**	601	1.131	1.732	35%	**65%**
6	**ApoE-KD/ Y36A-L159A**	85.883	3.563	89.447	96,0%	**3,98%**	389	1.182	1.571	25%	**75%**
7	**ApoE-KD/ L30A-L159A**	63.441	6.475	69.916	90,7%	**9,26%**	187	1.066	1.253	15%	**85%**
8	Naive-cell	697.591	3.563	701.154	99,5%	0,51%	2.073	2.183	4.257	49%	51%

App. Tab/Fig 3. Accumulation of HCV intracellular infectivity and core in Lunet-ApoE^{CRAC*} expressing cells

Lunet/ApoE-KD cells were transduced with lentiviruses containing either an empty vector (Empty V.), ApoE^{wt}, ApoE-C-terminal deletion (CTDdel), or ApoE CRAC mutants including Y162A, L30A-Y36A, L159A-Y36A, L30A-L159A, respectively and electroporated with *in vitro*-transcribed HCV Jc1 RNA. The HCV intra/extracellular infectivity were determined by the measurement of TCID$_{50}$/ml at 48 h.p.e. The intra/extracellular core protein amounts were also measured in parallel (n=2).

Note that ApoE CRAC mutants including L30A-Y36A, L159A-Y36A, L30A-L159A expression leads to the accumulation of the infectious HCV and core protein intracellularly suggesting the defect in the secretion step of the HCV life cycle.
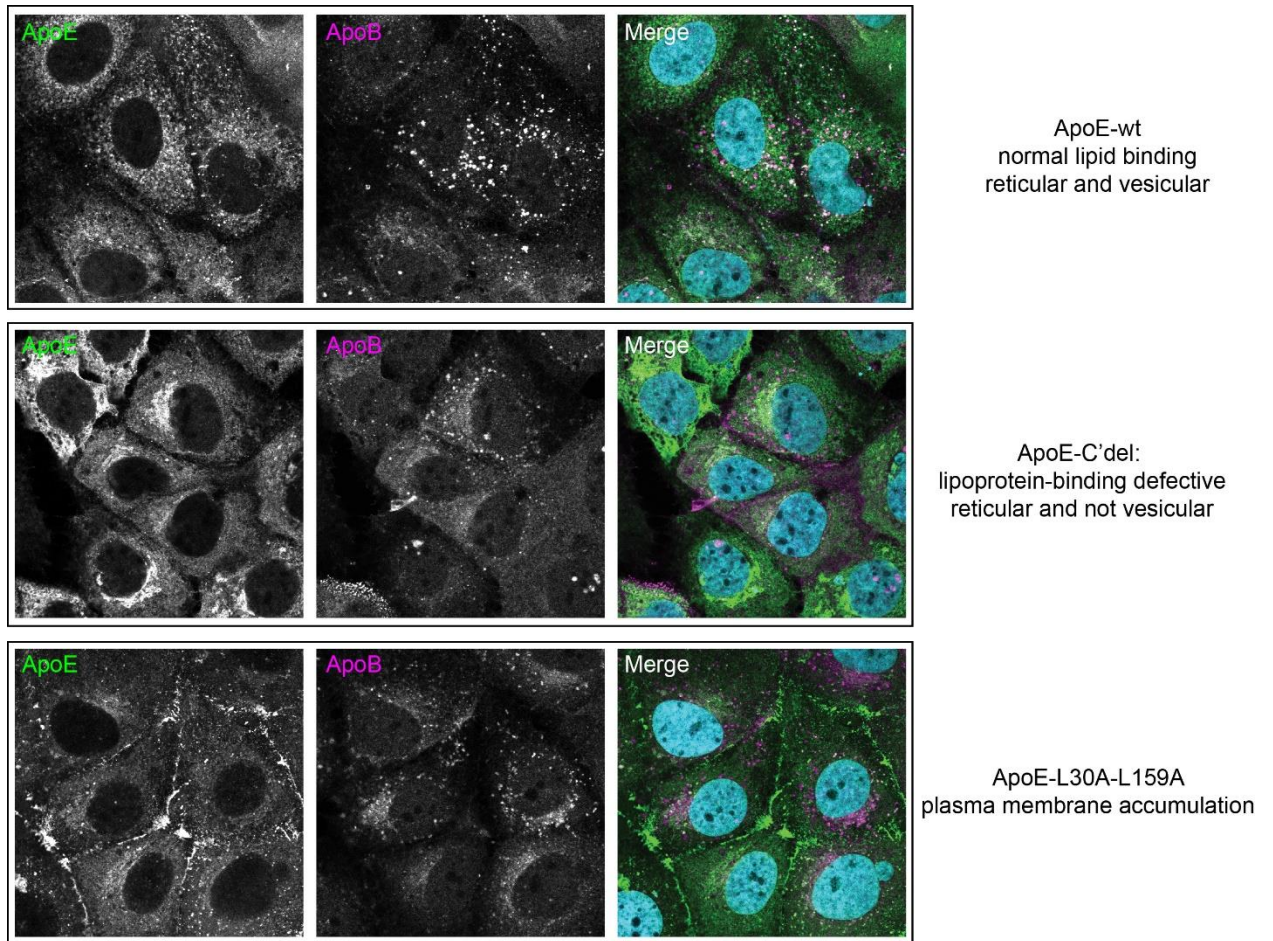
App. Tab/Fig 4. Plasma membrane accumulation of the ApoE^CRAC mutant

Lunet/ApoE-KD cells were transduced with lentiviruses containing either ApoE^wt, ApoE-C-terminal deletion, or ApoE L30A-L159A, respectively and were stably selected. Cells were fixed and subjected to IF staining of ApoE and ApoB by the respective specific antibodies and imaged by a confocal microscope.

Note that the ApoE^CRAC* preferentially distributes to the plasma membrane in Lunet cells. C-terminal deletion of ApoE abolishes the lipid-binding ability of ApoE. This mutant shows no vesicular signals overlapping with ApoB.
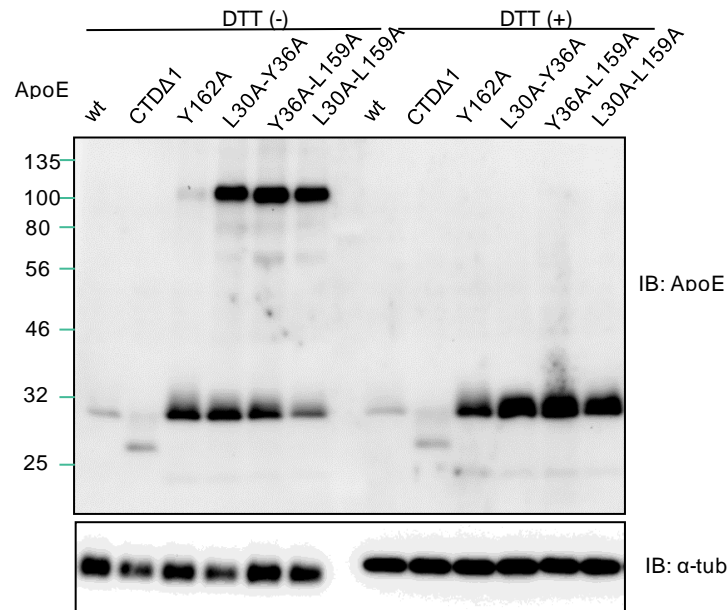
App. Tab/Fig 5. ApoE^CRAC* mutants are predominantly present in the tetrameric form

Lunet/ApoE-KD cells were transduced with lentiviruses containing either with ApoE^wt, ApoE-C-terminal deletion (CTDΔ1), or ApoE CRAC mutants including Y162A, L30A-Y36A, L159A-Y36A, L30A-L159A, respectively and stably selected. Cells were lysed in either non-reducing lysis buffer (DTT⁻) or DTT-containing lysis buffer. The presence of ApoE oligomer was visualized by Western blot analysis (first 6 lanes) using ApoE-specific antibody. α-tubulin was used as a loading control.

Note that intracellular ApoE^wt is predominantly present in the monomeric form. In contrast, the ApoE^CRAC* show high tetramer to monomer ratios.

Lunet ApoE empty/ApoE^wt/ApoE3^CRAC*

PAC-chol assay (20uM)
(UV-CL)
↓
SDS-PAGE (non-reducing)

% Eluate compared to Input		
Lane 1	HCV- NS2	8.3%
Lane 2	ApoE-wt	9.8%
Lane 3	**ApoE-CTDΔ1**	**0.6%**
Lane 4	ApoE-Y162A	10.9%
Lane 5	ApoE-L30A-Y36A	8.7%
Lane 6	ApoE-Y36A-L159A	9.5%
Lane 7	ApoE-L30A-L159A	8.3%
	HCV-core	1.3%
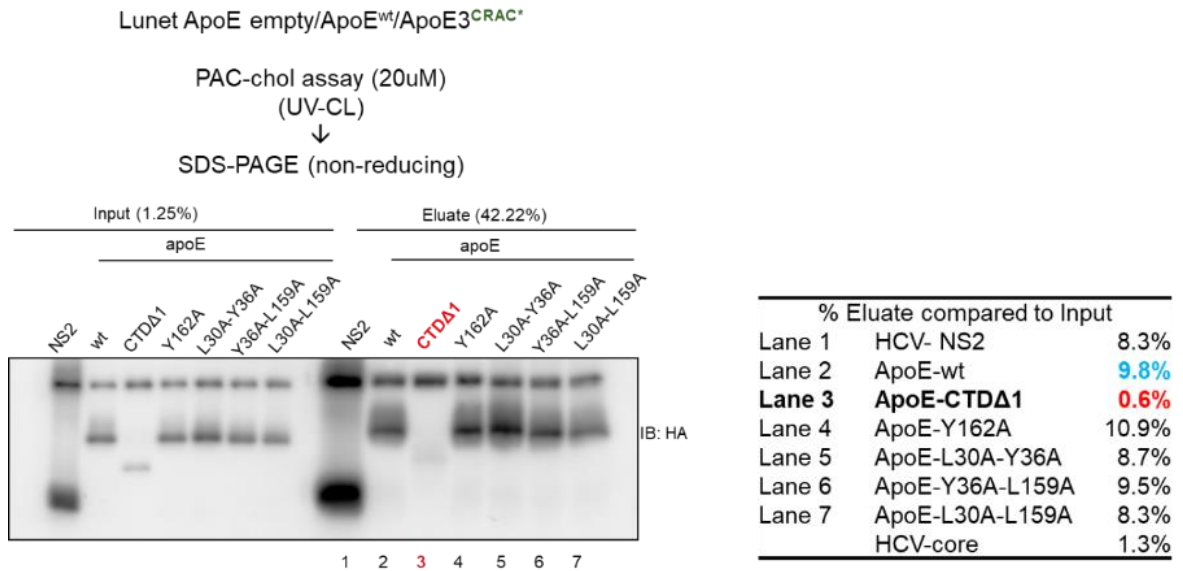
App. Tab/Fig 6. Monomer of ApoE^CRAC mutants can be crosslinked to the photoactivatable and clickable cholesterol (PAC)

[Left] Experimental procedure: Lunet/ApoE-KD cells were transduced with lentiviruses containing either HA-tagged ApoE^wt (wt), ApoE-C-terminal deletion (CTDΔ1), or ApoE CRAC mutants (ApoE^CRAC*) including Y162A, L30A-Y36A, L159A-Y36A, L30A-L159A, respectively. HCV NS2 or core transfected cells were used a positive control and negative control, respectively. At 48 h post-transduction or transfection, cells were fed with photoactivatable and clickable cholesterol (PAC) and subjected to the PAC binding assay after UV-crosslinking (CL) for 5 min. The ApoE forms crosslinked to PAC were detected by Western blot using HA-specific antibody.
[Right] Percent of bound proteins (eluate) compared to input are shown.

Note that C terminal deletion of ApoE (ApoE-CTDΔ1) abolishes the interaction between ApoE and cholesterol (lane 3).
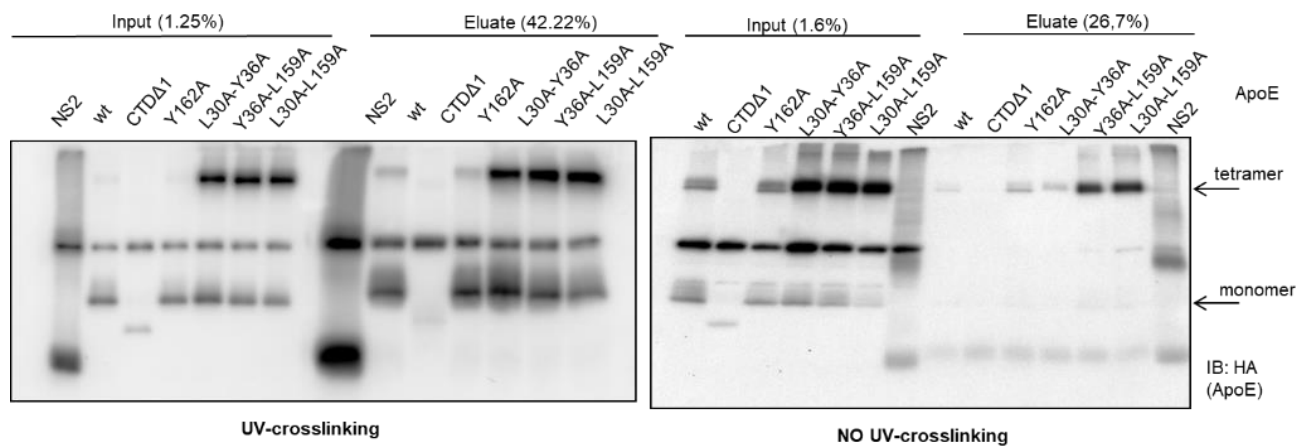
App. Tab/Fig 7. The high affinity of ApoE tetramer with cholesterol

[Left] Refer to the App.Figure 6. Note that both ApoE monomer and tetramer can be crosslinked efficiently with PAC in the condition of UV-crosslinking.

[Right] Lunet/ApoE-KD cells were transduced with lentiviruses containing either HA-tagged ApoE^wt (wt), ApoE-C-terminal deletion (CTDΔ1), or ApoE CRAC mutants (ApoE^CRAC*)) including Y162A, L30A-Y36A, L159A-Y36A, L30A-L159A, respectively. HCV NS2 transfected cells were used a positive control. At 48 h post-transduction or transfection, cells were fed with photoactivatable and clickable cholesterol (PAC), collected, and lysed in the lysis buffer (0.3% NP40, 50mM NaCl, 38mM MβCD, 1x PBS) and subjected to the PAC cholesterol binding assay (without UV crosslinking). ApoE forms bound to PAC were detected by Western blot using HA-specific antibody (n=1).

Note that only ApoE tetramer can be detected in the PAC binding assay without UV cross-linking. This result argues for the strong binding between ApoE tetramer and cholesterol.

2. Characterization of HCV mutant viruses with a defect in virion morphogenesis (E530A/G)

In need of finding the HCV assembly sites, I have searched for intermediate assembling virus particles having distinct signatures that could be detected at the virus budding sites by CLEM. Preliminary data provided by Norbert Tautz and Olaf Isken (Institute of Virology and Cell Biology, University of Luebeck, Luebeck ,Germany) showed that a mutation in HCV NS3 at E530 residue to A/G resulted in the abrogation in HCV particle assembly but does not affect RNA replication. Therefore, I confirmed the RNA replication competence and tested the assembly defect of the HCV E530A/G virus by investigating extracellular core secretion, intracellular core sedimentation, HCV assembly hallmark with NS5A-E2 foci formation, DMV formation, and virus budding by CLEM. I found that it is highly likely that these viruses have a defect in the nucleocapsid formation step. Unfortunately, I failed to identify any distinct ultrastructure that could

be unambiguously assigned to assembling HCV particles. However, my work resulted in the second-author manuscript "characterization of a multipurpose NS3 surface patch coordinating HCV replicase assembly and virion morphogenesis" which was submitted to Plos Pathogen and are currently under revision.

No.	Sample name		Intra core (fmol)	Extra core (fmol)	total core (fmol)	Extra core/total core
1	JcR2a-wt 1	24h	121.2	64.9	186.1	34.9%
2	JcR2a-wt 2		133.3	74.1	207.4	35.7%
3	JcR2a-E530A 1		9.6	0.0	9.6	0.0%
4	JcR2a-E530A 2		5.5	0.0	5.5	0.0%
5	JcR2a-E530G 1		36.8	0.0	36.8	0.0%
6	JcR2a-E530G 2		46.9	0.0	46.9	0.0%
7	JcR2a-wt 1	48h	954.8	866.3	1821.1	47.6%
8	JcR2a-wt 2		1021.8	893.9	1915.7	46.7%
9	JcR2a-E530A 1		257.0	2.6	259.6	1.0%
10	JcR2a-E530A 2		334.4	9.4	343.9	2.7%
11	JcR2a-E530G 1		577.8	3.0	580.9	0.5%
12	JcR2a-E530G 2		809.5	3.1	812.6	0.4%
13	JcR2a-wt 1	72h	1805.3	1466.1	3271.4	44.8%
14	JcR2a-wt 2		1863.3	1564.4	3427.7	45.6%
15	JcR2a-E530A 1		1027.9	7.2	1035.1	0.7%
16	JcR2a-E530A 2		1053.9	8.4	1062.3	0.8%
17	JcR2a-E530G 1		1346.8	15.2	1362.0	1.1%
18	JcR2a-E530G 2		1177.0	12.1	1189.2	1.0%

App. Tab/Fig 8. Abrogation of core release in HCV NS3 E530A/G-infected cells

Huh7.5 cells were electroporated with *in vitro*-transcribed HCV-JcR2a RNA wt or NS3 E530 A/G mutants. The amounts of intra/extracellular core protein (fmol) at indicated time points were measured by Core CMIA. Ratios of extracellular core to total core are calculated. Data from a representative experiment are shown (n=2).

Note that HCV RNA replication of HCV with NS3 E530A/G is affected, especially at early time points but these viruses replicate at a high level at 72 h post-electroporation of HCV RNA. Importantly, NS3 E530A/G mutations abrogate almost completely the secretion of core.
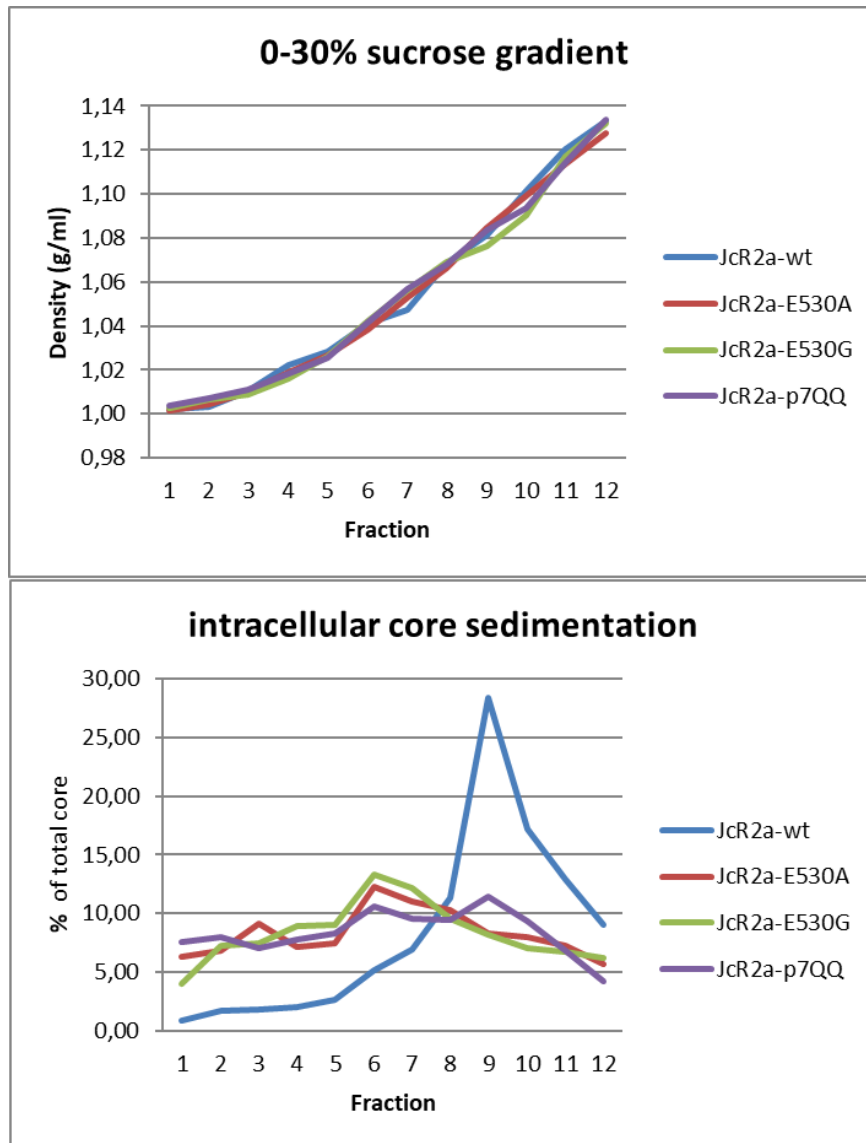
App. Tab/Fig 9. Abnormal core sedimentation profile of intracellular HCV with NS3 E530A/G mutation

Huh7.5 cells were electroporated with either *in vitro*-transcribed HCV JcR2a RNA wt, mutants NS3 E530 A/G, or p7QQ, respectively. Note that p7QQ is the HCV with a mutation in p7 protein, showing a defect in the capsid envelopment [27]. At 48 h.p.e, cells were collected and subjected to repeated freezing-thawing cycles to release intracellular HCV. HCV-containing lysates were subsequently subjected to rate-zonal centrifugation using 0-30% sucrose gradients to examine the sedimentation profiles of core (lower). The density of collected fractions is shown in the upper panel.

Note that intracellular HCV E530A/G mutants show abnormal core sedimentation profiles compared to HCV wt indicating the possible defect in the nucleocapsid formation step.
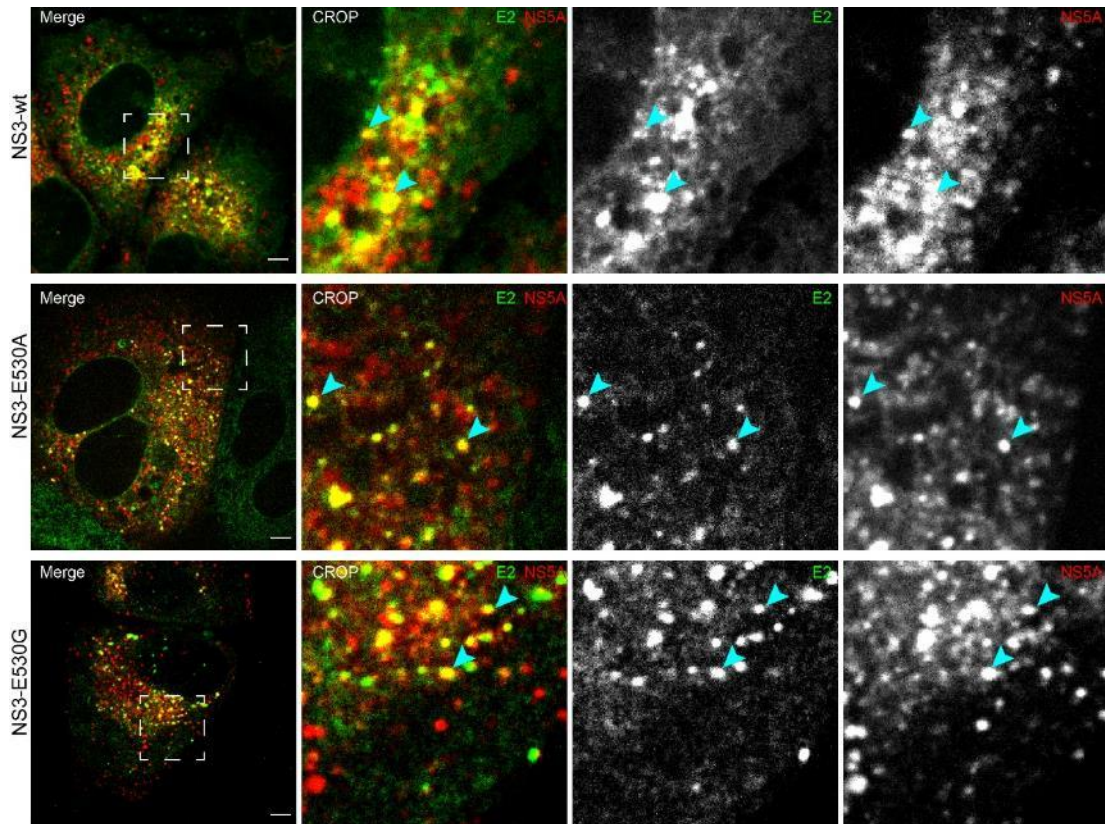
App. Tab/Fig 10. Normal HCV NS5A-E2 foci formation of HCV with NS3 E530A/G mutation

Lunet-ApoE^{mT2} cells stably expressing Core-NS2/E2^{eYFP} were electroporated with *in vitro*-transcribed sgJFH1/NS5A^{mCherry} RNA or sgJFH1/NS5A^{mCherry}/NS3-E530A/G. Cells were subjected to time-lapse live-cell confocal imaging to observe ApoE-, NS5A- and E2-positive signals. Extracted time frames at 48 h.p.e were shown. Images on the right of each row are magnified views from the selected area in the left overview image. Scale bar: 5 μm. Cyan arrowheads: E2-NS5A foci.

Note that HCV "assembly module"-induced E2 foci formation of HCV with NS3 E530A/G were still readily observed, indicating the assembly sites of HCV were somehow still formed in spite of a defect in HCV capsid assembly. This perhaps reflects the coordination of different steps of HCV assembly.

A

B
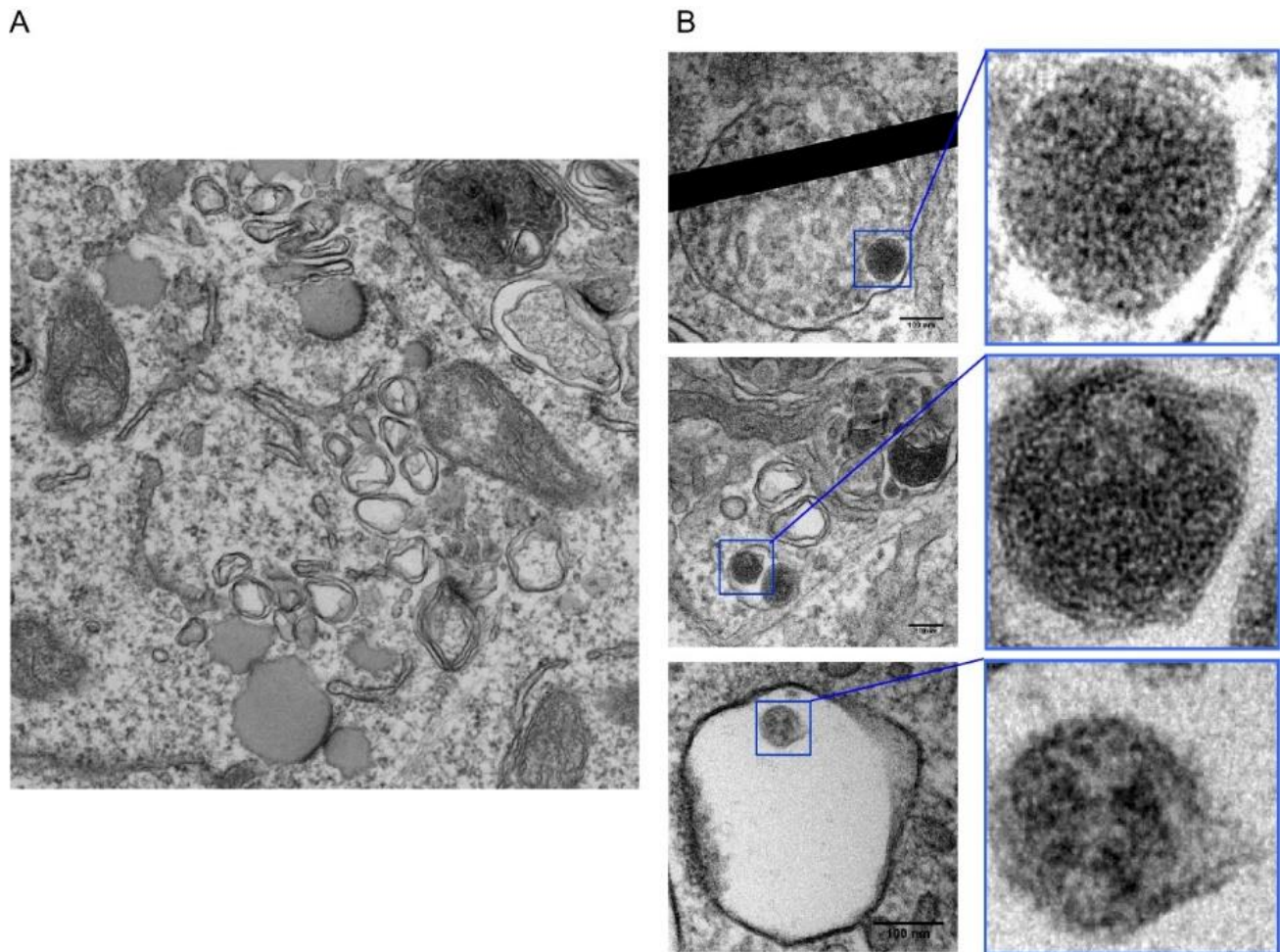
App. Tab/Fig 11. Normal DMV formation in cells infected with HCV with NS3 E530A/G mutation

Lunet-ApoE^mT2 cells stably expressing Core-NS2/E2^eYFP were electroporated with *in vitro*-transcribed sgJFH1/NS5A^mCherry/NS3-E530A/G RNA. At 48 h.p.e, cells were analyzed by a CLEM method to examine the DMV formation and find the arrested HCV particles. Representative electron micrographs of the HCV NS3-E530G-infected cells are shown.

Note that DMV formation induced by HCV with E530A/G mutation was still functional (A), indicating that the competent RNA replication of these viruses. The electron-dense spherical structures found in these virus-infected cells were shown in (B). However, I did not observe unambiguous IF signatures of these electron-dense structures.

3. Ultrastructure of HCV double membrane vesicles studied by cryo-FIB-SEM

This chapter shows my first attempts to visualize HCV DMVs by *in situ* cryoEM with the aim to determine the topology of DMVs and where NS5A resides. All steps of sample preparation,

i.e. RNA electroporation, cell culture on EM grids, grid plunging, and lamella FIB-SEM milling were performed by myself. Image acquisition was conducted by Petr Chlanda, Schaller research group leader at the Department for Infectious Diseases-Virology, Heidelberg University Hospital, Heidelberg, Germany.

Tomography snapshot 3

Tomography snapshot 4

protruding density at pore-like structrure

protruding density at pore-like structrure
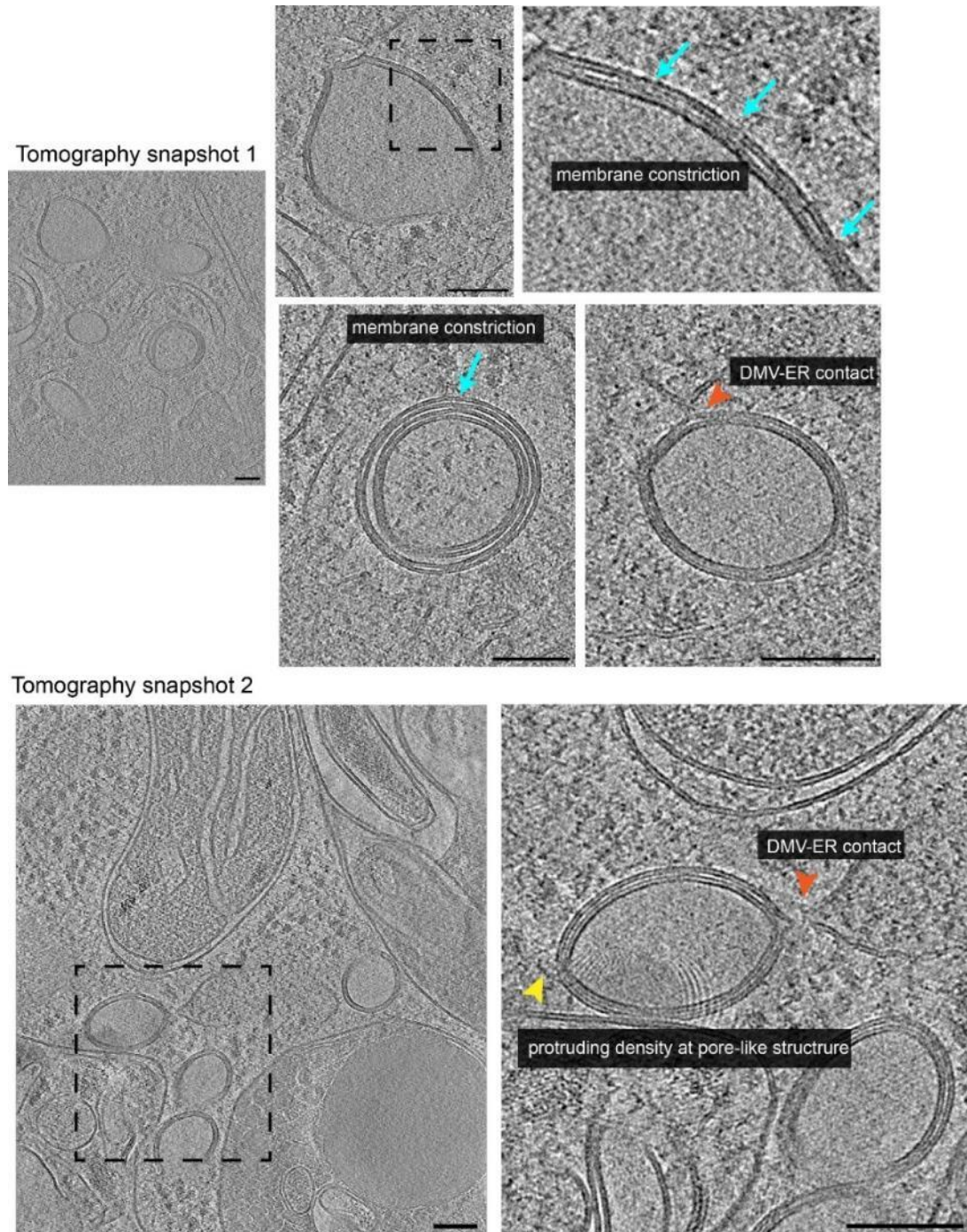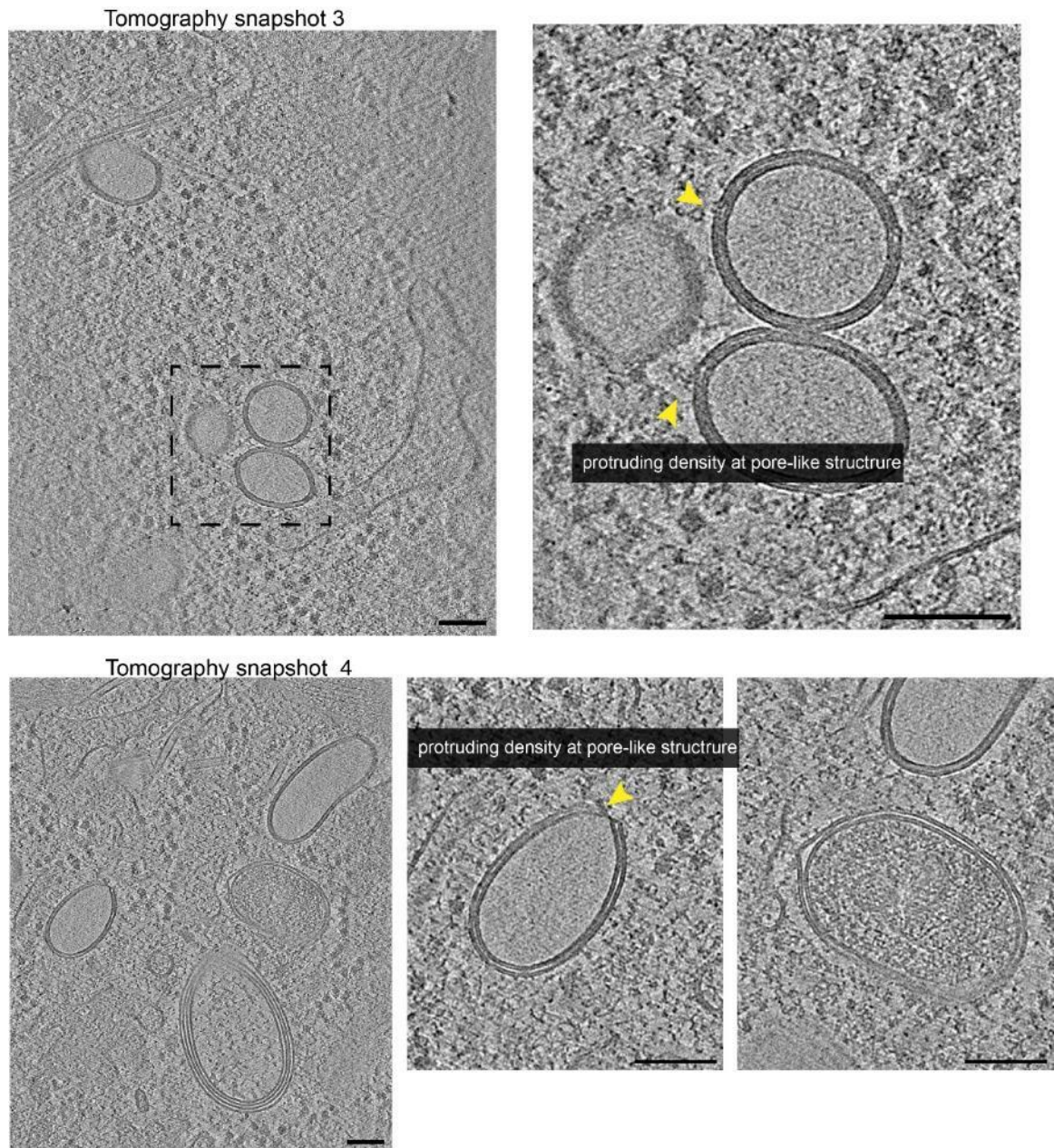
App. Tab/Fig 12. Putative pore-like structures with protruding densities of HCV DMVs as revealed by the cryo-electron tomography

Lunet cells were electroporated with *in vitro*-transcribed sgJFH1 RNA. At 48 h.p.e cells cultured on carbon-coated EM grids were vitrified by plunge-freezing in cryogenic liquid ethane and stored in liquid nitrogen for long-term storage before milling. Thin lamella (~150nm) of cells were prepared by a cryogenic FIB-SEM method. HCV DMVs morphologies were examined by cryo-electron tomography.

Note that there are protruding electron density at the pore-like structures of HCV DMVs. At this moment, I do not have any evidence and can only speculate that HCV NS5A is present at the putative pores of DMVs and makes up these densities. In addition, these results also clearly show the DMV-ER connection, possibly reflecting the ER origin of DMV biogenesis.